Influence of Maturation, Pathology and Functional Lateralization on 3D Sulcal Morphology using MRI

Jensen, Betina Vase; Larsen, Rasmus

Publication date:
2016

Document Version
Publisher's PDF, also known as Version of record

Influence of Maturation, Pathology and Functional Lateralization on 3D Sulcal Morphology using MRI

Betina Vase Jensen

Kongens Lyngby 2015

Technical University of Denmark
Department of Applied Mathematics and Computer Science
Richard Petersens Plads, building 324,
2800 Kongens Lyngby, Denmark
Phone +45 4525 3031
compute@compute.dtu.dk
www.compute.dtu.dk

Summary (English)

The folding of the cortex results in a characteristic pattern of folds called sulci and ridges called gyri. The cortical folding varies greatly both within and between individuals. Despite a century of sustained research, the mechanisms underlying the observed variation in folding is still largely unknown. The shape of cortical sulci and gyri are determined in part by forces exerted by white matter fiber connections between various cortical regions. Studying the shape of the cortical sulci hence contributes to the understanding of the variation in the folding.

This thesis concerns sulcal morphometry using Magnetic Resonance Imaging (MRI) and spatial statistical methods. The sulcal morphology has been studied with respect to: the normal development of a central sulcus; in relation to functional lateralization of the motor hand area in central sulcus and, finally, in relation to a pathological condition, anosmia, in the olfactory sulcus. This thesis describes and uses methods for sulci segmentation, sulci registration, sulci representation, and statistics for modeling sulci shape and testing sulcal morphology.

This thesis describes methods to analyze sulcal morphology and show how sulci variability are influenced under normal development, by a functional ability, and by pathological conditions.

Summary (Danish)

Hjernen er det mest komplekse organ i menneskekroppen. Den modtager konstant information, bearbejder den og reagerer i henhold til den. Hjernens overflade, cortex, består hovedsageligt af neuroner. Disse neuroner er forbundet ved underliggende myoliniserede axoner, der er med til at forme hjernen. Cortex er karakteristisk ved et foldningsmønster, der består af udposninger gyri, og foldninger, sulci. Disse er karakteriseret ved en meget stor variabilitet, der på trods af en enorm interesse og forskningsaktivitet, til stadighed er delvis ukendt. For at forstå, hvad denne variation skyldes, kan formen af sulci undersøges. Dette gøres oftest ved hjælp af magnetisk resonans (MR) skanninger af hjernen, hvilket giver mulighed for at studere hjernens bløddele. I denne afhandling undersøges, hvorledes formen af den centrale sulcus udvikles normalt. Dernæst undersøges, hvordan den asymmetri, der er findes i brugen af højre og venstre hånd, påvirker den asymmetri, der ses i det funktionelle motorområde i central sulcus. Endeligt undersøges, hvordan den olfaktoriske sulcus påvirkes ved personer, der har mistet lugtesansen.

Ovenstående undersøges med baggrund i metoder inden for billedanalyse, hvilket har inkluderet segmenteringer, registreringer, reprœsentationer af sulcus og endeligt statistiske metoder til at modellere en sulcus og sammenholde dens form med demografiske variable.

Denne afhandling beskriver og anvender metoder indenfor sulcal morfologi, og bidrager med ny viden inden for den normale udvikling, i forbindelse med en egenskab og i forbindelse med patologiske lidelser.

Preface

This thesis was prepared at the Section for Image Analysis and Computer Graphics at DTU Compute, and submitted to the Technical University of Denmark (DTU) in partial fulfillment of the requirements for acquiring the Ph.D.

This project was one third funded by the ITMAN Graduate School Programme at DTU, one third by the Danish Research Centre for Magnetic Research (DRCMR) at Hvidovre Hospital, and the last third by DTU Compute.

The aim of this thesis is to address research questions regarding sulcal morphology, with a primary focus on maturation, functional lateralization, and pathology. The thesis consists of two parts: an introductory part and a part with papers. The introductory part holds a section with a background and an overview of the methods used in the thesis, followed by a discussion. The second part consists of three papers.

The project was supervised by Professor Rasmus Larsen (DTU) and Professor Hartwig Roman Siebner (DRCMR).

Lyngby, 4-12-2015

Betina Vase Jensen

Papers included in this thesis

The following papers are included in this thesis:

A B.V. Jensen, W.F.C. Baaré, K.S. Madsen, S. Angstmann, R. Larsen, H.R. Siebner. *Right-left depth asymmetry of central sulcus predicts right-left asymmetry in manual dexterity: a structural MRI study in right-handed children and adolescents*, 2015. Manuscript.

B M. Vestergaard, B.V. Jensen, H.G Karstensen, B. Djurhuus, D. Herz, B. Numelin, C. Klausen, A. Leffers, N. Tommerup, H.R. Siebner. *Congenital atrophy of the olfactory bulb is coupled to changes in the depth of the posterior olfactory sulci revealed by factor analysis*, 2015. Manuscript.

C B.V. Jensen. *Mapping Longitudinal Maturational Changes in Central Sulcus Morphology during Adolescence*, 2015. Technical report.

Acknowledgements

I would like to acknowledge several people who put their time, effort, and energy into this project.
First of all, I would like thank my supervisors, Rasmus Larsen, DTU Compute, and Hartwig R. Siebner, from DRCMR, Hvidovre Hospital, for encouraging guidance, patience, and supervision throughout the project! I owe a big thanks to William F.C, Baaré for his fast and meticulous feedback and guidance during the last months of this project.
Thanks to all current and former colleagues at the Image Analysis and Computer Graphics Group at DTU Compute for providing an inspiring working environment and enjoyable company. Thanks to Knut Conradsen for motivating and inspiring discussions on statistics. Thanks to Signe Strann Thorup for our technical discussions and your friendship.
Also thanks to all current and former colleagues of at DRCMR, especially Arnold Skimminge for many discussions and enjoyable company. Thanks to Kathrine Skak Madsen and Martin Vestergaard for their motivating inputs.
A very special thanks to the Department of Health Science and Technology at Aalborg University for letting me be a part of your group for the last eight months. It has been like coming home. Thanks to all for inspiring discussions and your friendly and enjoyable company. I have to point out one person that has facilitated the above. My deepest and most grateful thanks and respect go out to Lasse Riis Østergaard for taking me under his wing and guiding me through this last period of the project.
Thanks to Tron Darvann from the 3D Craniofacial Image Research Laboratory, University of Copenhagen, for taking the time to guide me through using 'Landmarker'.
Thanks to my friends and family for their help and support, especially to my

dear parents for keeping our girls happy and alive during the thesis writing period. Lastly, the biggest thanks to Brian, Astrid, and Benedikte for your patience, love, and support.

Contents

Part I

Introduction

Chapter 1

Introduction

The brain is the most complex organ in the body. Together with the spinal cord it controls the body by constantly receiving information, interpreting it and executing a response [191]. Language, memory, perception, behavioral, and social activities are processed in the cerebral cortex -a thin layer consisting mainly of dense neuron cell bodies, referred to as the gray matter (Figure 1.1). These neurons are connected by axons wrapped in a fatty white layer, that conduct quick electrical signals transition between neurons. These axons are the main part of white matter. [191]

1.1 Gyrification

Evolution has adjusted the brain according to the demand of higher cognitive abilities to react and adjust to the environment [208, 116, 8]. A dramatic expansion of the area of the cerebral cortex has accommodated a larger number of neurons and cortico-cortical connections [279, 276, 112, 113]. The large cerebral cortex is folded to fit in the limited cranial volume. The folding of the cortex, also called gyrification, results in a characteristic pattern of folds called sulci and ridges called gyri (Figure 1.1).

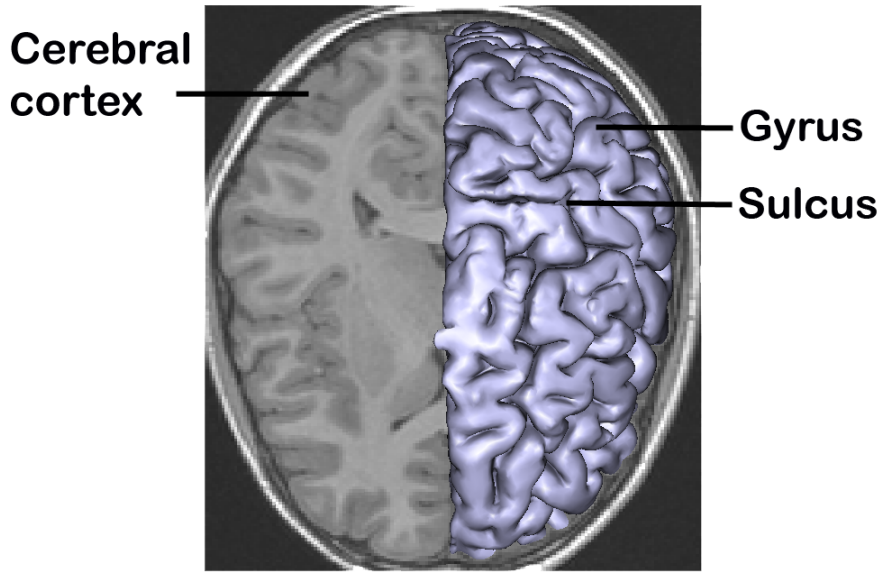

Figure 1.1: The Cerebral cortex, the outer layer of brain, consists mainly of dense neuron cell bodies. The folding of the cortex results in sulci and gyri.

The cortical folding and, consequently, the sulcal patterns varies greatly between human individuals [199]. All sulci are characterized by large variations both between individuals and hemispheres [199, 269, 280, 217, 178, 277, 212]. A sulcus corresponding to one long fissure in one subject may be made up of several small fissures in a second subject [178]. In regions with the most variation, only experts can reliably recognize sulci [212].
Despite a century of sustained research, the mechanisms underlying gyrification is still largely unknown [10, 9, 293, 174, 169, 149, 106, 234, 292, 117, 228, 90]. Gyrification has been explained by the restricted space in the skull during cortical folding [279]. However, another commonly accepted theory is that the neuronal connections that develop during the second trimester in gestation produce local fiber tension that pulls regions with greater connectivity closer together [276]. This produces outward bulging gyri as regions of greater interconnectivity move closer together in the enclosed brain. In addition, more sparsely connected regions are separated and form sulci. Based on this theory, the shape of cortical sulci and gyri are determined in part by forces exerted by white matter fiber connections between various cortical regions. Studying the shape, termed morphology, of the cortical sulci hence contributes to the understanding of the variation in gyrification [6, 281, 166, 5, 63, 76, 60, 186, 290].

1.2 Development of gyrification

There is evidence that the cortical folding pattern is subject to developmental change in both childhood and adolescence [91, 89, 23].
The outer cortex begins to fold from midgestation with the formation of neuronal connectivity inducing an expansion of the outer cortex [220]. After the first year of life, the gyrification decreases throughout life [174, 237, 10, 211, 193, 117, 33] and is characterized by synaptic pruning. Synaptic pruning eliminates extra neurons and synaptic connections to increase the efficiency of neuronal transmissions. [56, 283].
Synaptic pruning is influenced by environmental factors and is thought to represent learning [125, 126]. Studies have suggested that environmental influences and hence pruning is one of the basic foundation for the variation in gyrification [250, 248, 127, 239, 92].
The environmentally induced variation also affects the maturation, as early as the 6th week of the fetal life, when new neurons are formed and migrate from the ventricles toward the outer surface of the brain [26]. This neuronal division and migration are associated with a cortical growth both in thickness and surface area [254, 257]. Both thickness and surface area can be affected by even small interferences. Studies on embryos of monkeys show that irradiation during the symmetric phase of cell division in week 6 to 12 results in a decrease in the total surface area of the brain. When the radiation is applied after six weeks, during the phase of asymmetric cell division, a decrease is observed in the cortical thickness [18].
Apoptosis or programmed cell death contribution to the variation in gyrification. In fetal life, apoptosis eliminates up to 50 % of the neurons generated. This naturally influences the total brain volume [55] and shape the brain [141]. Apoptosis continues into both childhood and adultness, where around ten billion cells are made each day just to balance those dying by apoptosis [214].
It is clear that the gyrification decreases in childhood and adolescence [145]; however, relatively little is still known about the developmental changes in the folding of the cortical surface. [145]

1.3 Influence of trained abilities on gyrification

The variability in the brain morphology can be correlated with cognitive, sensory, and motor abilities. One of the best known examples is the case of London taxi drivers. These taxi drivers had an increased volume in the part of the brain involved with spatial navigation, the hippocampus, with more years working as drivers [175].

The variability in gyrification has been correlated with motor abilities. Musicians show a significantly greater local variability in the functional motor area in Central Sulcus (CS) than non-musicians. [160] Earlier music training even showed a bigger variability.
The huge variation in the brain morphology is not just present between subjects, but also within individuals [285, 284, 250]. This asymmetry or lateralization has been shown to map the hand motor area to the left CS in right handers and vice versa in left handers [6, 289, 60]. A lateralization is also seen in the language area, which is mapped to the peri-Sylvian [250] in the left hemisphere in 70 % to 95 % of all humans. Lateralization manifests as deeper and larger surface area in the dominant hemisphere [147, 159].
Several studies have correlated white matter and gray matter to specific functional abilities [163, 239, 127, 99, 66, 146]; however, the relation between functional abilities and gyrification is very limited [6, 5, 60].

1.4 Influence of pathology on gyrification

As well as a functional ability affects the cortical folding, the lack of an ability can also alternate the gyrification. A pathological condition is often related to a significant increase in apoptosis [73]. Patients suffering from schizophrenia show a decrease in the whole brain and hippocampal volume [251], and the bilateral average sulcal depth [58, 87]. A significantly greater sulcal width and shallower depth is also seen in patients suffering from Alzheimer's disease compared to controls [129]. The lack of motor functions in patients suffering from primary lateral sclerosis is seen as a decrease in cortical thickness of the motor hand area in CS [38]. On the other hand, patients with autism show an increase in the gyrification and sulci depths [278, 13, 161].
The loss of the ability to smell, also called anosmia, is related to loss of volume in the olfactory bulb and a less deep Olfactory sulcus [1, 123].
A number of studies have shown how sulcal morphology changes in the case of pathological conditions. Understanding the mechanisms underlying these disorders may contribute to distinguishing changes in maturation from neurological diseases from healthy aging processes.

1.5 Studying sulcal shape

The cerebral anatomy and functionality were traditionally studied using post-mortem samples [30, 41, 280, 281]. The first comprehensive descriptions of

sulci shape were based on pictures and metrics of the sulci from 25 postmortem brain specimens (Figure 1.2) [199]. Other specimen dissection studies have followed by further describing the location and shape of the sulcal morphology [6, 289, 232, 93].

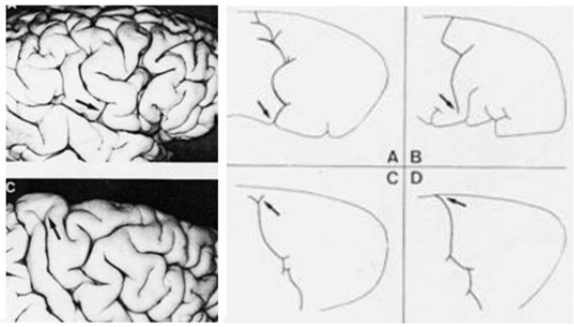

Figure 1.2: An example from the first comprehensive description of sulci shape made only 25 years ago [199]. These descriptions were based on pictures and metrics on 25 postmortem brain specimens.

Today, the study of gyrification is often performed with neuroimaging methods. Neuroimaging falls into two categories: functional neuroimaging and structural neuroimaging. Functional neuroimaging is typically used to map activities in the brain using, for example, functional Magnetic Resonance Imaging (fMRI) [209, 168, 97, 290], Transcranial Magnetic Stimulation (TMS) [99, 2], and Electroencephalography (EEG). Structural neuroimaging is used to describe shape, size, and integrity of the structures in the brain using Computed Tomography (CT) [174], Diffusion Tensor Imaging (DTI) [207, 151, 164, 57], and Magnetic Resonance Imaging (MRI) [136, 262]. Structural MRI is the typically used modality since it produces high quality 3D images of the soft tissue in the body. This technique uses magnetic fields and radio waves to form images of the body [105]. Within structural neuroimaging, spatial statistical models have shown powerful to describe patterns, spatial correlation, and shape based on, for example, probability theory, stochastic modeling, and mathematical statistics. Spatial statistics have proven powerful in studying the biological growth in numerous studies [153, 140, 252, 255, 51]. Spatial statistical models typically involve image acquisition, segmentation of the object of interest, an alignment to compare objects across subjects, and, finally, statistics to model or test hypotheses.

1.6 Objectives

The cerebral cortex is highly folded and variable in its shape across individuals and hemispheres. Based on the theory that the shape of cortical sulci and gyri are determined in part by forces exerted by white matter fiber connections, studying the shape, termed morphology, contribute to the understanding of the variation in gyrification. Despite a century of sustained research, the mechanisms underlying the observed variation in these sulci are still largely unknown. Studying the sulcal shape in relation to normal development, functionality, and pathological conditions contribute to the understanding of gyrification. Spatial statistical methods have been shown to be powerful in studying biological growth and shape.

The objective of this thesis is to study sulcal morphology using MR images and techniques within spatial statistics to investigate:

1) The normal development of central sulcus

2) The influence of functional lateralization on the motor hand area of central sulcus

3) The influence of a pathological condition, anosmia, on the morphology of olfactory sulcus

Scientific contributions

The above objectives have been addressed in the following three contributions (part II, Chapter 8, 9 and 10):

A B.V. Jensen, W.F.C. Baaré, K.S. Madsen, S. Angstmann, R. Larsen, H.R. Siebner. *Right-left depth asymmetry of central sulcus predicts right-left asymmetry in manual dexterity: a structural MRI study in right-handed children and adolescents*, 2015. Manuscript.

B M. Vestergaard, B.V. Jensen, H.G Karstensen, B. Djurhuus, D. Herz, B. Numelin, C. Klausen, A. Leffers, N. Tommerup, H.R. Siebner. *Congenital Atrophy of the Olfactory Bulb is coupled to changes in the Depth of the posterior Olfactory Sulci revealed by Factor Analysis*, 2015. Manuscript.

C B.V. Jensen. *Mapping longitudinal maturational changes in CS morphology during adolescence*, 2015. Technical report.

Paper A: The influence of functional lateralization on the motor hand area of central sulcus
Handedness is one of the most obvious asymmetries in the human body. The right-left asymmetry is seen as an increased surface area and depth of the central sulcus (CS) in the dominant hemisphere. Handedness is often classified into either left or right handers. To relate functional lateralization of the motor hand area to CS, we map the ability to draw superimposed circles in a regular fashion to the depth of the CS in right-handed individuals. We applied factor analysis to model causal observer-independent depths of the central sulcus. The novelty in this study is the mapping of the degree of handedness to the asymmetry of CS.

Paper B: The influence of a pathological condition, anosmia, on the morphology of olfactory sulcus
Olfactory deficits may be second to infections, Parkinson's disease, or dementia, which makes the olfactory systems important to understand. In individuals with anosmia, the bulb and sulci demonstrate respectively atrophy. In this study, we investigate whether specific subareas along the Olfactory Sulci (OS) are affected by the atrophy in the olfactory bulb. The novelty in this study is the modeling of the subareas to locate anosmia within the OS.

Paper C: The normal development of central sulcus
The overall gyrification decreases after the first year in life. However, relatively little is still known about the local development of CS, a major fold on the lateral surface of the brain. In this longitudinal study, we characterize the developmental changes in the surface area, depth profile, and positional variation of CS. The novelty in this study is the longitudinal analysis of the structural shape of CS. Furthermore, we address the positional movement of CS in time, to understand the local development.

1.7 Thesis overview

This thesis includes a background part (Chapter 1 to 7) and a scientific contribution part (Chapter 8 to 10). The background part describes the steps taken to study sulcal morphology (Figure 1.3). The first chapter gives an introduction to the data used to answer the objectives. The next chapters describes how a sulcus can be segmented from the brain. This is followed by a chapter

that describes how to align sulci both within and between subjects. The next chapter describes how to represent a sulcal shape. Finally, a chapter describing statistical methods, is followed by a discussion.

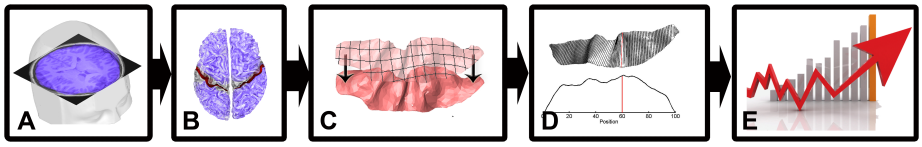

Figure 1.3: A pipeline to study sulci morphology typically include the following disciplines. Firstly, an MR image acquisition of the head, to produce high quality 3D images of the soft tissue in the brain (A). Based on the image of the entire brain the sulci of interest is segmented (B). This is typically followed by a one-to-one mapping between sulci (C) and a representation of the sulcal shape (D), also called sulcal morphology. Finally, to relate sulci shape to demographic variables statistical tests are applied (E).

The contribution part holds three papers. The papers in Chapter 8 and 9 are ready for submission. Paper 10 is a technical report, and is work in progress performed in collaboration with Kathrine Skak Madsen (DRCMR), Rasmus Larsen (DTU), Hartwig Roman Siebner (DRCMR) and William F.C. Baaré (DRCMR). This report will ultimately be published as an article in an international Journal. Appendix A, describes step-by-step extraction of CS.

Chapter 2

Sulci

The central sulcus (CS) and the olfactory sulcus (OS) are used to study the variability in sulcal morphology throughout this thesis. The CS (paper 8 and 10) is a large sulcus that is well studied because of its stability in both location and shape. The OS (paper 9) is small and very little is actually known about it. This chapter introduces CS and OS with respect to the anatomy, functionality, and acquisition of MR images to study their shape.

2.1 Central sulcus

The CS, also known as the fissure of Rolando [30], is made up of two merged folds [240]. It is characterized by a double S-shape that extends obliquely upward and backward on the lateral surface of each cerebral hemisphere [199] (Figure 5.1). CS is developed from the 18th week of fetal life [10, 3] and therefore has several stable structures [199, 280]. CS is often used as a gross landmark in planning of brain surgery [32]. However, the superficial appearance of CS has shown to vary greatly both between and within subjects [199].
CS separates the frontal and parietal lobes [280, 293]. The banks of the parietal lobes hold the primary somatosensory areas, Brodmann's area 3. The other banks, on the frontal lobes, hold the primary motor areas, Brodmann's area 4

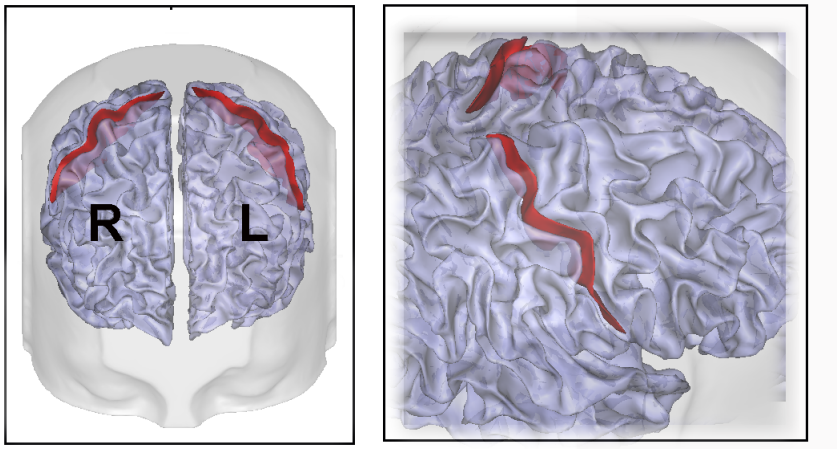

Figure 2.1: CS shown in red in axial view (left) and sagittal view (right).

[30]. Prior gross anatomical studies have demonstrated that the motor cortex is approximately twice as thick as the sensory cortex [187]. A 'homunculus' can be mapped onto the anatomy of each of the two banks along the CS. This map holds sensory input on the caudal banks and motor output on the rostral banks [79, 203, 204]. Each area along this 'homunculus' has been studied in detail, e.g. the functional movement of the tongue [235, 76, 182], jaw [98], fingers and toes [72], hands [63, 5, 27, 178, 111], and neural organization of speech [31, 34].

Motor hand area

The cortical representation of the motor hand function was first shown to be mapped on to the superior part of the precentral gyrus [79, 203] in the 1930s. Sixty years later, functional Magnetic Resonance Imaging (fMRI) techniques were used to explore the mapping of the motor hand area in greater detail. Simple paradigms, like contraction and extension of the index finger [101], repetitive opening and closing the hand [289], thumb to index finger [132], and finger tapping of all fingers except for the thumb [209] showed contralateral activation in the primary motor cortex. Increasing the complexity of the paradigms, for example, to successive finger-thumb opposition from little finger to index finger [101, 209], have showed an additional activation of the ipsilateral primary motor cortex and bilateral somatosensory areas [101]. These fMRI studies and other structural studies [233, 289, 111] have mapped the location of the motor hand area to a knob like structure in the precentral component often known as the 'hand knob' [289].

Functional lateralization
The motor hand area holds the most pronounced behavioral asymmetry in the brain; the preference towards using either the left or right hand. The CS of right-handed individuals is deeper and larger in the left hemisphere [6, 80, 178, 60, 260]. This pattern is flipped for left-handed subjects. This asymmetry is related to genetics [166, 259, 186] and environmental factors [247, 147, 158].

2.1.1 CS images

MR images to study CS in this project are from HUBU ('Hjernens Udvikling hos Børn og Unge', Brain maturation in children and adolescents). HUBU is a Danish longitudinal study initiated in 2007. The project is funded by the Danish Council for Independent Research, the Lundbeck Foundation, The Danish Agency for Science, Technology and Innovation, Hvidovre Hospital Research Foundation, and the Faculty of Health Sciences of the University of Copenhagen.
The aim of the HUBU project is to study the maturation of the brain among healthy children and link this to cognitive abilities and social behavioral data. Ninety-four 1st to 6th graders from Køge Municipality, located 40 km southwest of Copenhagen, were initially assigned to the study. Participants should have had no earlier history of trauma or psychiatric conditions. At the time of writing eleven semi-annual rounds have been completed and an overview of age and gender can be found in Table 2.1.

Round	Average age (CI 95 %)	Gender (M/F)	N
1	9.99 (8.36, 11.62)	39/55	94
2	10.56 (8.9, 12.22)	38/55	93
3	11.13 (9.45, 12.81)	26/53	89
4	11.68 (9.99, 13.37)	28/49	77
5	12.09 (10.41, 13.77)	30/48	78
6	12.67 (10.91, 14.43)	28/46	74
7	13.23 (11.56, 14.9)	27/47	74
8	13.72 (12.04, 15.4)	27/46	73
9	14.24 (12.53, 15.95)	27/41	68
10	14.85(13.15, 16.55)	25/38	63
11	16.3 (14.63, 17.97)	15/27	42

Table 2.1: Average age with 95 % Confidence Interval (CI), gender (F=females, M=males) and number of subjects for each round in HUBU.

All children underwent structural 3D MRI and neuropsychological tests, questionnaires assessing personality traits, stressful life events, alcohol use (from age 12), collection of saliva samples, and test of math and reading skills in the first five rounds. In all rounds, subjects had to be excluded due to lack of sufficient image quality and braces or pathological findings.

2.2 Olfactory sulcus

OS is located in the most medial position forming the lateral border of the gyrus rectus (Figure 2.2).

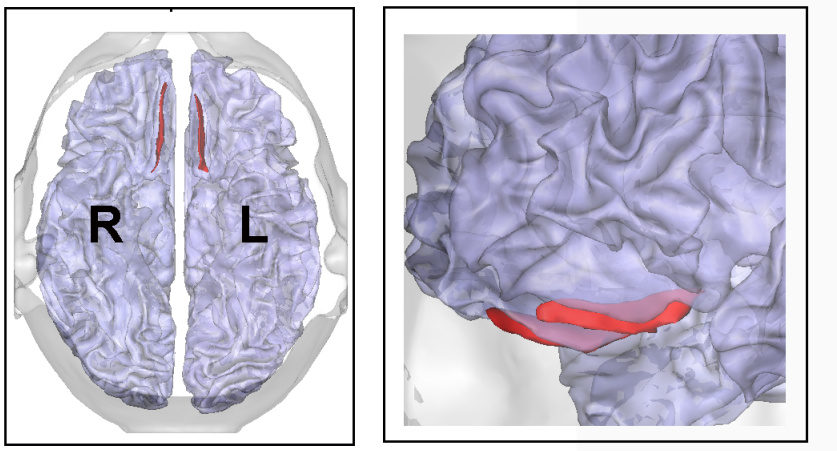

Figure 2.2: OS shown in red axial view (left) and sagittal view (right).

The OS has been related to the ability of smell [84, 66]. Studies have also shown that patients suffering from anosmia have a decreased mean depth and length of OS [288, 123, 157, 124]. These are important findings since olfactory deficits can be secondary to a primary disorder such as Parkinson's disease, Alzheimer's disease [107, 139, 68] and Kallmann syndrome [189].

2.2.1 OS images

MR images to study OS are from a project that aims at establishing a characterization of the phenotype in individuals with congenital anosmia. The project

is funded by the Lundbeck Foundation and the Faroese Research Council. Inclusion criteria were no previous history of psychiatric illness or head trauma. Thirty-seven individuals were recruited and divided into 20 anosmia cases (50.3 years ± 14.8) and 17 controls (47.3 ± 15.64). Participants were included in the anosmia group if they reported lifelong history of impaired olfactory capability. The groups were matched on age, gender, educational level, and cognitive ability measured with the Montreal Cognitive Assessment (MoCA) test.
All participants underwent 3D MRI and a test was performed to determine the ability to process odors by the standardized olfactory Sniffin' Stick test. The test comprises three tasks: odor detection by a threshold-score (1-16 points), odor discrimination in 16 triplets (0-16 points), and odor identification of 16 common odors (0-16 points). Based on the number of correctly answered tasks, these results are combined into a TDI (Threshold-Discrimination-Identification) score, with a maximum score of 48. Anosmia is defined as a TDI-score below 16.5 [148].

Chapter 3

Sulci segmentation

To study the variation in sulci morphology, a segmentation is required. Manual segmentation is the gold standard since it has a high accuracy. However, it is very time consuming and the precision might be low. Automatic segmentation is a non-trivial task due to the structural complexity of the cortex and the inter-subject variability.
This chapter first defines segmentation. Next, local sulci segmentation is described, including manual segmentation of OS (Paper chapter 9)) and automatic segmentation of CS (Paper chapter 8). Finally, global sulci segmentation is described, including registration-based segmentation of CS (Paper chapter 10).

3.1 Image segmentation

Image segmentation partitions a digital image into multiple segments that either cover the entire image or a set of contours. A label is assigned to every voxel in an image, and voxels that share chosen characteristics, share the same label. Frequently used characteristics are color, intensity, or texture.
Two main strategies are used to perform sulci segmentation: registration-based segmentation and a direct segmentation in the space of an individual. A direct

segmentation extracts sulci based on intensities and morphometry [177, 96, 167, 217, 218, 245, 246, 108]. The registration-based approach aligns an image with an atlas and propagates labels from the atlas to the image [21, 67, 155].

3.2 Local sulci segmentation

A local segmentation can extract sulci invariant of orientations and locations. This is an advantage as major variation in both orientation and location is present. The variability in location is seen, for example, in CS, that despite being one of the most stabile folds, can vary in location by up to 2 cm between individuals [261]. A local segmentation of the cerebral sulci can be performed manually, semi-automatically or fully automatically.

3.2.1 Manual segmentation

Manual segmentation is done by tracing an anatomical structure either in each slice or in a 3D volume. Manual sulci segmentation has been performed on sagittal slices [188, 253, 142, 269, 6, 280, 120], on the axial plane [162] and on the lateral brain surface [250, 248], dependent on the sulci of interest. The variability in brain anatomy poses serious challenges for an automatic sulci segmentation and thus manual annotation remains the gold standard.
Manual segmentation can detect individual anatomical differences and is therefore more accurate. The increasing amount of data available challenges this very time-consuming task and restricts the number of subjects and regions to be examined. Expert knowledge is required to precisely locate sulci on the cortex. Often, two experienced neurosurgeons or neuroradiologists must trace the same structure at least once, since the annotator might induce a subjective bias to the segmentation result. All together, manual segmentation is both difficult and time-consuming, but still supplies the most accurate sulci segmentation.

3.2.1.1 Segmenting OS

Manual segmentation is often the only possible solution in individuals with pathological induced structural changes. When a functional ability is trained [239, 127, 66] or lost [251, 58, 38, 1, 123] the corresponding area in the brain is structurally reorganized.

In paper Chapter 9, the OS is manually segmented. This is done since subjects with anosmia are expected to have structural changes in the depth and length compared to healthy individuals [288, 123, 157]. The OS was outlined in continuous 2D slices in the coronal plane on T2-weighted images (Figure 3.2). Two independent raters traced both the left and right OS twice. Adding a surface to

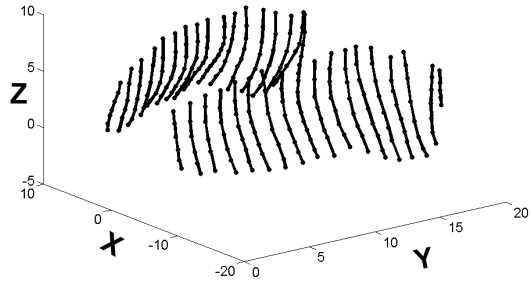

Figure 3.1: Manual segmentation of OS. The raw annotations from each slice are shown in 3D in mm. X=left and right, Y=Backward, Z=up.

the annotated points by a delaunay triangulation, the segmented OS is better visualized (Figure 3.2).

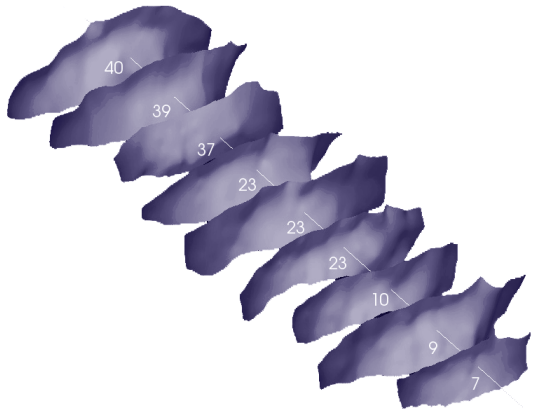

Figure 3.2: The segmented OS shown as a mesh from the annotated points. The number shown on each OS, reflect each individuals ability to smell.

3.2.2 Automatic and semiautomatic segmentation

Automatic sulci segmentation can potentially produce fast and precise results. An automatic segmentation consists of a series of morphological operations to separate the sulci from the remaining tissue. In the case of multiple sulci segmentations within the same individual, a sulci recognition is often also carried out [21, 221].

Two general approaches are used in automatic and semi-automatic segmentation:

- **Edge-based segmentation** is the process of identifying and locating sharp discontinuities in an image. These are found using edge filtering, which classify voxels into edge or non-edge. Voxels that are not separated by an edge are allocated to the same category [241]. Examples of edge-based segmentation methods used to segment a sulcus are zero crossings from a Laplacian of Gaussian [231, 128, 206] and active contours [155, 274, 63].
- **Region-based segmentation** iteratively groups related voxels and splits dissimilar voxels. Examples of region-based segmentation methods used to segment a sulcus are region growing [262, 166, 217, 190], watersheds [217, 219, 287], and Markov random fields [245, 158].

Automatic sulci segmentation is, as mentioned earlier, very challenging because of the high variability in brains. To address the need to segment sulci in order to study their variability, several tools have been developed. PALS (Program for Assisted Labeling) is a user interface that enables labeling of multiple segmented sulcal regions [219]. This labeling is guided by a landmark- and surface-based atlas of the human cerebral cortex [277]. PALS has been used to study abnormalities in sulci patterns in patients suffering from schizophrenia [58]. CRUISE (Cortical Reconstruction Using Implicit Surface Evolution) performs an automatic sulci segmentation using fuzzy tissue classification and topological information to find the interface of the gray matter and white matter [272]. CRUISE has been used to study the effect of aging on the sulcus shape [218]. Lastly, BrainVisa, one the most used tools in the sulci literature [178], segments and labels multiple sulci. BrainVisa has been used to describe the normal variability in sulci [200, 197, 150, 260, 256], define landmarks [118, 53], study the effects of alcohol consumption during pregnancy [64], and the effect of neurologic disorders on sulci morphology [213, 135, 161].
The above tools are used by the majority of groups working with sulci [118, 197, 112, 158, 102, 186, 256, 258], and only a few use their own methods

[167, 218, 245, 246, 108]. An advantage of this trend is that results become more comparable between studies.

3.2.2.1 Segmentation of CS

In this project, BrainVisa has been used to segment CS (Paper Chapter 8). BrainVisa performs a very advanced segmentation and has been shown to be able to model 96 % of the sulci variability in 21 brains [178]. The first prototype of BrainVisa was developed in 2000 and new versions have been added since, with the latest being in 2013.
The following describes the steps in BrainVisa to segment a sulci. Firstly, T1-weighted MR images are corrected for spatial inhomogeneities induced by weaknesses in the acquisition [180]. The brain is then segmented by the intensity distribution using a scale-space-based approach [177]. The image is next binarized using a Markovian regularization relying on the Ising model. The binary image is eroded and this result is used as a seed to reconstruct the brain shape by a dilation [177]. A second sequence of erosion and dilatation is used to split the brain mask into the two hemispheres and the cerebellum. The erosion process is guided by an affine normalization to a white matter mask. A segmentation of the gray matter and white matter interface is found and skeletonized by another erosion. Intensities are used to define the localization of the skeleton. Surface points are gathered into topologically simple surfaces without junctions. Each simple surface is modeled by its relations to the topological junctions, split induced by a buried gyrus and neighbor geodesic to the brain hull [179]. Finally, a probabilistic atlas labels these simple surfaces to automatically identify approximately 60 sulcal labels per hemisphere [206]. A sulcus is represented as the medial surfaces of two opposing gyral banks that span from the white matter/gray matter border, at the most internal point, to the envelope of the brain surface [178].
An example of the result of an automatic segmentation of CS using BrainVisa in this project (Paper chapter 8) can be seen in Figure 3.3. A pipeline of how to segment CS from the raw MR images in BrainVisa can be found in Appendix A.

3.3 Global sulci segmentation

The most common approach to segment sulci is registration-based segmentation [49, 185, 269, 268, 274, 155, 231, 48, 14, 263, 77, 206]. Registration-based segmentation models a priori information, such as the shape, features, or relative

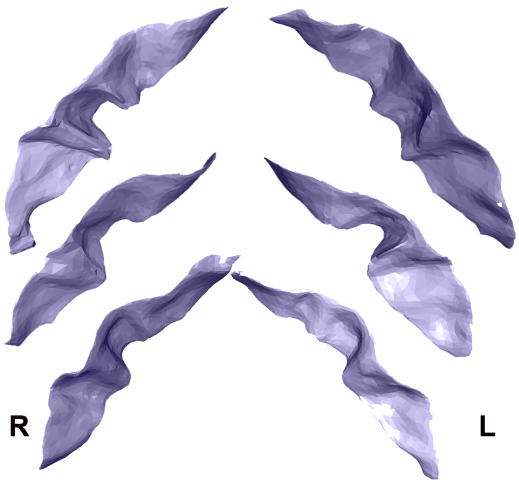

Figure 3.3: Automatic segmentation of left and right CS using BrainVisa.

positions, into an atlas. This atlas is warped to a new image and the labels from the atlas are propagated on to the new image [39]. Registration methods are described in detail in Chapter 4.
Registration-based segmentation can apply knowledge to multiple images. The challenge is, however, to align whole brain images from all individuals in a common atlas space. Even the advanced non-linear warping techniques are thought to be insufficient to account for the variations in the cortical anatomy between individuals [177, 48, 167, 40, 144]. The variation within subjects are, however, much more limited and could provide meaningful alignments.

Constructing an atlas
To perform registration-based segmentation, an atlas has to be constructed to hold the labels to be propagated to the new image. The most simple atlas is based on a single labeled volume, such as the Visual Human Project [273]. A determistic atlas cannot represent the variability of the cortex. However, this might be possible using a probabilistic atlas that models a priori knowledge of structural and spatial information from a large sample [185, 154, 184]. By incorporating new images, these atlases can be ever improved -an example is the widely used Internet Brain Segmentation Repository (IBSR) [183]. Several publicly available atlases have been created with manual segmentations, performed by expert radiologists, to benefit the research community.

A probabilistic atlas can be density-based, label-based, or deformation-based

depending on the features used to generate it:

- A **density-based atlas** is an average representation based on intensities. All images are linearly transformed into a stereotaxic space, normalized with respect to intensities, averaged on a voxel-by-voxel basis and, finally, smoothed. Density-based atlases have been used to study the cortical sulci [74].
- A **label-based atlas** is constructed by manually labeling parts of the brain. Images are first mapped into a stereotaxic space. A probability map is then constructed for each segmented part by determining the proportion of subjects assigned a given anatomic label at each voxel position. Label-based atlases have been used to segment sulci in several studies [185, 271, 269, 268].
- A **deformation-based atlas** is constructed by storing a 3D map that represents the amount of deformation required to deform an atlas template into the shape of a brain. This approach has been used in several studies to segment sulci [269, 268, 11, 62]. Active shape models [51] and active appearance models [50] are also within this category since they bring spatial prior knowledge to the segmentation process. These approaches have been used with success to segment sulci [264, 96, 217].

Warping of atlas
A 3D warping algorithm deforms the atlas to match the image to be segmented [74, 224, 270]. This warp can be affine, which includes translation, rotation, scaling, and shearing, or non-rigid to allow for local elastic deformations.
The warping of an atlas is often done in two steps. Firstly, by a global affine registration to perform an initial alignment. This is followed by a local registration that adapts to the local anatomy by non-rigid registration [114, 39]. Affine transformations are usually enough when dealing with intra-subject matching in healthy adults. However, inter-subject registration can only be achieved using non-rigid registration.

3.3.1 Registration-based segmentation of CS

In this project, we used registration-based segmentation to extract CS from longitudinal MR images. One CS was segmented for each subject using BrainVisa. This segmented CS served as a template. The within-subject registration was done using DARTEL (Diffeomorphic Anatomical Registration using Exponentiated Lie algebra) (Paper chapter 8).

A study by Klein et al. (2009) compared 14 registration algorithms. No ground truth exists for a registration, so the registration was compared using eight measures regarding overlap and distances. Among these registration algorithms, DARTEL was in the top five, with results showing only minor effects on the registration between subjects [144].
DARTEL performs non-rigid inter-subject alignment, with six millions parameters, that allows enough degrees of freedom to achieve a very precise inter-subject alignment [136]. DARTEL is an iterative procedure aligning gray and white matter tissue maps. A flow field is created for each subject which encodes how individual images should be warped. The algorithm iteratively computes average templates of the tissue maps and updates the flow fields. As the images become better aligned, the average tissue map becomes sharper. A clear advantage of DARTEL is that no predefined template or stereotactic space is needed [12].
In this project, the segmentation results of CS from longitudinal MR images, based on within-subject registration using DARTEL, can be seen as one example in Figure 3.4 (Paper Chapter 10).

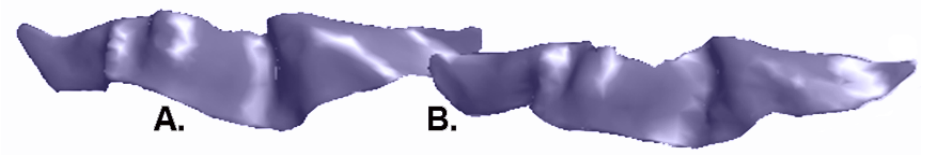

Figure 3.4: An example of the results from a registration-based segmentation of CS from longitudinal MR images. An atlas is created for each subject based on an automatic segmentation. A) Segmentation from BrainVisa. B) Registration-based segmentation of the same image.

Chapter 4

Sulci registration

To quantify the biological variability of sulci morphology beyond a feature representation, an alignment of the structural anatomy between subject is required [152]. This chapter first defines image registration and introduces intensity-based and feature-based registration. Both intensity-based registration and feature-based registration can be used to align the entire brain and thereby all sulci [49, 48], and to establish a one-to-one correspondence between segmented sulci. Next, local registration to align segmented sulci or sulci representations (Paper Chapter 10 and 9) is described. Finally, global registration of the whole brain is briefly mentioned.

4.1 Image registration

Image registration bring images into spatial alignment by a geometrical transformation. A registration aims at establishing a one-to-one mapping between the coordinates in one space and those in another [176, 78].
In image registration, the target, the new image, is spatially transformed to align with a stationary reference image. The goal is to find a transformation that maps the target image to match the reference image [176]. Image registration involves two steps:

1. An estimation of a set of parameters describing the mapping from each voxel's position in a reference image to a corresponding position in the target image. Such a mapping can be based on intensity patterns or image features such as points, lines, or contours [176].
2. A geometrical transformation re-samples the target image at new positions based on the estimated correspondences from the previous step. This new representation of the target image is established with a point-by-point correspondence to the reference images. During the registration, a regularization term secures that only reasonable transformations are obtained [152]. A transformation can be linear and include rotation, scaling, translation, and other affine transforms, or non-linear to conduct irreversible large-deformation warps [78].

A similarity measure quantifies the alignment of the transformed target image to the reference image. An optimization algorithm maximizes the similarity. This process is repeated until some matching criterion is met [78].

4.1.1 Intensity-based registration

Intensity-based registration estimates the transformation between two images using the voxel values of either an entire images or subparts of an image. Preprocessing ensures comparable intensities. An advantage of this registration approach is that no user-interaction is required to define landmarks.

4.1.2 Feature-based registration

Feature-based registration establishes the correspondence between landmarks, lines, or contours [176].

Landmarks
Landmarks are defined as pairs of unique points with correspondence between subjects. Landmarks are aligned in the transformation step and interpolate the mapping of the other points in an image or on a surface. Landmarks can be divided into three groups:

- **Anatomical landmarks** are biologically meaningful and have a correspondence between subjects. Examples of anatomical landmarks are the anterior commissure [194] and the pli de passage fronto-pariétal moyen (PPFM) in CS [4].

- **Mathematical landmarks** are located in the same mathematical or geometrical location between subjects. An example of a mathematical landmark is the deepest point in the hand knob in CS [54].
- **Pseudo-landmarks** are constructed points that are located between other landmarks.

Lines and contours
When a feature-based registration is performed for curved objects, the landmarks can often be aligned exactly; however, the mapping of the other points can vary depending on the used transformation. To overcome this problem, the transformation can be based on the deformation between two sulci shapes using continuous differentiable functions, such as interpolating polynomials, polynomial splines, and thin-plate splines (TPS) [78]. Corresponding landmarks on a sulci are matched first. A displacement is calculated between these sets of corresponding landmarks to estimate the displacement from one sulcus (x, y, z) to another $(x + dx, y + dy, z + dx)$. Based on this displacement, three smooth interpolation surfaces can be estimated -one for each direction of displacement (dx, dy, dz). These surfaces hold the displacement to deform sulci to match each other at every vertex.

4.2 Local sulci registration

A local registration aligns segmented sulci or sulci representations. An advantage of this method is that the registration only aligns the features of interest and bias from the variation between brains is removed. The segmented sulci are typically represented by a binary image or a mesh, hence the choice of registration has to be based on features since no intensities are present.

4.2.1 Aligning OS in healthy and patients with anosmia

A point-wise registration of sulci in healthy individuals and individuals with pathological conditions is typically not a valid option, since an actual correspondence is non-existing [267, 287].

In this project, we aligned the OS for healthy individuals and patients suffering from anosmia with respect to the lack of depth and length in the individuals with anosmia [123] (Paper Chapter10). The following steps were taken. All OS had their first position at the posterior extension. OS lengths were scaled with

respect to the length from the anterior commissure to the intersection with the skull. Furthermore, all OS depths were scaled with respect to the height from AC to the intersection of the skull in a line perpendicular to the length.

4.2.1.1 Aligning the shape of CS

A point-wise correspondence of the segmented sulci can describe the variability in shape and positional movement. In this project, we aligned segmented CS using a Thin Plate Spine (TPS) to obtain a smooth interpolation of the deformation between landmarks [69] (Paper chapter 10).

The basic idea of TPS is to model the behavior of infinitely thin metal plates forced through 3D points. The metal plates will naturally resist bending, as will the TPS subjected to a penalty against bending. The bending energy J is a function of the curvature of f:

$$J(f) = \iiint \left(\frac{\partial^2 f}{\partial x_1^2}\right)^2 + \left(\frac{\partial^2 f}{\partial x_2^2}\right)^2 + \left(\frac{\partial^2 f}{\partial x_3^2}\right)^2 + 2\left(\frac{\partial^2 f}{\partial x_1 x_2}\right)^2 + 2\left(\frac{\partial^2 f}{\partial x_1 x_3}\right)^2 + 2\left(\frac{\partial^2 f}{\partial x_2 x_3}\right)^2 dx_1 dx_2 dx_3. \quad (4.1)$$

With $\bar{\boldsymbol{x}}_i, \bar{\boldsymbol{y}}_i$, $i = 1, ..., N$, and $\bar{\boldsymbol{x}}_i$ as the target shape and $\bar{\boldsymbol{y}}_i$ as the reference. This bending is used to determine the weights w of the mapping between the two sulci by minimizing the sum of squared distances:

$$f(\bar{\boldsymbol{x}}, \bar{\boldsymbol{y}}, \lambda) = \arg\min_{w} \sum_{i=1}^{N} \|T(\bar{\boldsymbol{x}}; \bar{\boldsymbol{w}}) - \bar{\boldsymbol{y}}_i\|^2 + \lambda J(f) \quad (4.2)$$

λ controls the degree of smoothing. A λ that equals zero produces an interpolation, and higher values of λ produce more smooth surface until it approaches a plane.

The minimization of f in 4.2 can be expressed as:

$$f(x) = \beta_0^k + (\beta_1^k)^T x + \sum_{i=1}^{N} \alpha_i^k \eta_3(||x - x_i||), \quad (4.3)$$

With $\eta_3(r) = \|r\|^3$ and r being the distances between points in the two sulci. This can be written into matrix notation of a linear system to find $\bar{\boldsymbol{\alpha}}$ and $\bar{\boldsymbol{\beta}}$.

$$\begin{bmatrix} \boldsymbol{K} + \lambda \boldsymbol{I} & \boldsymbol{P}^T \\ \boldsymbol{P} & \boldsymbol{0} \end{bmatrix} \begin{bmatrix} \bar{\boldsymbol{\alpha}} \\ \bar{\boldsymbol{\beta}} \end{bmatrix} = \begin{bmatrix} \boldsymbol{y} \\ \boldsymbol{0} \end{bmatrix} \tag{4.4}$$

with $\bar{\boldsymbol{y}} = [\bar{\boldsymbol{y}}_1, ..., \bar{\boldsymbol{y}}_N]^T$, $\bar{\boldsymbol{\alpha}} = [\alpha_1, ..., \alpha_N]^T$ and $\bar{\boldsymbol{\beta}} = [\beta_0; \beta_1]$, $\boldsymbol{K_{ij}} = \eta_3(||\bar{\boldsymbol{x}}_i - \bar{\boldsymbol{x}}_j||)$ and $\boldsymbol{P} = \begin{bmatrix} 1 & ... & 1 \\ \bar{\boldsymbol{x}}_{\boldsymbol{1}} & ... & \bar{\boldsymbol{x}}_{\boldsymbol{N}} \end{bmatrix}$.

In this project, we performed TPS registration in a program called Landmarker by Darvann et al. (2008) [61] (Paper chapter 10). This program supplies user-friendly annotations and registrations.

4.3 Global sulci registration

Mapping of the whole brain was introduced within subjects to locate activation in Positron Emission Tomography (PET) images with bad resolution [81]. This has led to many approaches using sulci in both landmark-based registration [46, 40, 264, 167, 47] and feature-based registration [47, 277, 269, 266, 265, 272, 77, 134, 170]. A problem in whole brain registration is that many features or landmarks are not represented in all brains [47, 134]. This especially gives rise to problems relating to sulci morphology, since the cortex is subjected to very large variability [199].

Chapter 5

Representation of sulcal morphology

Sulci morphology is the study of the geometrical information that remains after filtering out scale, location, and rotation. Sulci morphology has been widely studied and the representation of the anatomy has spawned many features. One representation, the sulcal depth position profile, has almost become a gold standard. This chapter describes the representation of sulci by features and by shape.

5.1 Feature-based representation

The high inter-subject variability might challenge a reasonable alignment of the whole brain and hence sulci. Instead features are often used in the majority of studies within sulcal morphology. Features are distinctive characteristics independent of rotation and location.

Gyrification
Gyrification has been shown to be associated with higher cognitive abilities [169]. A local gyrification quantifies the amount of cortex buried within the

sulcal folds compared to the amount of cortex on the outer cortex. A local gyrification index has been used to quantify age-related changes in sulci [218].

Surface area
The area of a sulcus is another widely used feature [80, 282, 15, 218, 149, 160, 162, 161]. The surface area of a sulcus can be represented by either the medial sheet or the areas on either side of the banks [162]. The medial sheet provides a balanced representation of a sulcus and the associated gyri [277, 275, 172]. The banks reflect specific functional areas, such as the motor cortex in the anterior banks of the CS.

Top and bottom length
The patterns of cerebral gyrification can be represented by the lengths of primary sulci [130, 131]. Two of the more recent features in the literature are the sulcus top and bottom length [160, 162, 161, 256] and an average of the two [80, 149, 186, 161].

GM volume
The cortex holds the neurons and glia cells, and hence the GM volume surrounding a sulcus is a direct measure of local cortical functionality. Common cortex features related to sulcal morphology are GM volume [218], cortical thickness [282, 129], and average cortical thickness [218, 161]. The surface area and the cortical thickness define the GM volume. The surface area and the cortical thickness seem to be genetically independent [202, 117] and are affected differently during maturation [282].

Sulcal width
To quantify the local GM atrophy, the sulcal width is a good indicator [150, 164, 162, 161] as well as the average width [150, 129, 164, 162, 256, 161]. Greater width reflects a decrease in the overall brain size and vasculature in the brain [59]. Furthermore, this feature is thought to be associated with a decrease in white matter and subcortical volumes in normal aging [165].

Distance to interhemispheric fissures
The distance from the interhemispheric fissures to a sulcus can provide information about alternations in maturations [133, 256]. Despite the great variability in the cortical folding, the organization of the deep structures are rather stable [199, 282], and hence large deviations might reflect pathological conditions [133, 256].

Depth profile
Age-related atrophy of the WM and GM volume result in less sharp gyri and more open sulci. This lower the distance from a top of a gyri to the inner most part of a sulcus. This depth is often measured along the entire sulcus and is

called the sulcal depth profile or depth-position profiles [6, 60]. Depth profiles provide a measure of the true cortical depth, as they take into account the twisting nature of the sulcus [283].
The depth profile parameterizes sulci to create a normalized coordinate system on its surface. One hundred successive depths are calculated along the entire sulcal contour (Figure 5.1). This uniform parameterization of sulci provide a good inter-subject matching [60].

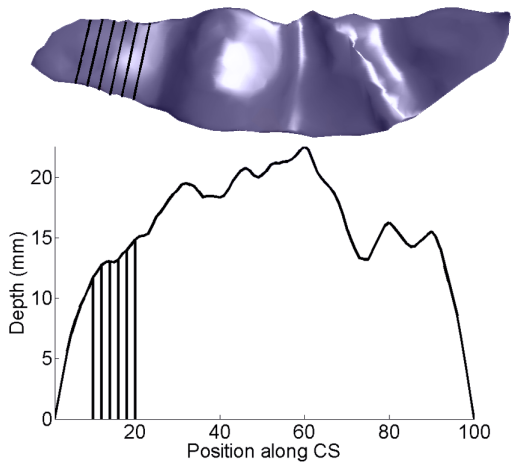

Figure 5.1: Representation of the sulcal morphology by the sulcus depth profile. The depth is calculated at 100 points along the sulcus.

Sulcal depth profiles have been used to identify landmarks as PPFM [60] and the hand knob in CS [54]. Furthermore, it has been used to describe the shape variability in CS [263, 63, 118] and its relation to genetics [186], gender [60, 256], handedness [6, 5], age [60], and pathology [161]. The depth profile is often used to calculate an average depth [123, 15, 150, 161, 129, 149, 186, 256, 161] or a maximum depth [15, 161].

The depth profile can be derived in several ways. The very simplest is found by manually tracing 2D slices [6, 280]. Another alternative combines manually tracing of the points along the top ridge, with a cost function, that firstly favor short depths to the bottom ridge and secondly favor points on a plane perpendicular to the long axis of the sulcus [63]. Coulon et al. (2006) generated an observer-independent depth profile that extrapolated a coordinate field over the entire surface by solving the heat equation on the surface. The top ridge, bottom ridge, and the two endpoints behaved as constant heat sources [52, 60]. McKay et al. (2013) presented an automatic method that connected 100 equivalently spaced points on the top and bottom ridge by a geodesic line [186].

Sulcal profile
An extension of the sulcal depth profile is the sulcal profile. The sulcal profile has been used to locate the hand motor area in CS [53] and to investigate the morphology between children diagnosed with attention deficit and hyperactivity (ADHD) and healthy controls [161]. This sulcal profile quantifies the variability in the curvature along the sulcus [53]. The sulcal profile measures the average deviation in 100 positions along the sulci to the plane of main orientation of the sulcus.

Calculating sulci profile
A sulcus can be represented as $S = \{X_i, Y_i, Z_i\}$, with $i = 1, ..., N$ and N being the number of vertices. The eigenvectors (P) and eigenvalues (Λ) of the covariance matrix $\Sigma = (N-1)^{-1} \sum_{i=1}^{N} (S_i - \overline{S})(S_i - \overline{S})$ can be found by $\Sigma P = \Lambda P$. The first two eigenvectors, p_1 and p_2, associated with the maximum eigenvalues yields the orientation of the plane. The third eigenvector, p_3, is the unit normal vector. The distance between a point on the sulcus and the plane of main direction is calculated as: $D_i = p_3 \cdot (S_i - \overline{S})$.

5.2 Shape-based representation

A feature-based representation uses only part of the information given in a 3D shape. To obtain a quantitative description of the overall shape variability, a feature extraction can transforms data from a high-dimensional space to a space of fewer dimensions. A sulci must then be described by a finite number of landmarks, that has correspondence between and within populations. The data transformation may be linear as in a Principal Component Analysis (PCA) or non-linear as in a ISOMAP.

Principal Component Analysis
PCA has been used to quantify the difference between shapes in CS in relation to genetics [95]. PCA seeks to reduce the dimensionality of the data by finding new orthogonal linear combinations of the original variables. shape correspondence is needed. If we again let a sulcus be represented by $S = \{X_i, Y_i, Z_i\}$, with $i = 1, ..., N$, and N being the number of vertices, and the covariance matrix $\Sigma = (N-1)^{-1} \sum_{i=1}^{N} (S_i - \overline{S})(S_i - \overline{S})$. PCA seeks to find a linear combination, $Y = P'S$, that maximizes the variance $D(Y) = D(P'S) = P'\Lambda P = \Lambda$. This yields the eigenvalue problem $SP = \Lambda P$, with the associated eigenvalues arranged in descending order: $\Lambda = diag\{\lambda_1, ..., \lambda_N\}$ and principal vector $P = [p_1, ..., p_N]$. The first principal component is the linear projection of $Y_1 = p_1' S$ that maximizes the variance in data. The second principal component maximizes the variance orthogonal to the first. These orthogonal components

are uncorrelated.

Manifold learning
The sulcal shape is not always well described by a linear projection as PCA. Non-linear techniques such as manifolds have also been used to describe the location of the hand knob [260] and functional variability in hand movement and silent reading [258]. An isomap is a multidimensional scaling technique that finds average quadratic distance between pairs of sulci in 3D. These distances are gathered in a high dimensional similarity matrix of the inter-individual shape variability. Manifold learning can represent this similarity in a non-linear structure to obtain a more compact representation of the inter-individual shape variability.

Chapter 6

Statistics

Statistical methods can relate sulci shape to demographic variables. This chapter describes the General Linear Model (GLM) that enables the influence of covariates in modeling the sulcal shape (PFaper Chapter 8 and 9). Covariates are not of primary interest, but potentially influence the response. An example of a covariate is the total brain volume, which affects the size of a sulcus. Repeated measurements on the same subject violate the standard independency assumption of the dependent variable. These correlation have to be modeled, which can be achieved in mixed model (paper Chapter 10). Finally, Factor Analysis (FA) is described since it can transform correlated sulci depths into uncorrelated interpretable subparts (Paper Chapter 8 and 9). The advantage of FA compared to PCA, which also performs an orthogonal transformation, is that PCA is driven by the variation in data and the resultant transformation is hard to interpret. FA has the advantage that it models an underlying causal relationship [143], which is in line with the topological organization of sulci. The depths along a sulcus can be tested independently, which introduces a multiple comparisons problem. In multiple comparisons, we risk to falsely reject the null hypothesis. This can be corrected, for example, by the false discovery rate [71].

6.1 General linear model

GLM predicts the dependent variable from one or more independent variables, and is often used in cross sectional studies of the sulcal shape [54, 286, 145, 119]. The dependent variable (Y) for any given observation is the sum of the intercept, the sum of the weighted independent variables, and the error [143]:

$$Y = \alpha + \beta_1 X_1 + \beta_2 X_2 + ... + \beta_n X_n + \epsilon \tag{6.1}$$

Y: Dependent variable.
α: Intercept
X_i: Independent variable
β_i: A series of n weights for each independent variable
ϵ: Prediction error or residual

The predicted value of the dependent variable is thus:

$$\hat{Y} = \alpha + \beta_1 X_1 + \beta_2 X_2 + ... + \beta_n X_n, i = 1...n, \tag{6.2}$$

From equation 6.1 and 6.2 the residual (ϵ) is just $Y - \hat{Y}$. The most frequently used criterion to estimate the GLM parameters is the least squares criterion, which minimizes the sum of the squared differences between observed and predicted values $\sum_{i=1}^{n}(Y_i - \hat{Y}_i)^2 = \sum_{i=1}^{n} \epsilon_i^2$. Writing it into matrix notation yields: $Y = X\beta + \epsilon$, with the solution for the estimation of β: $\hat{\beta} = (X'X)^{-1}X'Y$ [143]. The errors are assumed to be independent and follow normal distribution with zero mean and constant variance, $\epsilon \sim N(0, \sigma^2)$.

6.2 Mixed models

The large amount of between-subject variation, especially in the cortex, reduces the sensitivity in cross-sectional studies. Longitudinal studies have been used to study age-related changes in the brain [159, 218, 218, 248]. A longitudinal study involves repeated observations of the same variables in the same subjects at more than one point in time [22]. Observed variation in a longitudinal study is, hence, related to changes within subjects, which makes the results more accurate [215, 236, 75, 196]. Longitudinal studies require large amounts of time, are expensive, and participants might drop out [22].

In longitudinal studies, the observations within subjects are correlated, which means the residuals are also correlated. This correlation in the residuals can be modeled in a general mixed model by modeling the covariation structure imposed upon the residuals. [103]
A mixed model contains both fixed and random effects. Fixed effects hold explanatory variables and random effects hold the variables for which the model is to be adjusted:

$$Y = X\beta + Z\gamma + \varepsilon \tag{6.3}$$

Y: Dependent variable
X: Design matrix of the independent variables related to fixed effects
β: Fixed-effects regression coefficients
Z: Design matrix for the random effects
γ: Random effects regression coefficients, $\gamma \sim N(0, G)$.
ϵ: Residuals, $\epsilon \sim N(0, R)$,

Generalized least squares is used to estimate β, γ and R in order to minimize: $(y - X\beta)'V^{-1}(y - X\beta)$. V is the variance of Y given by $V = ZGZ' + R$. V can be modeled by setting up the random-effects design matrix Z and by specifying the covariance structures for G and R. In repeated measured with no nesting of the data, the Z matrix contains dummy variables.

Modeling the error covariance
The error covariance structure, R, holds the correlation in errors between observations from the same subject. If, for example, the variance is homogeneous in time, the diagonal will hold σ^2. Measurements on the same subject made close together in time are often more correlated than measures made further apart. An irregular time interval is often seen between measurements, which can be modeled by a spatial power covariance function imposed upon the residuals [103]. This is a continuous-time model taking into account the irregular time intervals and the decline in correlations over time:

$$D(\epsilon_{ij}, \epsilon_{i'j}) = \sigma^2 \rho^{di'j} \tag{6.4}$$

$D(\epsilon_{ij}, \epsilon_{i'j})$ is the covariance matrix of the errors ϵ between time i and time i' for subject j, σ^2 is the variances of the errors and $\rho^{di'i}$ is the correlation of the errors measured at distance, d, between the time i and the next i'.

6.3 Factor analysis

Factor analysis includes a factor extraction followed by factor rotation that prompts the interpretation of the transformed data [143].
If we have an observation $X = [X_1 ... X_K]'$, e.g. the depths along a sulcus from one subject. These depths can be modeled as to how they depend on some underlying factors:

$$X = AF + G \tag{6.5}$$

F: A vector of factor scores
A: Factor loadings, which give weights to single factors. This is the correlation between an observation (X) and a factor score (F).
G: Unique factors, which are errors or special for a specific depths. $D(F, G) = 0$.

With k observations, in m subjects and n models, this yields:

$$\begin{bmatrix} X_{11} & \cdots & X_{k1} \\ \vdots & & \vdots \\ X_{1n} & \cdots & X_{kn} \end{bmatrix} = \begin{bmatrix} a_{11} & \cdots & a_{1n} \\ \vdots & & \vdots \\ a_{k1} & \cdots & a_{kn} \end{bmatrix} \begin{bmatrix} F_{11} & \cdots & F_{1n} \\ \vdots & & \vdots \\ F_{m1} & \cdots & F_{mn} \end{bmatrix} + \begin{bmatrix} G_{11} & \cdots & G_{1n} \\ \vdots & & \vdots \\ G_{k1} & \cdots & G_{kn} \end{bmatrix}$$

Extraction of factors
The factor loadings, A, can be found by the principal factor solution $AA' = (P\Lambda^{1/2})(P\Lambda^{1/2})'$, with P being the eigenvectors and Λ the eigenvalues.
The variability in each observation (X), explained by the m common factors (A), can be found by $h_j^2 = a_{j1} + ... + a_{jm}$ with $j = 1, ...k$. h_j^2 is called communalities and expresses the amount of variability in each subject explained by the model [143]. The factor loadings can be estimated by, for example, principal components, maximum likelihood, generalized least squares, and unweighted least squares [143].

Rotation of factors
To prompt the interpretation of the factor loadings, a FA also encompasses a rotation to assign factor loading to load primarily to one factor score [143]. The rotation can be done by, for example, varimax, quartimax, parsimax, and equamax. The factor loadings are uncorrelated after factor extraction. To retain these orthogonal factor loadings an orthogonal rotation is often preferred using

the varimax rotation [137]. A varimax rotation maximize:

$$\sum_{j=1}^{m} \left\{ \sum_{i=1}^{k} \left(\frac{a_{ij}^2}{h_i^2} \right)^2 - \frac{1}{m} \left[\sum_{i=1}^{k} \left(\frac{a_{ij}^2}{h_i^2} \right) \right]^2 \right\} \tag{6.6}$$

This maximization prompts a lot of the a_{ij}'s to become close to 0 and others to become close to -1 or 1. This makes the loadings much easier to interpret. [143]

Chapter 7

Discussion and conclusion

This thesis has addressed the variation in the folding of the cerebral cortex which, despite numerous studies, is largely unknown. The cerebral folding can be described by the sulcal shape, since the shape of cortical sulci and gyri are determined in part by forces exerted by white matter fiber connections.
The objective of this thesis was to study sulcal morphology using MR images and techniques within spatial statistics to investigate:

1) The normal development of central sulcus

2) The influence of functional lateralization on the motor hand area of central sulcus

3) The influence of a pathological condition, anosmia, on the morphology of olfactory sulcus

These objectives were addressed in the scientific contributions in Chapter 8 to 10. The methods used in these contributions were described in greater detail in Chapter 1 to 6. The results found in the contributions are first summarized. This is followed by a discussion of the used methods.

7.1 Summary of methods and results

1) The normal development of central sulcus
Gyrification decreases in childhood and adolescence; however, relatively little is still known about the local development in the folding of the cortical surface.
Methods: Sulci maturation was studied in a longitudinal study of CS. Longitudinal studies reduce the sensitivity caused by the large subject variation. The CS was automatically segmented in one round for each subject. These segmented sulci were used in a registration-based segmentation, using DARTEL to align images within subjects. The shape of CS was represented by the surface area, the depth, and the positional movements. The longitudinal data were modeled and tested using mixed models. Sulci were aligned with TPS to obtain a point-wise correspondence between subjects. Eight landmarks for each subject were automatically calculated based on the curvature along CS.
Results: This study showed significantly reduced left surface area of CS over time, especially in females. These results are in line with cross-sectional studies; however, our results suggest that the overall maturation might locally both increase and decrease.

2) The influence of functional lateralization on the motor hand area of central sulcus
To understand how specific functions and abilities affect the sulcal shape, the ability to use the hands are related to the motor hand area in the CS.
Methods: The CS was automatically segmented in both hemispheres. The surface area and depth profile represented the shape of CS. The subject's ability to draw superimposed circles in a regular fashion was measured to obtain a right-left asymmetry in dexterity. An asymmetry index was calculated for the dexterity measure, the area, and each depth. The depths were modeled into causal subareas of the CS using factor analysis. Statistical tests were performed using GLM.
Results: Handedness has been mapped to the motor hand area before, but here we show that higher manual proficiency is associated with increased cortical folding, resulting in a deeper sulcus in the dominating hemisphere.

3) The influence of a pathological condition, anosmia, on the morphology of olfactory sulcus
To understand how the sulcal shape is affected in patients with a pathological condition, we studied how the subareas along OS are affected by the atrophy of the olfactory bulb.
Methods: The OS and olfactory bulb were manually segmented. The traced points were gathered into a sulci mesh. The sulci shapes were represented by the area and depth position profile. The sulci were aligned using a method that respected the lack of depth and length in individuals with anosmia. The depths

were modeled using factor analysis and statistical tests were performed using GLM.
Results: The depth of OS in individuals with anosmia has been shown to be reduced in other studies, but this study finds that the atrophy of the olfactory bulb results in reduced depth in the bilateral OS. This reduction is most prominent in posterior and middle subareas of the OS.

7.2 Discussion of methods and results

To answer the objectives, sulci morphology has been studied using high quality MR images of the brain, sulci segmentation, sulci alignment, and sulci shape representation.

7.2.1 Sulci segmentation

Two main strategies can be pursued to segment sulci: direct segmentation and registration-based segmentation. In this project, we used both by performing manual segmentation, automatic segmentation, and a registration-based segmentation. All three methods yielded nice segmentations. Manual tracing is necessary to segment small sulci like the OS, especially in patients with pathological diseases. Manual tracing remains the gold standard to produce accurate segmentation, but stable sulci, such as the CS, can with success be segmented using an automatic algorithm. Automatic algorithms are used by the majority of groups working with sulci morphology [118, 197, 112, 158, 102, 186, 256, 258] and only few use their own methods [167, 218, 245, 246, 108]. An advantage of this trend is that results become more comparable between studies.

7.2.2 Sulci registration

In the sulcal literature, registration is mainly performed by aligning the sulcal depths in a depths-position profile. In this project, we aligned sulci with a depth position profile, with a feature-based registration (TPS), and by a global registration in DARTEL in order to segment sulci. The variation within subjects provides meaningful registrations, as these images are almost alike. Global registration has been widely used to align the whole brain, which generally aligns the brain very nicely between subjects [144]; however, the variability between brains might mean that no meaningful correspondence exists. This problem

might also apply to the local registration of the shape of CS and in the depth profiles. This question if or how brains can be compared in general.

7.2.3 Sulci representation

The sulci shape can be represented by sulci metrics or by the overall shape. In this project, we have used the surface area and the sulcal depth. These features are the most frequently used in the literature and provide general information about sulci. In the future, these metrics could be combined with local gray matter thickness to address the amount of neuron cell bodies surrounding a sulcus. Furthermore, the two banks in sulci could provide more accurate information in the mapping of a functionality, for example, by mapping a functional measure of the hands to the banks on frontal lobe in the CS.

7.2.4 Future sulci morphology studies

Future studies of the sulci morphology could include 7 T MR imaging. Given the size of the brain and the magnitude of the within subject changes over time, the measurable changes are expected to be small within a year or two. This might challenge the resolution of 1.5 T or 3 T images. The 7 tesla MRI techniques might meet the demands to map sulci changes on a finer time scale in relation to the positional movements in the brain. [291]
Sulcal morphology studies could in the future combine several modalities, such as DTI with fMRI or MRI with TMS, to combine functional and structural studies.

The ultimate goal is to understand the brain's variability both in healthy individuals and patients suffering from brain disorders. This thesis has addressed sulcal variability in relation to maturation, functionality, and pathological conditions. Hopefully, this thesis has made a small contribution to the understanding of the large variability in the brain.

Part II

Contributions

Chapter 8

Right-left asymmetry in depth of central sulcus predicts right-left asymmetry in manual dexterity: a structural MRI study of right-handed children and adolescents

Betina Vase Jensen[1,2], William F.C. Baaré[1], Kathrine Skak Madsen[1], Steffen Angstmann[1], Rasmus Larsen[2], Hartwig Roman Siebner[1,3*]

[1] Danish Research Centre for Magnetic Resonance, Centre for Functional and Diagnostic Imaging and Research, Copenhagen University Hospital Hvidovre, Denmark
[2]DTU Compute, Technical University of Denmark - DTU, Kgs. Lyngby, Denmark

[3]Department of Neurology, Copenhagen University Hospital Bispebjerg, Copenhagen, Denmark

Abstract

Handedness, the preferred use of one hand for manual dexterity tasks, is associated with right-left asymmetries in the surface area and depth of the central sulcus with the dominant hemisphere showing a larger surface area and depth. It is less clear how right-left differences in manual dexterity are reflected in right-left asymmetries in the depth and surface area of the central sulcus. This study was designed to examine the relationship between the depth of the central sulcus and manual dexterity in consistently right-handed children and adolescents. We applied factor analysis as a observer-independent modeling of central sulcus depth. Central sulcus have been segmented from high-resolution structural magnetic resonance images (MRIs) in cohort of 51 typically-developing individuals. Right-left asymmetry in dexterity was assessed using a drawing task, which tested subject's ability to draw superimposed circles in a regular fashion. All participants showed a strong preference for the right hand, avoiding any confound influence of differences in handedness. Factor analysis revealed 11 factors of which two were spatially expressed in the 'hand knob' region of the primary motor cortex (M1-HAND). Only these two factors significantly predicted the right-left asymmetry in manual proficiency during a circle-drawing task. The deeper the left relative to the right central sulcus in M1-HAND, the stronger was the right-hand advantage in drawing performance. This effect was not related to age, gender, or the total cortical surface of the cerebral hemispheres. It also cannot be explained by handedness, because all participants were consistent right-handers. The results indicate that manual proficiency is associated with increased cortical folding, resulting in a deeper sulcus in the more proficient hemisphere.

Introduction

The proficient use of the hand for skilled activities is a hallmark of human motor control. A large repertoire of manual skills, such as writing or picking up small items, is already acquired during childhood. The ability to skillfully use the hand, referred to as dexterity, requires the finely tuned coordination of multiple muscles to synchronize the movements of hands and fingers. Dexterity strongly

relies on a proper function of primary motor hand area (M1HAND) and its monosynaptic cortico-motor neuronal connections supplying the hand muscles [229, 156].
Another striking property of manual motor control in humans is a high degree of functional lateralization of hand use. Nine out of ten humans show a life-long preference for using the right hand during skilled manual actions [85]. The strong bias towards right-handedness is a unique human motor trait, which appears to be universally expressed in all human populations anywhere in the world. No other primate species shows a tendency to favor the right over the left hand that comes even close to the right-hand bias expressed in humans [43]. Right-handed people are usually more skillful with their right hands as opposed to their left hands when performing manual tasks. This is implied in the latin word "dexter", which means "right" but also "skillful". Yet, even in highly consistent right-handers, who show a strong bias towards using the right hand for daily activities, right-left asymmetry of manual dexterity may vary from subject to subject [82] although this variability of right-left asymmetry in dexterity has not attracted much attention.
Structural magnetic resonance imaging (MRI) of the brain has been used by several groups to identify macrostructural correlates of handedness in the human M1HAND. The M1HAND region forms a characteristic precentral 'knob' and can be easily identified on axial structural MRI scans, because of the omega-like shape of the central sulcus [289]. Shape analysis of the central sulcus yielded a difference in the 'hand knob' position along the dorso-ventral axis of the central sulcus [260]. In consistent right-handers, the overall location of the 'hand knob' is located more dorsally in the left (dominant) hemisphere than in the left (non-dominant) hemisphere in consistent left-handers [260]. Other studies have found an association between handedness and the right-left asymmetry of the area and depth of the central sulcus. Consistent right- and left-handers consistently showed a larger surface area of the central sulcus in the dominant hemisphere contralateral to the preferred hand [6, 80, 147, 63]. Cykowski et al. (2007) used an observer-independent depth measurement of the central sulcus to study the influence of handedness on the depth profile of the central sulcus: Healthy adult right-handed subjects revealed a deeper central sulcus in the left dominant hemisphere. In male right-handers, this leftward depth asymmetry was expressed in the superior extent of the central sulcus, whereas the leftward depth asymmetry was located near the midpoint of the central sulcus in female subjects [60].
While these morphometric MRI studies in adults provided converging evidence for a structural asymmetry of the central sulcus that is related to handedness, the interpretation of these studies is ambiguous. Since the asymmetry in preferred hand use (i.e., handedness) is confounded by an asymmetry to the ability to use the right and left hands skillfully (i.e., dexterity), it is difficult to attribute structural asymmetry in sulcal anatomy specifically to handedness or dexterity. In left-handed adult individuals, who were forced to write with their

non-preferred right hand at school, forced dextrality was associated with an asymmetry in sulcal size typical of right-handers, but forced dextrality did no shift of the handedness-specific location of the "hand knob" [260]. These findings indicate that in adults, sulcal morphology reflects both, innate hand preference as well as environmental influences shaping early developmental experience.
This study was designed to specifically assess the relationship between asymmetry in manual dexterity and right-left asymmetry in the depth profile of the central sulcus. To this end, we applied observer-independent depth analysis of the central sulcus to high-resolution structural MRIs, which had been collected in a cohort of 51 typically-developing right-handed individuals. Right-left asymmetry in dexterity was assessed using a drawing task, which tested subject's ability to draw superimposed circles in a regular fashion. We studied typically-developing adolescents, because we wished to minimize the influence of developmental experience. Critically, all participants showed a strong preference for the right hand, avoiding any confound influence of differences in handedness. We hypothesized that the individual right-left asymmetry in manual dexterity would show a spatially specific negative correlation with right-left asymmetry in sulcal depth within the hand knob region of the central sulcus.

Methods

Participants

The initial group consisted of 66 typically-developing right-handed children and adolescents, who participated in the HUBU ('Hjernens Udvikling hos Børn og Unge' - Brain maturation in children and adolescents) project. The HUBU project is a magnetic resonance imaging (MRI) study in which developmental changes in cognition, brain structure and function are prospectively assessed every six months [173]. The data reported here were collected in the eighth assessment round. Participants had no known history of neurological or psychiatric disorders or significant brain injury according to parent reports. To minimize the confounding effect of inter-individual differences in handedness, we only included participants who reported a consistent preference for using the right hand for everyday manual skills. The median handedness score was 100 %, ranging from 44 % to 100 % according to the Edinburgh Handedness Inventory (EHI) [198]. The EHI provides a laterality score for preferred hand use which ranges from −100 % (completely sinistral) to +100% (completely dextral). Prior to participation and after receiving oral and written explanation of the study aims and study procedures, all children assented to the procedures and informed written consent was obtained from the parents or guardians of all

participants. The experimental procedures were approved by the ethics Committee of the Capital Region of Denmark (H-KF-01-131/03), and conducted in accordance with the Declaration of Helsinki. Fifteen participants were not included in the final data analysis because due to dental brace (n=8), abnormal MRI findings (n=2), image artifacts (n=2), failure to segment the central sulcus (n=2), missing recordings of dexterity (n=1). The final cohort consisted of 51 children (18 males and 33 females) with a mean age of 13.6 ± 1.7 years (mean ± SD age range: 11 to 16 years).

Measurement of manual proficiency

To obtain a measure of dexterity for the right and left hand, participants were asked to perform a simple circle drawing task with their right and left hand. Circle drawing was performed on a regular piece of paper with a digitizing inking pen. Participants were asked to continuously draw concentric superimposed circles on a sheet of paper using an inking digitizing pen. Firstly, circles were drawn with the right hand in clockwise direction for 10 s, then circles were drawn with the left hand in counter-clockwise direction for 10 s. Participants were informed that we were mainly interested in testing their ability to produce circles in a regular fashion. Therefore, we emphasized that they should try to draw circles as smoothly as possible at a constant speed. To facilitate fluent open-loop performance, we told subjects that one circle did not need to exactly overlay the other.

We chose this circle drawing task because it involved a precision grip to hold the pencil, required the rapid synchronization of finger movements and had been previously used to compare dexterity of the right and left hand [110, 147, 247]. Further, the task was easy to understand, not previously trained at school, and could be completed with both the preferred right and non-preferred left hand. Circle drawing performance was continuously recorded using a digitizing tablet (UD-1212; WACOM Europe, Neuss, Germany). The position of the pen tip was stored at a sample frequency of 200 Hz. Kinematic analyses were performed using commercially available software (CS-Win; Version 10.05, MedCom, München, Germany).

We were mainly interested in assessing the temporal regularity of drawing movements. Smooth and fluent circle drawing is characterized by a low variance of the velocity profiles produced during the circle drawing task. Using the CS-Win software, the vertical drawing traces and the corresponding velocity profiles produced with the right and left hand were automatically segmented into consecutive up-and-down strokes. Curves of vertical velocity were calculated and smoothed by nonparametric regression methods [181]. Based on these velocity curves, we calculated vertical peak velocity of all up-and down drawing movements and derived the coefficient of variance (CV = standard deviation / mean)

of peak vertical velocity for right hand drawing (CV_R) and left hand drawing (CV_L). This measure was used as index of manual dexterity. The smaller the CV of peak velocity, the more regular were the velocity profiles during continuous circle drawing, indicating a high level of manual proficiency for circle drawing (Figure 8.1). The individual CV_R and CV_L values were used to calculate a an

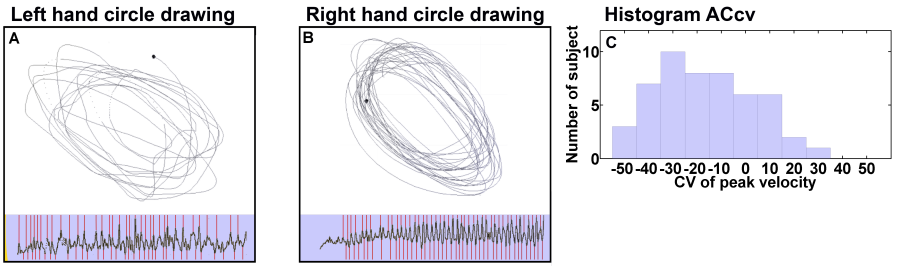

Figure 8.1: Measurement of manual proficiency. A and B) Top: The left and right hand circle drawing. Bottom: Velocity profile of the drawing traces. More fluently drawings results in less variability in the velocity profile. C) Histogram of the asymmetry coefficient of the dexterity.

Asymmetry Coefficient (AC) score to quantify right-left asymmetry in manual dexterity for each subject. The AC was calculated using the following formula and is expressed in percentage:

$$AC_{CV} = \frac{CV_R - CV_L}{CV_R + CV_L} \cdot 100 \tag{8.1}$$

AC_{CV} values between -100 and -1 indicated more regular velocity profiles during right-hand circle drawing relative to circle drawing with the left hand. Conversely, AC_{CV} values between 1 and 100 indicate a left-hand advantage for regular circle drawing.

Structural brain imaging

Three-dimensional T1-weighted MRI scans (Figure 8.2) were acquired using 3.0 Tesla Siemens Magnetom Trio Scanner (Siemens, Erlangen, Germany) equipped with an eight-channel surface head-coil (Invivo, Fl, USA). A sagittal magnetization prepared rapid acquisition gradient echo (MPRAGE) sequence was used with a repetition time (TR) of 1550 ms, echo time (TE) of 3.04 ms, inversion time (TI) of 800 ms, and a flip-angle of 9 °. The MRI scans had a 1mm isotropic resolution covering the whole brain using 192 sagittal slices with no gap (matrix

256 x 256). All images were visually inspected to insure sufficient image quality. This was done blind to behavioral data. Images were preprocessed using SPM 8 (Wellcome Department of Cognitive Neurology, University College London, UK). The T1-weighted images were corrected for spatial distortions due to non-linearity in the gradient system of the scanner and oriented to the MNI coordinate system using a six-parameter mutual information rigid transformation [136].

Segmentation of the central sulcus

The central sulci were extracted from the T1-weighted MRI scans using BrainVisa 4.3.0 (http://brainvisa.info) [178]. BrainVisa represents a sulcus as a three-dimensional mesh of the medial surface of the cerebrospinal fluid filling the central fold. A mesh represents the geometry of sulci as triangles. The edges of these triangles are called vertices and their relationships faces. All sulci were extracted and identified using the build-in pipeline ('Morphologist 2012'). An automated sulcal-recognition algorithm assigned standard anatomical labels to sulci using neural network-based pattern classification [178]. The pipeline was used with a global and local registration to recognize each sulci ("Statistical Parametric Anatomy Mapping"). Two sulci (2 left) had to be identified with another labelling method in BrainVisa (Artificial Neural Networks). Trying both recognition methods the central sulci of one subject were only successfully extracted at the medial end and hence had to be excluded. After sulcus extraction, 81 % of the sulci had to be edited manually in MeshLab (1.3.2), a 3D program for mesh manipulation (MeshLab, 2015) to remove other sulci or noise. Finally, an expert (HRS) confirmed that the software correctly identified sulci. All right central sulci were flipped relative to the interhemispheric plane for asymmetry studies.

Depth profile of the central sulcus

Since the depth profiles of a given sulcus treat each depth along the sulcus as a continuous variable, depth profiles offer a good inter-subject matching for morphological studies of cortical sulci [6, 60]. With respect to the central sulcus, profiling the sulcal depth has been used to identify landmarks of the hand knob [53], assess regional variations in sulcal area in relation to genetics [186] and to investigate the influence of handedness [6, 118]. For sulcal depth profiling, we used a simple representation adopted from McKay et al. (2013). This method finds the geodesic distance between 100 equidistantly points along the fundus and top ridge of the central sulcus. We first annotated the medial and lateral

endpoints of the central sulcus. The endpoints were defined as the medial and lateral intersection of the brain envelope and the central sulcus. This result was checked for all subjects and manually corrected in 14 % of the sulci. The next step was to define the sulcus fundus and top ridge. Candidate border points were located by only considering vertices where associated faces had at least one angle above 60° between adjacent face normals. Starting from the medial endpoint the upper and lower borders of the central sulcus were found by constraining a forward search along the candidate points towards the lateral endpoint. The two curves were smoothed by a moving average using a kernel size of 10 and re-parametrized into 100 equal spacing points. At each of the 100 locations, the geodesic was found along the mesh producing homologous left and right depth profiles. The resulting depth profiles of the central sulcus started at a medial position "1" near the inter-hemispheric fissure and ended at a lateral position 100 on the lateral surface of the cerebral hemisphere.
The area of each central sulcus was obtained by summing the area of all faces. Each triangular area was calculated as the cross product of the two sides in each face divided by 2.
As for the kinematic analysis of circle drawing (AC_{CV}), we calculated a lateralization index for the sulcal area AC_{AREA}, sulcal depth profile at each of the 100 positions for each central sulcus $AC_{DEPTH1,2...,100}$ and the mean depth $AC_{MEAN\ DEPTH}$. Negative AC values indicate a leftward asymmetry with a larger sulcal depth or area in the left hemisphere, whereas positive AC values indicate a rightward asymmetry with a larger sulcal depth or area in the right hemisphere.

Statistical analysis

Factor analysis

Factor analysis, a latent statistical data reduction technique, was used to describe the variance of the highly inter correlated 100 lateralization indices of the depth along the central sulcus ($AC_{DEPTH1,2,...,100}$). Factor analysis models depths with a causal relationship into a lower number of uncorrelated variables called factors. Factor analysis was chosen over other common data reduction techniques, such as principal component analysis and independent component analysis, because it provided a better anatomical interpretation of the results. Factor analysis involved two steps. First, a number of factors were extracted, which expressed the depths as linear combinations of the potential factors plus an error term. The second step was a rotation that prompts the interpretation of the factors by assigning depths load primarily to one factor. We used the Varimax rotation criterion, because it maintains the groups uncorrelated and

ensures an objective rotation [137]. The numbers of factors were chosen based on Kaiser Criterion ($1 \geq \lambda$).

Multiple regression analysis

Our hypothesis was that the left-right asymmetry in manual proficiency of fluent circle drawing would predict a right-left asymmetry in sulcal depth in the M1HAND region of the central sulcus. Specifically, we hypothesized that a higher right-hand advantage in dexterity would be associated with a relatively deeper central sulcus in the left as opposed to the right hand knob region of the central sulcus. To test this hypothesis, we calculated the individual AC values using depth factors located in the hand knob region of the central sulcus. Multiple linear regression was used to investigate whether the asymmetry in manual proficiency of circle drawing, as indexed by the individual AC_{CV}, would be predicted by the individual AC values of factors modeling the depth positioned in the M1HAND region. Age, gender, the interaction of age and gender and the area of the left and right hemisphere were included in the model to control for their influence. Descriptive follow-up analyses included analogous multiple regression models to test whether the individual AC values of all other positional depth factors, as revealed by factor analysis, predict right-left asymmetry in manual proficiency. We also tested the predictive value of individual depth position along the central sulcus. Further we tested the predictive value of AC_{CV} by the total sulcal area (AC_{AREA}) and sulcal mean depth ($AC_{MEAN\ DEPTH}$). Like the main regression analysis, these follow-up analysis were corrected for the influence of age, gender, interaction of age and gender and the area of each hemisphere.

Additional analyses

The Pearson Correlation Coefficient was computed to test for linear relations between the sulcal area, the mean sulcal depth and the right and left hemispheres. We also performed separate two-tailed t-tests to test for a significant right-left asymmetry in manual dexterity (AC_{CV}), total area (AC_{AREA}) and mean sulcal depth ($AC_{MeanDEPTH}$).
All statistical analyses were done using SAS 9.4. Group data are given as mean $\pm$ SD if not stated otherwise. A p-value below 0.05 was considered significant. Gaussian distribution was evaluated with the Shapiro-Wilk test.

An overview of the methods is seen in figure 8.2.

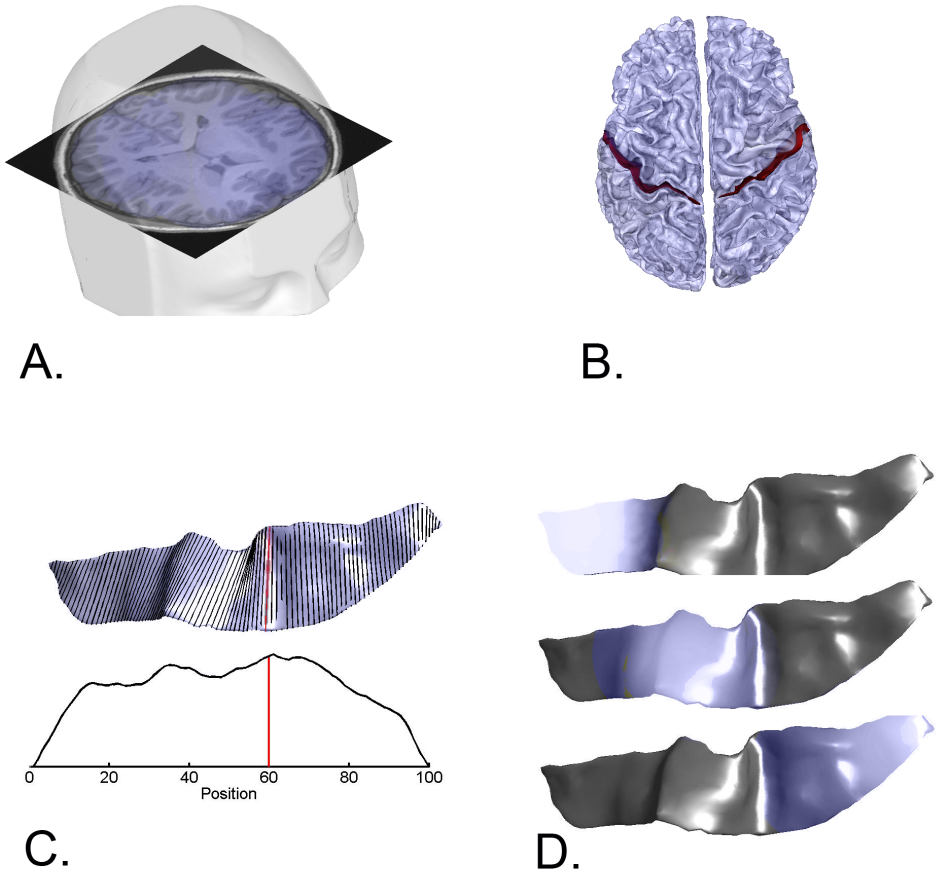

Figure 8.2: An overview of the method used. High quality 3D MR image were acquired (A). The central sulcus is segmented using BrainVisa (B). Depth profiles are generated by the geodesic distance between 100 equidistantly points along the fundus and top ridge of the central sulcus(C). The depths are modeled into causal sulcus subparts using factor analysis (D).

Results

Circle drawing

The right-handed typically-developing adolescents produced on average less variable peak velocities with their right dominant hand than with the left non-dominant hand. Mean AC_{CV} was -16.76 % with a SD of 19.56 % and differed significantly from zero (t=-6.12, p<0.0001), indicating a right-hand advantage for regular circle drawing at the group level. Although all participants consistently used their right hand for every day manual activities, the relative right-hand advantage for fluent circle drawing varied considerably across participants, ranging from -49.57 % to 31.06 % .
Some subjects showed no clear difference in CV of peak velocity between the right and left hand or even a slight left-hand advantage, whereas others showed a clear right-hand advantage. The variability of the velocity profile during circle drawing gradually decraesed with age. This age effect was seen for both the right dominant hand (t=19.94, p<0.001) and left non-dominant hand (t=16.85, p<0.001) and the lateralization index AC_{CV} (t=-5.92, p<0.001), but this age effect was no longer significant when the statistical model corrected for gender and area of the left and right hemisphere.

Sulcal area and depth profile

The area of left central sulcus was 1397.92 ± 171.66 mm^2 and the area of right 1364.06 ± 56.83 mm^2. This right-left difference in area did not reach significance (t= −1.7, p= 0.096), but multiple regression showed a trend towards a linear relation between the asymmetry of manual dexterity, as indexed by AC_{CV}, and right-left asymmetry in sulcal area, as indexed by (AC_{AREA}) ($R^2 = 0.48$, t=-1.90, p=0.065). There was no main effect or interaction effect of gender and age (p=0.23).
Mean depth of the left central sulcus was 13.70 ± 1.81 mm, and mean depth of the right central sulcus 13.47 ± 1.04 mm. The asymmetry between the mean depth of the left and right central sulcus was significant with a deeper central sulcus in the left dominant hemisphere (t=-2.2, p=0.032). Yet the asymmetry in mean sulcal depth, as reflected by $AC_{MEAN\ DEPTH}$, was not significantly related to the right-left asymmetry in proficiency of circle drawing as indexed by AC_{CV} (R^2=0.46, t=-1.28, p=0.209). The prediction of the laterality index AC_{CV}, by AC_{AREA} and $AC_{MEAN\ DEPTH}$ is summarized in Table 8.1.

	$\mathbf{AC}_{Area}$	$\mathbf{AC}_{Mean\ depth}$
R^2	0.48	0.46
Age	t=0.8 p=0.940	t=-0.22 p=0.825
Gender	t=0.12 p=0.235	t=-0.08 p=0.934
Interaction age and gender	t=-0.11 p=0.909	t=0.10 p=0.922
Area right hemisphere	t=1.03 p=0.307	t=1.07 p=0.292
Area left hemisphere	t=-1.08 p=0.284	t=-1.0 p=0.321
ACcv	t=-1.90 p=0.065	t=-1.28 p=0.209

Table 8.1: Manual dexterity index AC_{CV} related to the laterality index of the sulcal area (AC_{AREA}) and laterality index of the mean depth ($AC_{MEAN\ DEPTH}$).

Factor analysis

Factor analysis revealed 11 factors, which explained 95.6 % of the total variance of asymmetry of the 100 positional depths along the central sulcus ($AC_{DEPTH1,2,...,100}$). Eight factors modeled the variance in sulcal depth asymmetry along the entire central sulcus (Factors 1, 2, 3, 5, 6, 8, 10 and 11, labeled in white in Figure 8.3).

The variance explained by each of these factors ranged from 6-17 % of the total variance. Factors 5 and 6 were positioned in the M1HAND and were therefore used as explanatory variables in our primary analysis to link asymmetry in the depth profile of the M1HAND to asymmetry in manual proficiency.
Three factors explained only 7 % of the total variance (range: 1-3 %) and spatially overlapped with other factors. They were located between position 32 to 36, 49 to 59, and 79 to 85 (Factors 4, 7, and 9; in grey in Figure 8.3.
Multiple regression showed that factor 5 significantly predicted the right-left asymmetry in manual proficiency after accounting for the contribution of age, gender and area of the hemispheres (R^2 =0.48, t =-2.05, p =0.046). No age or gender effects or interaction between age and gender were found. The deeper the left central sulcus relative to the right central sulcus at sulcal positions in factor 5 (i.e., position 34 to 49), the more the subjects showed right-hand advantage in fluent circle drawing. The same relationship was also found for $AC_{DEPTH1,2,...,100}$ modeled by factor 6 ranging from position 49 to 65 (R^2 =

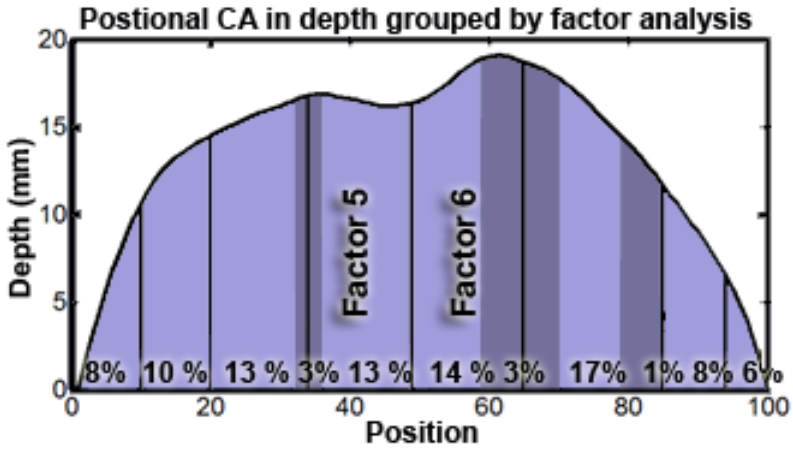

Figure 8.3: The 11 factors found by the factor analysis. The percentage of variation explained by a factor each factor is given in percent. The factors in gray show the least variance (totally 7 %) and spatially overlap the other factors

0.048, t =-2.02, p =0.0492). Again no age, gender or interaction between the two was found. The results of the multiple regression testing for a linear relation between the asymmetry of the depth of M1Hand modeled by factors 5 and 6 to the manual dexterity index (AC_{CV}) are listed in Table 8.2.

Relationship of all other factors outside M1-HAND

Overall, the first three factors (from position 1 to 34) show a rightward asymmetry in the depths and the last eight factors (from position 35 to 100) a leftward asymmetry. None of the factors outside the M1(HAND) predicted asymmetry in manual dexterity. A significant age effect was seen for all factors, showing negative t-values . No significant gender or interaction between age and gender effects were found in any of the regions of sulcal depths modeled by the factors
.

Factor (position on depth profile) (position on depth profile)	**Factor 5** (34-49)	**Factor 6)** (49-65)
R^2	0.48	0.48
Age	t=-0.23 p=0.82	t=-0.56 p=0.58
Gender	t=-0.25 p=0.905	t=0.52 p=0.61
Interaction age and gender	t=0.18 p=0.86	t=0.48 p=0.64
Area right hemisphere	t=1.47 p=0.15	t=1.35 p=0.19
Area left hemisphere	t=-1.42 p=0.16	t=-1.13 p=0.26
ACcv	t=-2.02 p=0.049	t=-2.05 p=0.046

Table 8.2: Results of multiple regression analysis testing factor 5 and 6. The t and p value are stated for age, gender, age and gender, the area of the two hemispheres and the manual dexterity measure.

Discussion

Here we used factor analysis as data-driven analytical approach to test for a relationship between the depth of the central sulcus and manual dexterity in consistently right-handed children and adolescents. Factor analysis revealed 11 factors of which two were spatially expressed in the "hand knob" region of the M1. Only these two factors significantly predicted the right-left asymmetry in manual proficiency during a circle-drawing task. The deeper the left relative to the right central sulcus in M1-HAND, the stronger was the right-hand advantage in drawing performance. This effect was not related to age, gender, or the total cortical surface of the cerebral hemispheres. They also could not be explained by differences in preferred hand use because all participants were consistent right-handers. The results indicate that manual proficiency is associated with increased cortical folding, resulting in a deeper sulcus in the more proficient hemisphere.

Right-left asymmetry in circle drawing

In most participants, fluent circle drawing movements were more regular when circles were drawn with the right hand. This right-hand advantage for regular circle drawing is not surprising, given the fact that all participants were consistent right-handers. However, at the individual level, the right-hand advantage for circle drawing varied substantially across subjects. This finding indicates that the individual expression of manual dexterity could not be exclusively be explained by preferred hand use. Together, our behavioral data confirm previous studies that the degree of hand preference (i.e., the preference to use the right or left hand to perform manual dexterity tasks) and hand dominance (i.e. the hand showing best motor performance) may dissociate at the individual level and therefore need to be distinguished in studies on human motor control [44]. In our study, we minimized possible influences of handedness, because we only studied participants with a strong preference for using the right hand for dexterity tasks.

Left-right asymmetry in sulcal area and depth

To pinpoint a relation between the depth profile of the central sulcus and manual dexterity, we used a factor analysis, which assigned sulcal depth values to uncorrelated groups. This data-driven approach identified two "sulcus depth" factors, which were positioned in the M1HAND. The right-left asymmetry of these M1HAND factors predicted right-left asymmetry in circle drawing skill. The other factors represented the sulcus depth outside M1HAND and were unrelated to the asymmetry in manual dexterity. The right-left asymmetry of mean sulcus depth also failed to explain right-left asymmetry in manual dexterity. Together, the results link differences in the depth of the central sulcus to the individual expression of manual dominance, but this structure-function relationship is somatotopically specific, as it is only expressed in the portion of the central sulcus that corresponds to the M1-HAND.

Cykowski et al. (2007) showed a deeper central sulcus in the left dominant hemisphere in adult right-handed individuals. Our study in healthy right-handed individuals significantly extends the work by Cykowski et al. (2007) showing that sulcus depth of M1-HAND also reflects manual proficiency in addition to hand preference. Cykowski et al. (2007) found gender differences in the spatial expression of the relationship between depth asymmetry and handedness in the central sulcus. The two "sulcus depth" factors corresponding to the M1-HAND were predominantly positioned medially and laterally in the hand area. For

both, the medial and lateral factor, the right-left asymmetry in sulcal depth predicted right-left asymmetry in manual proficiency, but this relationship was not influenced by the gender of participants. This negative finding does, however, not exclude a subtle gender effect in adult participants or in a larger cohort of children and adolescents.

Right-left asymmetry of the central sulcus

In healthy right-handed children and adolescents, we found that the dominant left central sulcus was deeper than the non-dominant right central sulcus. A weak trend towards a left-hemispheric asymmetry was also found for a larger surface area of the central sulcus in the dominant left hemisphere. Our findings are consistent with previous studies in adult right- and left-handers, showing a larger surface area of the central sulcus in the dominant hemisphere contralateral to the preferred hand [6, 63, 80, 147, 63]. We conclude that an overall increase in mean sulcus depth of the left dominant hemisphere is already present in right-handers during late childhood and adolescence, but does not scale with the relative right-hand advantage in dexterity. Of note, adult "converted" left-handers, who had been forced as children to become dextral writers, show a reversal of the interhemispheric asymmetry in the surface area of the central sulcus. The attempt to convert left-handers resulted in a larger surface of the central sulcus in their left, nondominant hemisphere [146]. This finding is in agreement with the present results, suggesting that sulcal surface covering the M1-HAND increases as a function of the level of acquired dexterous manual skills in the contralateral hand.

Limitations

The study has several limitations. One limitation is the lack of left-handed subjects in this study. It has previously been reported that in left-handers, the central sulcus of the dominant right hemisphere is deeper than the central sulcus in the left non-dominant hemisphere [5] but asymmetry in sulcal depth is less pronounced compared to right-handers [5] Future studies must clarify whether consistent left-handers show a similar relationship between right-left asymmetry in sulcus depth and dexterity than consistent right-handers. Another limitation is that this study is cross-sectional. This might explain why we did not detect any significant effect of age on the asymmetry in sulcal depth. A longitudinal study removes the inter-subject variability and therefore might be more sensitive to reveal age-effects on the right-left asymmetry of sulcal surface and has the potential to reveal individual developmental trajectories.

Chapter 9

Congenital atrophy of the olfactory bulb is coupled to changes in the depth of the posterior olfactory sulci revealed by factor analysis

Martin Vestergaard[1], Betina Vase Jensen[1,3], Helena G. Karstensen[2], Bjarki Djurhuus[4], Damian Herz[1], Brian Numelin Haagensen[1], Camilla Klausen[2], Anne-Mette Leffers[2], Niels Tommerup[2] and Hartwig R. Siebner[1,5]

[1] Danish Research Centre for Magnetic Resonance, Centre for Functional and Diagnostic Imaging and Research, Copenhagen University Hospital Hvidovre, Hvidovre, Denmark
[2] Wilhelm Johannsen Centre for Functional Genome Research, Department of Cellular and Molecular Medicine, Faculty of Health Sciences, University of Copenhagen, Denmark.
[3] DTU Compute, Technical University of Denmark - DTU, Kgs. Lyngby, Denmark

[4] Department of ENT Head and Neck Surgery, The National Hospital of the Faroe Islands, Tórshavn, Faroe Islands
[5] Department of Neurology, Copenhagen University Hospital Bispebjerg, Copenhagen, Denmark

Keywords: Anosmia, hyposmia, smell, olfaction, MRI

Abstract

The olfactory bulb conveys the perceptual qualities of odorants to the medial orbitofrontal cortex (mOFC) via the piriform cortex. Anatomically the olfactory bulb and tract is situated in within the olfactory sulci within the mOFC. This intimate coupling is evidenced by individuals who suffer from congenital olfactory impairment demonstrate olfactory bulb atrophy as well as reduced depth of the olfactory sulci. It is unclear, however, whether specific subareas along the olfactory sulci are affected by lifelong atrophy of the olfactory bulb. To address this question, we examined fifteen adults with isolated congenital olfactory impairment (COI) matched with sixteen normosmic controls. Magnetic resonance imaging (MRI) was acquired in all subjects to assess the volume of the olfactory bulb and the depth along the entire olfactory sulci. The olfactory sulci were co-registered between all subjects and factor analysis was performed to identify subareas along the olfactory sulci within the mOFC. Relative to controls, individuals with COI showed reduced depth along the olfactory sulci most prominently in posterior and middle subareas. Specifically, atrophy of the olfactory bulb in the COI group showed a stronger positive relationship with factors loadings in posterior subareas of the bilateral olfactory sulcus compared to olfactory bulb volume in controls. Our results suggest that lifelong atrophy of the olfactory bulb preferentially induce structural reorganization in subareas within the posterior mOFC roughly corresponding to the agranular and dysgranular layers connected with the olfactory system as previously demonstrated in monkeys.

Introduction

It is well established that the medial orbitofrontal cortex (mOFC) is a key neocortical target for olfactory inputs conveyed through the olfactory nerve via the

piriform cortex [42, 192]. While the integrity of the olfactory bulb is critical for encoding perceptual qualities of odorants, higher-order appraisal of odours are represented in the mOFC [163, 222]. The application of magnetic resonance imaging (MRI) has provided compelling evidence that link olfactory proficiency with structural variation in the mOFC. Smell ability in healthy individuals exhibits a positive association with grey matter volume or thickness along the olfactory sulci [66, 84]. Furthermore, depth measurements of the olfactory sulci, measured in a single plane posterior to the eyeballs, is proportionate with smell ability in healthy individuals [123] and in subjects with acquired smell deficits [124]. The close link between the human functional sense of smell and the mOFC is perhaps most clearly evidenced by observations that relative to normosmic controls, individuals suffering from congenital olfactory impairment have atrophic olfactory bulb [1, 83] together with substantially smaller olfactory sulci [1] and thicker cortex in mOFC [83]. Consistent with these prior findings, we recently showed that subjects with isolated congenital olfactory impairment (COI) had atrophic olfactory bulbs and reduced area of the olfactory sulci [138] (please see supplementary material).

While the empirical data clearly demonstrate a connection between the human functional sense of smell and grey matter along the olfactory sulci and adjacent gyri, namely gyrus rectus and medial orbital gyrus, it remains unknown whether depth measures in specific subareas along the olfactory sulci are modulated by the integrity of the olfactory bulb. Because volume of the olfactory bulb shows a proportional relationship with smell ability in normosmic individuals [37] and in subjects who suffer from acquired olfactory loss due to various medical conditions [124], we speculated that inter-individual variations in olfactory bulb volume was closely associated with the depth of the olfactory sulci. Hence, we hypothesized that congenital atrophy of the olfactory bulb in COI participants would reveal a differential relationship with depth reductions of the olfactory sulci relative to olfactory bulb integrity in controls. To address this question, we used structural MRI to obtain depth measurements along the entire olfactory sulci in a unique group of relatives from the Faroe Islands with isolated COI who were otherwise healthy. The population of the Faroe Islands is descendent from a small number of settlers in the 800s, and since then the population has expanded without severe bottlenecks or immigration, which has contributed to a relatively high prevalence of rare conditions caused by genetic founder effects [115, 201, 238]. We applied factor analysis to examine, whether subareas along the olfactory sulci differed between individuals with COI and normosmic controls. Moreover, interaction analyses was used to estimate if the localized reductions in olfactory sulcal depth were differently associated with olfactory bulb volume in COI individuals relative to normosmic controls.

Methods

Participants

The present study included 15 COI individuals (12 familial cases clustering in four subfamilies and 3 distantly related cases) and 16 matched healthy normosmic controls (six familial with the COI group and 10 non-familial). The family were originally described by Lygonis in 1969 [171]. Additional family members were recruited through local advertisement. Voxel-based morphometric (VBM) analyses of regional grey matter volume differences across the whole brain have previously been reported for the COI family compared to the controls. A thorough description on recruitment, screening and exclusion procedures as well as group assignment is described thoroughly in that study [138]. Shortly, all participants were interviewed concerning their olfactory ability and subjects were ascribed to the COI group only if they reported to suffer from lifelong smell impairment with no apparent underlying condition. Olfactory ability was assessed with the standardized TDI "Sniffin' Sticks" test (Burhart, Wedel, Germany) [122]. Anosmia was defined according to a TDI score below 16.5 [122, 148], and hyposmia was defined according to normative data adjusting for age and sex (Hummel et al., 2007). Ten COI subjects had anosmia while five COI subjects had hyposmia. All controls were normosmic.
The study took place at the Danish Centre for Magnetic Resonance (DRCMR), Denmark. All subjects, except for one control were right-handed assessed by the Edinburgh handedness Inventory. The groups were matched on age, sex, cognitive ability measured with the Danish version of the Montreal Cognitive Assessment test (MoCA) [195], years of education and number of smokers (Table 1.1). We have previously shown that COI participants and controls did not differ in taste detection sensitivity, vision and hearing ability [138]. All participants received thorough written and oral information concerning the study procedures and aims. Written consent was obtained before study initiation. The study was approved by the National Scientific Ethics Committee (H-A-2009-063) and the Faroese Scientific Ethical Committee (200812) and followed the Declaration of Helsinki.

Image acquisition and evaluation

All subjects were scanned using a 3T Siemens Magnetom Verio MR scanner (Siemens, Erlangen, Germany) with a 32-channel head coil (Invivo, FL, USA). For definition of the olfactory bulb and olfactory sulci we used a 2D T2-weighted sequence with high in-plane resolution acquired of the frontal cortex and the ol-

	COI (n = 15)	**Controls** (n = 16)
	Demographics	
Age in years	48.3 ± 14.3	47.2 ± 16.1
Sex (male/female)	5/10	7/9
Smokers/non-smokers	7/8	6/10
MoCA score	27.1 ± 2.5	27.3 ± 2.5
Years of education	11.3 ± 3.4	12.5 ± 2.7
	Olfactory ability	
Sniffin' Sticks (TDI) score	14.8 ± 4.8	31.6 ± 4.8
	Brain measures	
Whole brain volume (mm^3)	1194 ± 135	1220 ± 100
Prefrontal length (mm)	64.4 (60.9, 64.7)	62.2 (60.3, 63.5)
Prefrontal height (mm)	68.6 (66.0, 71.2)	70.2 (67.7, 70.9)
Left olfactory sulcus area (mm^2)	120.4 ± 46.0	159.1 ± 23.9
Right olfactory sulcus area (mm^2)	134.1 ± 41.6	167.0 ± 28.8
Left olfactory bulb volume (mm^3)	4.0 (0.0, 11.5)	19.3 (12.5, 25.4)
Right olfactory bulb volume (mm^3)	0.0 (0.0, 12.5)	19.9 (12.3, 26.7)

Table 9.1: Normally distributed variables are presented as mean ± standard deviation and non-normally distributed variables, as tested with the Shapiro-Wilk test, are presented with medians and lower and upper quartiles. MoCA = Montreal Cognitive Assessment test.

factory bulb (TR= 6180 ms, TE= 79 ms, matrix=512x420, FoV=230x230, 49 coronal slices, 0.45x0.45 mm^2 pixels, 2 mm slice thickness with 10 % gap between slices).
In the present study we combined the total grey matter and white matter volume for each subject as a measure of whole brain volume extracted from a previously published VBM analysis of a whole-brain T1-weighted image [138]. Group data for whole brain volume are presented in table 1. Furthermore, a T2-weighted image and a FLAIR image were acquired of the whole brain for clinical evaluation of the nasal cavities and sinuses. Sequence specifications for the T1-weighted image, T2-weighted image and the FLAIR image, VBM analysis and clinical image evaluations have been described in detail elsewhere [138].

Olfactory bulb volume measurement

The olfactory bulb were defined according to established anatomical criteria [35], and were manually segmented on the 2D T2-weighted images in native space using software from Xinapse Systems version 6.0 (www.xinapse.com/home.php), described in detail elsewhere [138] (please see Supplementary material). Olfac-

tory bulb volumes are displayed in table 1.

Demarcation of the olfactory sulci in native space

The olfactory sulci were defined bilaterally using The Human Brain Atlas as guidance [70]. Shortly, the shape of each sulcus was defined by annotated points using a piece-wise linear curve, drawn from the midpoint between the apex of the gyrus rectus to the apex of the medial orbital gyrus to the fundus. The anterior border of the olfactory sulcus was defined when a division of the lateral and medial banks was observed while the posterior border of the olfactory sulcus was delineated by the olfactory trigone. The demarcation of the olfactory sulci are described in further detail elsewhere [138] (please see Supplementary material). The length and height of the prefrontal cortex (PFC) was drawn manually from the subjects' non-anonymized image by a single rater. The PFC length was defined as the distance from the anterior commissure to the anterior border of the PFC following the intercommissural (AC-PC) line. The height of the prefrontal cortex was defined placing a line in a 90-degree angle on the AC-PC line, and taking the distance from the anterior commissure to the dorsal border of prefrontal cortex. The total area of the olfactory sulci and PFC measures are displayed in table 1.

Between-subject co-registration of the olfactory sulci

The statistical analysis of the olfactory sulci depth measures was performed using SAS 9.4 software (http://support.sas.com/software/94), and the transformations were calculated with matlab software. To accomplish a between-subject correspondence that could adequately account for inter-individual variations in the depth profile of the olfactory sulci across the COI and controls, a series of preprocessing procedures were performed. First, the depth of the olfactory sulci was calculated as the sum of the Euclidian distance between each of the annotated points for each coronal slice. As the posterior border was defined at the olfactory trigone in all subjects, we aligned all subjects' left and right olfactory sulcus, respectively, according to the most posterior slice (see Figure 9.1). Next, to account for the between-subject variability in the size of the prefrontal cortex, we scaled the olfactory sulci for each subject with the individual measurements of the length and height of prefrontal cortex. This rescaling resulted in the loss of a point-wise correspondence between the subjects' slices. To reestablish the point-wise correspondence, the depth profiles were reparametrized by first interpolating a cubic spline to the sulci depth profiles followed by resampling. To avoid subsampling the original slices, sampling of the depth profiles were

performed across twenty-two points along the olfactory sulci as this number corresponded to the maximum number of slices used to define the right olfactory sulcus in a control subject.

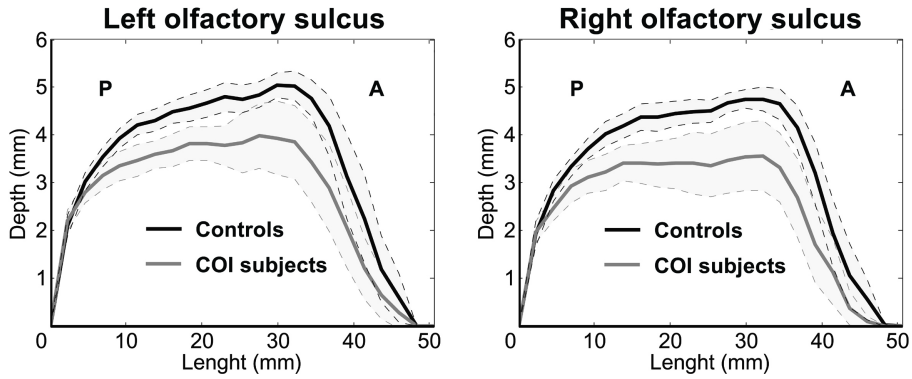

Figure 9.1: Mean and 95 % confidence interval of the depth profiles for the left and right olfactory sulci, respectively, for the COI group and controls. Depth and length of the olfactory sulci are displayed in millimeters (mm). The most posterior slice is X-axis = 0. P = posterior. A = anterior.

Estimation of olfactory sulci subareas using factor analysis

To identify anatomical subareas along the olfactory sulci, we assumed that the highly correlated depth measurements along the olfactory sulci were linked to underlying causative factors. Therefore, we used factor analysis, a multivariate aproach, that models the olfactory sulci depth measures as latent variables assumed to share a causal relationship. Factor analysis identifies anatomical clusters of the intercorrelated depths in terms of a lower number of uncorrelated unobserved variables called factors. Factor analysis includes a factor extraction followed by factor rotation. The factors are modelled as linear combinations of the potential factors plus an error terms. We extracted the factors as principal components. The rotation of each observation prompts the interpretation of the factors, since it forces the clusters of depths to load primarily on to a single factor. We used the Varimax rotation criterion [137] to obtain orthogonal rotation of the factors to ensure that the estimated depth factors of the olfactory sulci were uncorrelated. We applied the Kaiser Criterion [137] to restrict the number of factors, which yielded four factors for each olfactory sulcus (Figure 9.2).

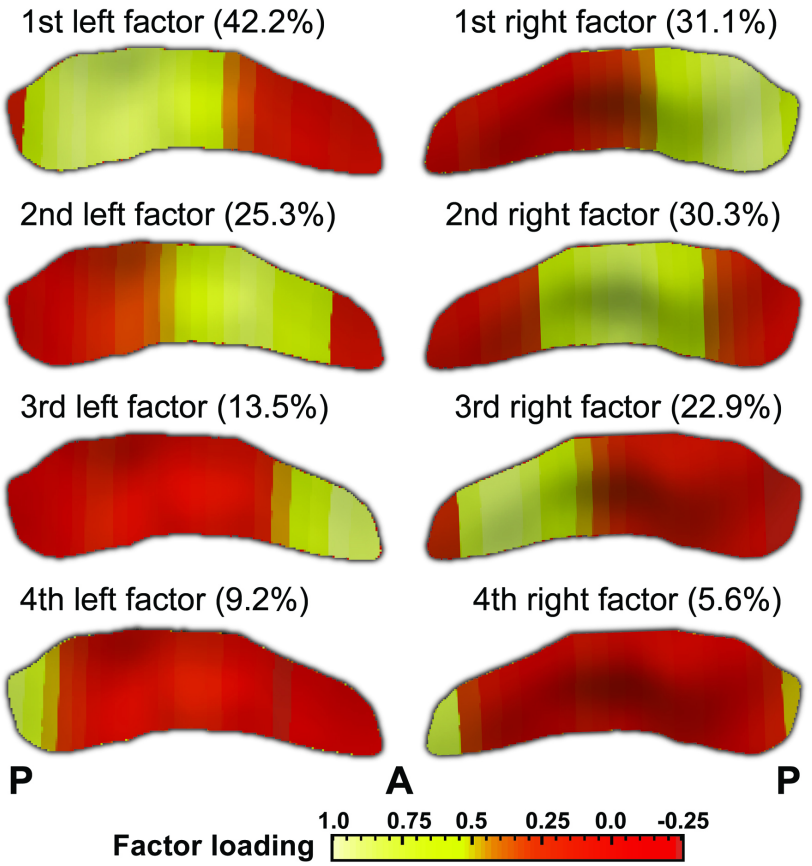

Figure 9.2: Extracted factors for the left and the right olfactory sulci, respectively, estimated from the depth profiles in all participants. The number of factors was based on the Kaiser Criterion [137] and resulted in four extracted factors for each of the olfactory sulci. The model variance explained by each factor is shown in parentheses. The factor loading values are coded in warm colors across the 22 sampling points along the left and right olfactory sulci, respectively, and overlaid on the largest olfactory sulcus for illustrative purposes. P = posterior. A = anterior.

Statistical analysis

Statistical analyses were done using SPSS20. A p-value below 0.05 was considered significant. Group differences in age, years of education and MoCa score were tested with two-tailed t-tests as neither age, years of education or the MoCa score were significantly non-normally distributed using the Shapiro-Wilk test. The Chi square test was used to test for sex differences between groups. Group differences in brain measures were tested with multiple linear regression models. Models testing for group differences in PFC length, PFC height or whole brain volume were corrected for age and sex.
First, we tested if COI participants and controls differed in each of the four factors for the left and right olfactory sulci, respectively. Models testing for group differences in each of the factors were corrected for age, sex and whole brain volume. Because the co-registration of the olfactory sulci depth measurements, used for factor analysis, was scaled according to PFC length and PFC height, we did not correct for neither of these variables in the regression models.
To examine whether atrophy of the olfactory bulb in COI individuals showed distinct relationships with subareas across the olfactory sulci relative to olfactory bulb volume in normosmic controls, we performed interaction analyses for the left olfactory bulb by group and the right olfactory bulb by group, respectively, for each of the olfactory sulci factors, correcting for age, sex and whole brain volume.

Results

COI and controls were matched for age (t= 0.38; p= 0.71), sex ($\chi^2 = 0.25$; p= 0.62), years of education (t= −1.38; p= 0.18), number of smokers ($\chi^2 = 0.27$; p= 0.61) and cognitive ability measured with the MoCA (t= −2.25; p= 0.82). The COI group and controls did not differ in PFC length (t= −0.521; p=0.61), PFC height (t= 1.700; p= 0.1), or whole brain volume (t= 0.47; p=0.64).

Group differences in the olfactory sulci subareas

Multiple linear regression analyses for each of the olfactory sulci factors confirmed that COI participants and controls differed significantly in the bilateral posterior subareas (left 1st factor: t= 2.904; p= 0.007, figure 9.3A; right 1st factor: t= 3.014; p= 0.006, figure 9.3B) and the bilateral middle subareas extending into the anterior mOFC (left 2nd factor: t=2.507; p= 0.019, figure

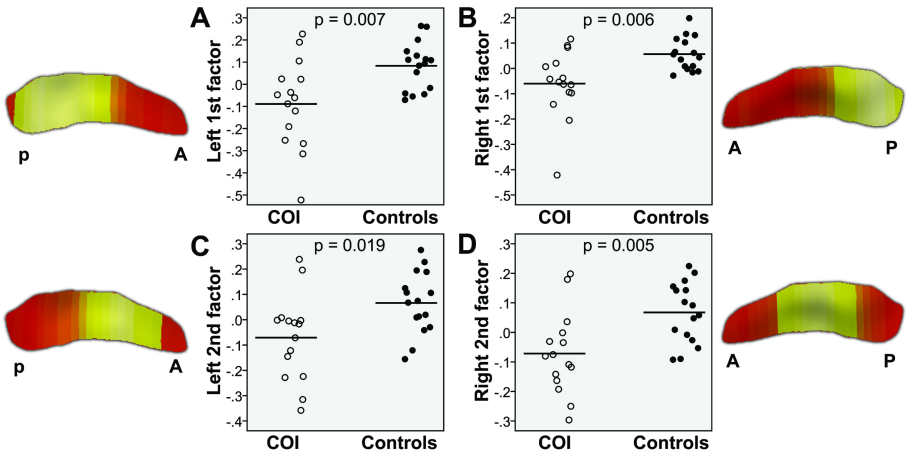

Figure 9.3: Extracted factors for the left and the right olfactory sulci, respectively, estimated from the depth profiles in all participants. The number of factors was based on the Kaiser Criterion (1) and resulted in four extracted factors for each of the olfactory sulci. The model variance explained by each factor is shown in parentheses. The factor loading values are coded in warm colors across the 22 sampling points along the left and right olfactory sulci, respectively, and overlaid on the largest olfactory sulcus for illustrative purposes. P = posterior. A = anterior.

9.3C; right 2nd factor: t=3.062; p=0.005, figure 9.3D) with no significant group differences for the additional factors ($t \leq 1.406$; $p \geq 0.17$).

Interaction analyses

Interaction analyses showed that relative to left olfactory bulb volume in controls, the volume of the left-sided olfactory bulb in COI individuals showed a positive association with subareas in the bilateral posterior olfactory sulci (left 1st factor: t= −2.445; p= 0.022, figure 9.4A; left 4th factor: t=−3.928; p=0.001, figure 9.4C; right 1st factor: t=−3.036; p= 0.006, figure 9.4E) with a trend for the right 4th factor (t=−1.751; p= 0.093, not shown), whereas the remaining factors showed no significant interactions ($t \leq \pm 0.192$, $p \geq 0.25$). Similar results were obtained for the interaction analyses with the right olfactory bulb. Compared to inter-individual variations in the volume of the right olfactory bulb in controls, volume of the right olfactory bulb in the COI subjects showed a

more positive association with subareas in the bilateral posterior olfactory sulci (left 4th factor: t=−2.839; $p = 0.009$, figure 9.4D; right 1st factor: t=−2.237; p= 0.035, figure 9.4F) with a trend for the left 1st factor (t= −1.937; p= 0.065, figure 9.4B). No significant interactions were found for the remaining factors ($t \leq \pm 1.120$, p≥ 0.27).

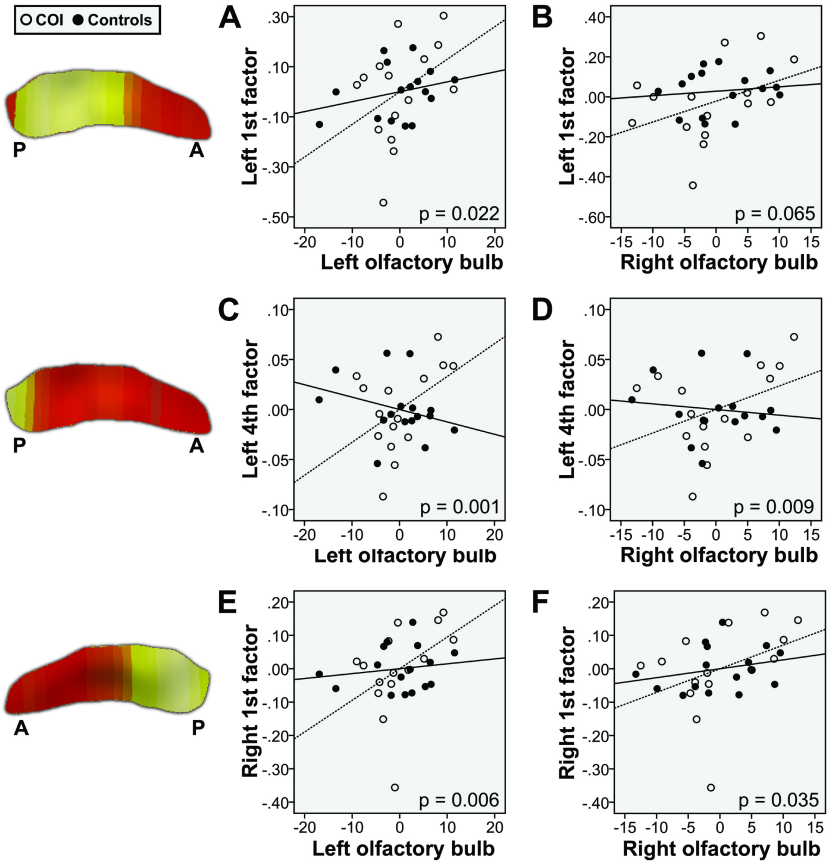

Figure 9.4: Extracted factors for the left and the right olfactory sulci, respectively, estimated from the depth profiles in all participants. The number of factors was based on the Kaiser Criterion (1) and resulted in four extracted factors for each of the olfactory sulci. The model variance explained by each factor is shown in parentheses. The factor loading values are coded in warm colors across the 22 sampling points along the left and right olfactory sulci, respectively, and overlaid on the largest olfactory sulcus for illustrative purposes. P = posterior. A = anterior.

Discussion

In a unique cohort from the Faroe Islands who suffered from isolated congenital olfactory impairment (COI) and a matched normosmic control group, we examined whether lifelong atrophy of the olfactory bulb was associated with regional depth reductions along the olfactory sulci. Because we applied factor analysis to the depth measurements along the entire left and right olfactory sulci, we were able to identify subareas within posterior, middle and anterior mOFC. Previous studies reported that individuals suffering from COI due to various conditions had a substantial reduction in the depth of the olfactory sulci measured in a single plane behind the eyes [1, 121]. Our results corroborate and extend these earlier findings. We provide novel evidence that reduced depth of the bilateral olfactory sulci in COI subjects is most prominent in posterior and middle subareas of the mOFC. Importantly, the olfactory bulb in COI individuals showed a preferential positive relationship with assumed depth reductions in mOFC subareas, specifically in the posterior olfactory sulci, which appeared less consistent for olfactory bulb volume in normosmic controls.

MRI studies have established that the human functional sense of smell is closely linked to integrity of the mOFC, yet it remains unclear whether a definite anterior-posterior gradient is evident along the human olfactory sulcus. While expert perfumers, relative to controls, had increased volume in the more posterior segments of bilateral mOFC [66]), healthy normosmic participants were reported to show positive associations between smell ability and cortical thickness along the middle right olfactory sulcus [84], as well as grey matter volume in lateral areas of right mOFC [242]. Functional MRI (fMRI) studies in healthy normosmic participants have also provided support that the dynamic recruitment of the mOFC is essential for higher-order olfaction as activation foci across the entire surface of the mOFC [29, 29, 94, 119] including the posterior mOFC [7, 163] have been observed during appraisal of odours. Recently, an interventional fMRI study showed that temporary olfactory deprivation in healthy normosmic adults disrupted brain activity in the mOFC including the right posterior mOFC when subjects performed associative encoding of odour quality [286]. Although it is currently unknown which subareas in the human mOFC are targeted by projections from the olfactory system, our findings are compatible with neuroanatomical discoveries in monkeys that orbital neurons implicated in higher-order appraisal of odour are primarily distributed across the posterior surface of the orbitofrontal cortex [225, 226]. Furthermore, the olfactory bulb mainly project to the ipsilateral posterior mOFC via the piriform cortex [42], and projections from the olfactory system terminate predominantly in the agranular and to a lesser extent the dysgranular layers of the posterior mOFC [17]. Hence, the present study indicates that lifelong olfactory deprivation in humans may induce the most profound changes in the agranular and dysgranular subareas along the posterior olfactory sulci and the adjacent gyri.

Converging evidence suggest that the cellular organization of the mOFC, guided by major maturational events, takes place well before adulthood and even childhood. The olfactory sulci emerge at an early gestational age as the gyrus rectus and the medial orbital gyrus begin to convolve [45], and cortical thinning of the posterior mOFC appear to show a characteristic linear thinning already present in preschool children unlike most regions of the cerebral cortex, which do not peak in density until later in childhood or adolescence [243]. Therefore, it appears probable that functional disruption of odor inputs to posterior mOFC, due to congenital atrophy of the olfactory bulb, may trigger substantial changes in the cellular organization along the olfactory sulci. This hypothesis is further substantiated by consistent observations that COI individuals have reduced olfactory sulcal depth [1, 121] whereas subjects who suffer from olfactory impairment acquired later in life appear to show no significant reductions of the olfactory sulci [227].

Method limitations

The present study has several limitations. First, the cross-sectional study design and the fact that we scanned the matured cortex in adult individuals prevented insights into the altered dynamics of mOFC development. Second, due to the use of linear general models for statistical analysis, non-linear relationships between olfactory sulci measures and olfactory bulb volume might have been overlooked. Moreover, we did not identify a causative genetic mutation in the COI group, which might have enabled a more specific separation of cases and controls.

Conclusion

In conclusion, our findings suggest that congenital atrophy of the olfactory bulb in otherwise healthy individuals induces structural reorganization in subareas within the posterior mOFC along the olfactory sulci, a region of the mOFC, which contains agranular and dysgranular layers connected with the olfactory system.

Disclosure

Hartwig R. Siebner (HRS) has served on a scientific advisory board for Lundbeck A/S, Valby Denmark. HRS has received honoraria as speaker from Biogen Idec, Denmark A/S, Genzyme, Denmark and MerckSerono, Denmark. HRS has

received honoraria as editor from Elsevier Publishers, Amsterdam, The Netherlands and Springer Publishing, Stuttgart, Germany. HRS has received travel support from MagVenture, Denmark, and a research fund from Biogen-idec. All other authors have no conflict of interest.

Supplementary material

Manual segmentation of the olfactory bulbi and olfactory sulci

The olfactory bulbi and olfactory sulci were manually segmented on the 2D T2-weighted images in native space using software from Xinapse Systems version 6.0. The olfactory bulbi were defined according to established anatomical criteria [35]. Images were interpolated using a bi-linear algorithm. Two trained raters (H.K. and M.V.) blinded to clinical status, independently performed the manual segmentation of the olfactory bulbi and olfactory sulci. To calculate intra-rater reliability measures each subject's 2D T2-weighted images were duplicated and left-right flipped to create additional images. Intra-class correlation coefficients (ICC), calculated as a two-way mixed model with measures of absolute agreement, showed that reproducibility of the bulbs was high with a mean intra-rater reliability of 0.93 (range: $0.92 - 0.95$) and a mean inter-rater reliability of 0.87 (range: $0.85 - 0.88$).
The planimetric measurements of the olfactory bulbs were multiplied by 2.2 (2 mm slice thickness with 10 % gap) in order to obtain bulb volumes in mm^3. The values were comparable with previous published measures of olfactory bulb volumes [36]. The median value from the four volume measures obtained for each left and right-sided olfactory bulb, respectively, was used as outcome variable to account for possible outliers. The olfactory sulci were defined bilaterally using The Human Brain Atlas as guidance [70]. Initially, a tangent was drawn from the apex of the gyrus rectus to the apex of the medial orbital gyrus, and the midpoint between the gyrus rectus to the medial orbital gyrus was used to demarcate the inferior border of the olfactory sulcus. Following the shape of the sulcus, a piece-wise linear curve, connected by annotated points was drawn from the border of the inferior olfactory sulcus to the fundus. The anterior border of the olfactory sulcus was defined when a division of the lateral and medial banks was observed. The posterior border of the olfactory sulcus was delineated by the olfactory trigone observed on the coronal image as a small protrusion of grey matter.

Group differences in olfactory bulbi volume and sulci depth and subareas

Multiple regression models tested for group differences in volume of the left and right olfactory bulbi, respectively, were corrected for age, sex and whole brain volume. Models testing for group differences in the total area of the left and right olfactory sulci, respectively, were corrected for age, sex, whole brain volume and PFC length, to further ensure that group differences were not accounted for by variations in PFC length.

As reported elsewhere [138], relative to normosmic controls, the COI group had reduced volume of the olfactory bulbi (left: $t = 5.179$; $p < 0.0001$; right: $t = 5.490$, $p < 0.0001$) and the total area of the olfactory sulci (left: $t = 3.295$; $p = 0.003$; right: $t = 3.116$, $p = 0.005$).

Chapter 10

Technical report: Mapping maturational changes in CS morphology during adolescence

Betina Vase Jensen [1,2].

[1] Danish Research Centre for Magnetic Resonance, Centre for Functional and Diagnostic Imaging and Research, Copenhagen University Hospital Hvidovre, Denmark.
[2] DTU Compute, Technical University of Denmark - DTU, Kgs. Lyngby, Denmark

Keywords : Cortical surface, Central Sulcus, Brain maturation, Adolescence, MRI, Brain Sulci, Gyrification, TPS.

Abstact

The maturation of the human brain is ever changing caused by an interaction of genetic and environmental factors. A large variation in the cortical folding is evident. This folding is known to decrease and after the first year in life, however relatively little is still known about the developmental changes in the folding of the cortical surface.
In this longitudinal study we investigate the maturation of Central Sulcus (CS), a major fold on the lateral surface of the brain, that separate the primary motor areas from the somatosensory areas. 51 participants aged 8 to 17 years were assessed using high resolution structural magnetic resonance imaging (MRI) in 8.9 times on average, resulting in a total of 454 MR images. Linear mixed models were used to investigate age and gender effects on CS surface area and depth. Thin plate spline registration aligned all segmented sulci and the three dimensional positional variations were studied.
Left CS area were significantly reduced with age, but only a trend was found for the right CS surface area. Moreover, females showed a significantly bilateral decrease in the sulcal area, not seen in males. We found no age or gender effects in the depth along the CS in time. The average positional movement from the first scan to the last is primary related to the sulci extremities. The left CS were subjected to a significant larger average positional movement than the right CS. The movement in the medial part of CS is larger than the one in the lateral. The positional movement is not constant from one year to another.

Introduction

The CS is a distinct anatomical landmark on the lateral surface of both cerebral hemispheres that separates the frontal and parietal lobes. The rostral bank of the CS contains the primary motor areas and the caudal bank the primary somatosensory areas [280, 293]. The motor and sensory cortices along the banks of the CS are somatotopically organized according a "homunculus" with representations of the lower part and trunk of the body in the medial superior, the arm, hand, and fingers in the middle, and the face, mouth, and tongue in the inferior part of the sulcus [204, 203].
Studies of the CS are not straight forward, since the superficial appearance of the cortex varies greatly both between and within subjects [199, 280]. The inter subject variability in the folding of the cortex and hence sulci, are a result of an interaction of both environmental and genetic factors factors [166, 205, 16]. A meta study (n=1422) has estimated the genetic variation to account for an individual variation in brain volume in 82.8 % (71.6, 94) of the subjects. The

heritability for the volume of the cerebral cortex is seen in 85.5 % (74.9- 92.2) of subjects (n=748) [25]. The cortical folding is less influenced by the genetics than the brain volume, with a significantly heritable observed in 30 % of individuals. [223]. This heritability in the cortical folding is largely reflected in the average depth of CS, with a 56 % heritability.
The genetics explain the majority of the variation in sulci, however environmental effects, such as prolonged learning or specific training, are well documented to have an effect on the structural changes in the brain [239, 127, 99]. As an example alterations in the neural connectivity is seen as a results of long-term motor skill training in musicians [160]. The training results in a significantly greater local variability in the middle section of CS in musicians than in non-musicians. ([160]. This variability was negative correlated with the age of commencement of musical training, meaning that earlier training induce more variability in the trained region. Another example is left-handers forced to write with their right hand as child. These left-handers displayed an asymmetry in the area of CS typical for right-handers. However the handedness-specific location, known as the "hand knob", remained at the dorsal location typical for left handers [260]. These results show how genetic and environmental factors affects the brain in different ways depending on the timing [45, 26, 254, 257, 166]. A larger heritability is seen in the deeper and earlier developed sulci than in the more superficial. The more superficial sulci are mainly developed after birth, and appear to be more affected by environmental influences [166]. The CS is formed as the fourth sulci in the 18th week of gestational [196, 3], which has prompt several stable features.
The functional topologic delimitation of CS and the stable features has prompt the mapping of e.g. handedness [6, 5, 60, 178, 27], the tongue area [76], location of landmarks [53, 60] and shape changes with motor training [160, 247, 260]. Further neurological disorders has been mapped to the CS morphology in e.g. schizophrenia [86], autism [13], ADHD [161] and Williams syndrome [133, 88].
The development of CS is also studied with respect to age [218, 60, 150], as the brain is ever changing through the span of life. The brain volume is expanding until age 13, and again in a slower rate from 18 to 35. In between these a decrease is seen, with the largest decrease after the age of 60 years [109]. Along with the decrease in brain volume, an age-related decrease is further seen in the gray matter (GM) and white matter (WM) [210, 174, 20], the surface area [219, 60, 256] and the length of both the anterior and posterior banks of CS [162]. The cortical folding increase into the first year in life [9] followed by lifelong reduction [211, 193, 237]. The decrease in folding and brain volume result in more open and less deep sulci with age [150, 164, 162]. Contradictions were found regarding the age-related effects in the average depths in CS. Kochunov et al. (2005) and Rettmann et al. (2006) found a significant reduction in the average sulcal depth with age, while no significant age effects were seen in other studies in average depth [218, 60, 150, 256].
A biological variation in gender exists in the size of the brain, with the weight

of males being 9.6 % greater than that of females (n=1963) [65, 249]. In females the surface area of the left anterior wall and the average width were greater in the left CS than the right [162, 256]. Females also showed greater left bottom length and bilateral top length than males [256]. The sulci width has been shown to be significantly wider in males than in females [162, 256, 164], this was however not found by [150]. However, no gender effects have been found in the depth position profiles [162, 60, 256, 150].
The study of sulci morphology in relation to demographic or genetic findings have spawn many features as e.g. area, top length, bottom length, sulci width, sulci depth, sulci depth profile [162, 6, 60, 130, 5, 150, 186, 244, 161]. The CS morphology have been widely studied using the surface area [160, 162, 161, 150, 218]. The surface area have e.g. shown interhemispheric asymmetry in the surface area with a greater surface contralateral to the dominant hand [146]. The sulci depth profile is an almost matter of cause to characterize the morphology of CS, and have shown to provide good inter subject matching [53, 60, 162]. Sulci depth has especially been used to relate asymmetry in the sulcal depth to functional asymmetry classification [6, 63].
Local vertex positional changes has been used to demonstrate the asymmetry in the surface of the cortex within the first two years of life. This was done by mapping the whole brain toward a common atlas and hence obtaining a one-to-one correspondence for each point on the cortex [159].
The large amount of between-subject variation caused by the environmental and genetic factors reduce the sensitivity in cross-sectional studies to detect changes in cerebral morphology. A longitudinal study of older (age 59-85 years at baseline), spanning a 4-year interval, reported a decreases in cortical GM using a voxel-based analysis [216]. These results were confirmed in other longitudinal study that mapped changes associated with aging in elderly [218, 248].
Evidence from the literature show that the brain undergoes structural changes throughout life. The CS is widely studied, also in relation to age. However the actual change in surface area and the depth profile need to be evaluated in a longitudinal study. In this study we investigate the growth of CS in relation to its morphology in ten repeated measurements throughout childhood and adolescent. The CS is represented by the surface area, depth profile and three dimensional positional variations. All CS were extracted in 3D and the area and depth profile were found. Segmented CS were aligned with a landmark based registration (TPS) to find the position movement in the shape. The repeated measures were tested using mixed models, which allow the correlation within the subjects' observations and residuals to be modeled.

Method and materials

Subjects

Seventy-two typically-developing children and adolescents (27 males, 45 females) aged 8 to 17 years (mean ± SD: 12.24 ± 2.22) from the longitudinal HUBU study (”Hjernens Udvikling hos Børn og Unge” Brain maturation in children and adolescents) [175] participated in this study. This current study build on a cross-sectional study we did, that used the eight assessment round. The subjects in this longitudinal study is based on the segmentations of CS from this study. HUBU is an ongoing project that aims at clarifying the maturation of the brain in children in relation to environmental and genetic influences. Every sixth month the participant's undergone structural MRI and complete behavioral and neuropsychological tests. The children attended three different schools in the Copenhagen area. None of the children have had any known history of neurological or psychiatric disorders or significant brain injury. Subjects were informed about the procedures both written and oral prior to participation. The protocol of the HUBU projects was approved by the local Danish Committee for Biomedical Research Ethics (H-KF-01-131/03) and conducted according to the Declaration of Helsinki.
21 participants were not included in this study. The reasons for exclusion were: Lefthanders (n=7), dental brace (n=8), diagnostic findings (n=2), image artifacts (n=2) and failure to segment CS (n=2). The final sample holds 454 MR images from 51 children (18 males, 33 females) aged 11 to 17 years (mean ± SD: 12.24 ± 2.23). Each subject was been scanned 3 to 10 times (mean 8.9).

Magnetic resonance imaging

MR images were obtained in all subjects on the same 3.0 Tesla Siemens Magnetom Trio Scanner (Siemens, Erlangen, Germany) using an eight- channel surface head-coil (Invivo, Fl, USA). For the present study we only used the acquired T1-weighted three-dimensional high resolution structural magnetization-prepared 180 degrees radio-frequency pulses and rapid gradient-echo (MPRAGE) images of the whole brain (TR = 1550 ms, TE = 3.04 ms, Inversion Time (TI)= 800 ms, matrix 256x256, 192 sagittal slices with no gap, 1 mm^3 isotropic voxels). To insure sufficient image quality a neuroradiologist visually inspected all scans blind to behavioral data. All images were visually inspected by a neuroradiologist.

Image preprocessing

Preprocessing pipelines were implemented in MATLAB, using mainly SPM 8 routines (www.fil.ion.ucl.ac.uk/SPM). Images were corrected for spatial distortions due to scanner gradient non-linearities [136] and oriented to the MNI coordinate system using a six-parameter rigid transformation using mutual information (i.e. no scaling). The quality of each processing step was visually inspected by an expert.

Segmenting CS

The segmentation of CS was done in two steps. The first step segmented all sulci from one round. The next step extracts all sulci based on correspondence from the sulci in step 1 to the other rounds. This correspondence was found based on a within-subject registration. Registration based segmentation is solid method, that have been widely used to describe sulci morphology [15, 206, 170, 266].

Step 1: Segmenting sulci
The CS was segmented using BrainVisa 4.3.0 [178]. BrainVisa is an image processing software, that hold a number of functions to extract and manipulate sulci. In BrainVisa a sulcus is represented as a three-dimensional mesh of the medial surface of a sulcus. A mesh consists of vertices, that represent the coordinates of the sulci, and edges that associate these vertices. The pipeline to segment a sulcus, "Morphologist 2012", contain the following operations: Removal of skull, spatial normalization to MNI, bias field correction, tissue segmentation, extraction of gray matter, white matter, and cerebrospinal fluid (CSF), extraction of sulcal folds and automated labeling of sulci. One female had to be excluded, since the CS was split in two and failed to be extracted. 81 % of the extracted sulci had either holes or attachments of parts of surrounding sulci and were subsequently manually corrected using standard guidelines in MeshLab (CNR 2015).

Step 2: Registration based segmentation
To segment sulci from all rounds, an average brain for each subject was created using DARTEL (Diffeomorphic Anatomical Registration using Exponentiated Lie algebra) [12]. This average brain holds the within subject correspondence from the segmented sulci to all other rounds.
Co-registrated T1 images were segmented into gray matter and white matter and used in a probability map. To remove extra cerebral tissue from the gray matter and white matter segmentations, brain masks were generated based on T2 co-registered images. These tissue maps are then feed to the high dimen-

sional warping tool DARTEL implemented in SPM8 [12]. DARTEL warp each subjects' image into a within-subject template. The resultant correspondences is used to find the corresponding sulci in the other rounds. The result of this segmentation is verified by segmenting the left and right CS from all 10 rounds in one subject using BrainVisa.

Between subject point correspondence

To bring all extracted CS in a standard coordinate space we used Landmarker [61]. Landmarker is a 3D software tool that enables manual annotations of landmarks in 3D. Landmarker further holds 3D registration based on Thin Plate Splines (TPS), which is a non-linear registration that brings surfaces of comparable anatomy into spatial correspondence [28]. The basic idea behind TPS is to model the deformation of thin metal plates that pass through a set of knots in order to minimize the bending energy. The landmarks on the template are perfectly overlapped with corresponding landmarks on each sulcus. All other points on the template were transformed using TPS. The result is an overlap that was refined using closest point deformations and establish a point to point correspondence.
Our registration is based on one subjects left and right CS. This template was chosen between the 5 subjects with the best resolution. We chose eight landmarks; the medial and lateral endpoints and six landmarks on the hand knob (Figure 10.1). Coulon et al. (2011) have showed that by matching two landmarks on the handknob the inter-subject matching was improved [53].

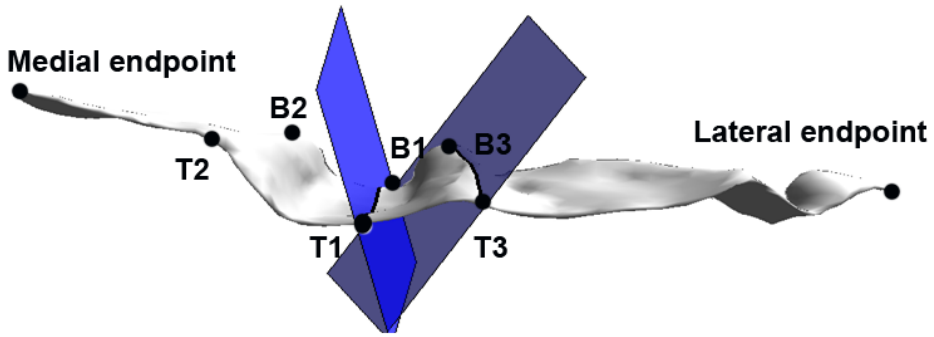

Figure 10.1: Eight landmarks were used in the between subject registration of CS. The location of the eight landmarks mapped onto CS: Medial endpoint, T1, T2, T3, B1, B2, B3 and the dorsal endpoint.

The medial and lateral endpoints of all sulci were found as the most superior

medial point and the most inferior dorsal point. All endpoints were visually inspected, and manually correction was performed in 14 % of all points. Correction of endpoints were done when the extremities resembled a straight line rather than a point. In these cases the endpoints were chosen as the middle point on this line. Based on the endpoints the top ridge and bottom ridge of the CS were subsampled into 100 equal spaced points.
Based on the distances from the 100 point on the top ridge and the bottom ridge to the plane of inertia, the minimum distance marked a landmark as the deepest part of the handknob Figure 10.1 (B1, T1). The two local maxima distances at each side of this minimum marked the landmarks of the medial (B2,T2) and lateral (B3,T3) border of the handknob (Figure 2). 14 % of the landmarks needed manual correction due to the large variety in CS shape.
The plane of inertia was spanned by the two first eigenvectors of CS. A sulcus can be represented as $S = \{X_i, Y_i, Z_i\}$, with $i = 1, ..., N$ and N being the number of vertices. The eigenvectors (P) and eigenvalues (Λ) of the covariance matrix $\Sigma = (N-1)^{-1} \sum_{i=1}^{N} (S_i - \overline{S})(S_i - \overline{S})$ can be found by $\Sigma P = \Lambda P$. The first two eigenvectors, p_1 and p_2, associated with the maximum eigenvalues yields the orientation of the plane. The third eigenvector, p_3, is the unit normal vector. The distance between a point on the sulcus and the plane of main direction is calculated as: $D_i = p_3 \cdot (S_i - \overline{S})$.

Sulcal area and depth profile

The area of CS was found by summing the area of all faces of the sulcus, which is found as the cross product of the two sides in a face, divided by 2. Sulcal depth profiles treat each depth along the CS as a continuous variable. The depth profile is found as the geodesic distance between the 100 equidistantly points along the CS fundus and top ridge. The depth profiles had position 1 at the most superior lateral point near the interhemispheric fissure. This method was inspired by the depth profile in McKay et al. (2013), they however allowed the depths to cross as they the depths had to be orthogonal to the top ridge. We experienced large errors especially in the ends using this approach, and restricted the depths not to cross.

Positional movement

The positional movement is found as the median positional movement from the first round to the last within subjects. The magnitude of this positional movement is found along with its median direction (x, y and z). A drawback of this method is the mixed ages. A second illustration deals with this problem, by

calculated the average within subject movement in a year. As each subject is not scanned on their birthday every year, a linear interpolation was made to estimate the position between rounds. By doing so each subject had measurement at comparable ages, and the movement from one year to the next could be calculated.

Statistics

Statistical analyses were done using SAS 9.4. A p-value below 0.05 was considered significant.
Gaussian distribution of CS surface area, depths along the CS and mean CS depth were evaluated with the Shapiro-Wilk test.
To model the repeated measurements of each subject we used linear mixed model. Mixed models accounts for the correlations of observations and their residuals (Hammond 2002). Age in years is the time scale at which the measurements were repeated. A Mixed model contains both fixed effects and random effects:

$$Y = X\beta + Z\gamma + \varepsilon \tag{10.1}$$

Where Y is the dependent variable, X was the design matrix and β its corresponding parameters for the fixed effects, Z is the design matrix and γ is the associated parameters for random effects. In the random effect we modeled that the measurements were grouped into subject [104]. We modeled the covariance structure imposed upon the residuals, by a spatial power covariance function. This is a continuous-time model to describe the covariance's among the errors, that account for the irregularly for of time intervals between measurement. In this model the correlations decline as a function of time:

$$D(\epsilon_{ij}, \epsilon_{i'j}) = \sigma^2 \rho^{di'j} \tag{10.2}$$

$D(\epsilon_{ij}, \epsilon_{i'j})$ is the covariance matrix of the errors ϵ between time i and time i' for subject j, σ^2 is the variances of the errors and $\rho^{di'i}$ is the correlation of the errors measured at distance, d, between the time i and the next i'.
Mixed models were used to the development of the surface area, the mean depth and each depth along the sulci. Two subgroup, males and females, were used to evaluate the gender effects. Testing each of the depths along the CS, the results were to control for multiple comparisons by the false discovery rate (FDR).
All statistic tests were corrected for the total brain volume. This was done as the total brain volume are significant correlated with the surface area (left: 0.46, $p<0.0001$, right: 0.67, $p<0.0001$) and the mean depth (left: 0.36, $p<0.0001$, right: 0.26, $p<0.001$). GM, WM and CSF volumes were calculated using SPM8. The t and the p value were given for each test. Group data are given as mean SD.

Results

Sulcal area

The CS areas are summed in Table 10.1. We found that the left sulci area (1400.01 mm^2) were significantly larger than the right CS (1373.73 mm^2) (t=19.45, p<0.0001). This was also the case in both males (left: 1484 mm^2, right: 1449.7.6 mm^2) and females (left: 1352.7 mm^2, Right: 1313.6 mm^2), where the left sulci area CS was significant larger than the right (female: t=10.06, p<0.0001, males: t=15.61, p<0.0001).

	CS area	**Average CS depth**
Left	1400.5 ± 169.05	13.71 ± 13.60
-Male	1484 ± 178.60	14.03 ± 13.60
-Female	1352.7 ± 143.00	13.53 ± 1.15
Right	1373.75 ± 159.95	12.54 ± 1.08
-Male	1313 ± 157.25	14.04 ± 1.17
-Female	1352 ± 144.80	13.26 ± 0.91

Table 10.1: The mean and standard division of the CS area and average depth, for the left and right CS in males and females.

The growth of the left sulcal area displayed a significant negatively reduction with age (t=-2.48, p=0.0136). The right sulci area also decreased, however this failed to reach significance (t=-1.75, p<0.081).
A gender effect were seen for the left sulcal area (t=-2.43, p=0.019). The decrease in right sulcal area showed a trend in gender effects (t=-2.00, p<0.051). No gender effects were seen for the left CS.
In the female subgroup the right CS decreased significantly (t=-2.04,p=0.042), this was not seen in the male subgroup (t=0.04, p=0.966). In the female subgroup the left sulcal area showed a significant decrease in time (t=-2.57, p=0.011), that did not reach significant in the right sulci (t=-0.62, p=0.534).
We found no interaction of age and gender on the sulcal area or mean depth in time.

Sulci depth

An overview of the average depth in left and right sulci and in males and females are found in table 10.1. The left sulci has a mean depth of 13.71 mm and is significant deeper than that of the right 13.53 mm. This difference between the left and right average is seen in both males (t=9.87, p<0.0001) and female (t=2.21, p=0.028).
A trend is observed in the decrease of average depth of the left CS in time (t= -1.91, p=0.057). The right average depth does not decrease significantly in time (t=-1.02, p=0.307). Either the males or females subgroups reached significance (male -1.64, p=0.104; female: -0.81, p=0.415).
Testing each of the 100 depths along the CS no gender effects (left: average p=0.36; right: p average=0.56) or change in depth is seen in time (left: p average=0.87, right: p average=0.67). The depth is significantly explained by the total brain volume in all positions.

Positional movement

The median positional movement is largest in the sulci extremities (Figure 10.2). The left sulci in general experience a significant bigger median positional movement (0.44 mm), than the right CS (0.35) (t=19.09, p<0.001). In the left CS the average positional movement is significantly greater in the medial proportion (average: 0.41 mm) than the lateral (average: 0.47 mm) (t=11.36, p<0.0001). The same is seen in the right CS, where the medial movement (0.47 mm) also is significantly bigger than the lateral (0.41 mm) (t=-5.64, p<0.0001).

The average movement of each point on CS within a year is illustrated in (Figure 10.3). In the right CS the movement decreased with age in the extensions. In the lateral end of the right CS the movement is mainly seen in the depths, where the medial end only involve the most medial positions. The left CS however show an increase of positional movement in the medial extension.

Discussion

In this study we set out to describe the changes in CS morphology from age 8 to 17 in a longitudinal study, with an average of 8.9 assessment rounds. The shape of CS was represented by the surface area, the average depth, the depth position profile and finally the positional change within CS in time. We have found a reduction in surface area in time in the left surface areas. No gender effects are observed, however the female subgroup show a significantly reduced

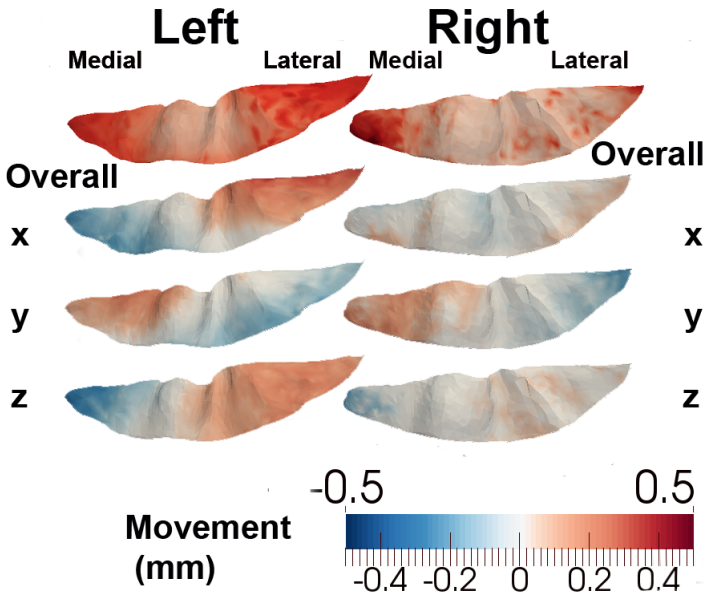

Figure 10.2: Median positional movement of each point on CS from each subjects first scan to the last. At the top, the overall average movement, below the movement in the x, y and z direction. Medial is at the left and lateral is at the right.

area in both the right and left CS in time. The average positional movement from the first scan to the last is primary observed in the sulci extremities, with the left sulci subjected to a general larger average positional movement than the right CS. In both hemispheres the medial movement is larger than the lateral. The movement from one year to the next show that the positional movement is not stable in time.

Surface area

We found the surface area in the left CS to bigger than the right, this result is line with other studies [5, 178, 60]. The brain is ever changing through life and this involve an age-related decrease in GM volume along with WM volume [20, 100, 230, 24]. The gyrification has been shown decreasing with age in most of the cortical regions [145, 19, 250]. The atrophy in the cortical lobes prompt the sulci to become wider and less deep [60, 150, 218]. In our study we found

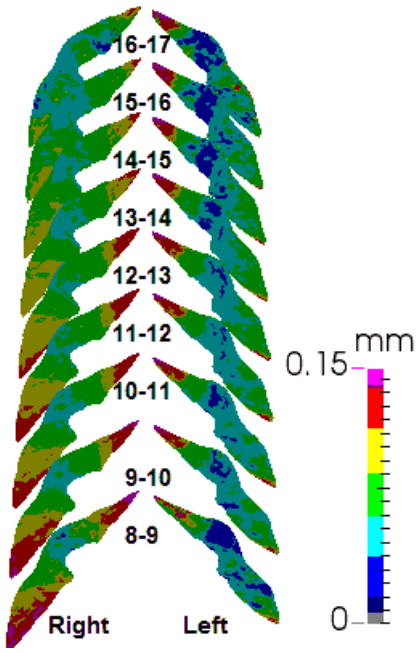

Figure 10.3: The average movement within one year for each subject.

a significant reduction of the left area in time, the decrease in the right CS did however only show a trend (p=0.08).

Depth

The average depth was 16.6 ± 1.3 mm for the left CS and 16.4 ± 1.2 mm for the right CS. This results is comparable to other studies [63, 60, 161, 256]. The left mean depth is significantly deeper than the right, which is also in line with the previous findings [6, 60].
We found no significant decrease in the average depth in time, however a trend is observed in left CS (p=0.057). The mean depth measure how far the sulci extends into the cortex on average. In time as the gyrification lowers this mean depth it is also lowered. Discrepancies are found in the relation of average depth in age. Kochunov et al (2005) found a decrease in the average depth of CS in healthy subjects (n=90) aged 20 to 82 years, based on structural segmentation of CS. This was also reported by Rettmann et al. (2006) in a longitudinal study with 35 adults aged 58 to 84 years [218]. This result was however not confirmed

in other studies [60, 256, 162]. Cykowski et al. (2008) studied 55 healthy subjects from the age of 21 to 89 and found a leftward asymmetry in the depth profile, but no correlation between the mean average depth and age. A study with a large sample (n=295) aged 19 to 94, investigated the effect of several sulci features in ageing, but found no age-related changes in the mean depth [162]. A recent study with 112 healthy participants aged 18 to 27, studying the morphology in CS in relation to age and gender also found no effects of age on the mean depth.

Gender

We found that females showed a significantly bilateral decrease in the sulcal area, not seen in males. Another longitudinal study found a decrease in the surface area (n=35) aged 69 to 84 years. However the gender effect was not investigated. Li et al. (2011) found greater left surface area in the anterior wall [162]. Gender effects are in the literature generally not consistent, since the correction for differences between males and female brain volume, is done either using different metrics or not done at all. Sowell et al. (2002) used height as a covariate in establishing gender effects [249]. Rettmann et al (2006) controlled cross-sectional results with intra cranial volume, however not in their longitudinal analysis. We observed significant correlation between the brain volume and both sulcal areas, the average sulci depth and the total brain volume. A meta study based on 56 longitudinal studies of healthy individuals (n=2211) aged 4 to 88, map the annual brain volume in time. A weighted regression analysis was used to calculate a 1 % increase in brain volume until the age of 13. From age 13 the volume gradually decreases until the age of 18. We observed an average positive increase in of 0.14 % a year in total brain volume in our sample. This is very small increase, however the total brain volume in our study reached significance in all tests.

Average positional movement

We wanted to investigate the positional movement of each vertex. All sulci were aligned by a TPS registration. The results show that the median positional movement within subject is largest in the sulci extremities. This result is in line with another study evaluating the cross-sectional movement in 295 subjects aged 18 to 94 [162]. To obtain correspondence across subjects they produced a surface representation based on the outlined CS boundary, which was originally described by Thompson et al. (1996) [267]. This method did, as we did, match the medial and lateral endpoints, and forced the boundary to match. One

variation is that we force the ”hand knob” across subjects to be aligned, based on a study improving the inter-subject alignment in by doing so [53].
Li et al. (2011) found the posterior walls to decrease faster than the posterior walls. In the posterior walls the left decreased faster than the right. This result is in agreement with our results, were we found an overall greater average positional movement in the left CS. We found a bilateral average positional movement that was significantly greater in the medial proportion than the lateral.
We found that the development of the CS is not constant in time. This can be seen on Figure 10.3, were some areas increase in positional movement and other decrease. Reznahan et al. (2011) found that the cortical folding decrease in adolescence, which was supported by Multu et al. (2013) that also found a reduction in the folding from age 6 to 29. In line with other studies we also found a decrease in surface area and depth, however our results show that the decrease might locally both increase and decrease.

Study Limitations

The extraction of CS for the longitudinal data was based on a registration based segmentation. This was done to handle the within subject errors introduced by the 3D manual corrections. A registration based segmentation is a fast way to obtain a god segmentation [14]. We used the registration method, DARTEL, which have shown to be among the most reliable [145]. DARTEL align images based on volumes of gray matter and white matter. It could be hypothesized that a surface based registration could align sulci better. However, the segmented sulci have been visually inspected to consolidate with a standard segmentation. Further the segmentation is done within subjects, which improves and the result of any registration.

Appendix A

Extracting Central Sulcus in BrainVisa

This chapter describe a pipeline to obtain a segmented Central Sulcus (CS). To extract CS an existing software, BrainVISA, is used [178]. CS has shown to have a frequency of accurate recognition of CS in $> 96\%$ [178]. BrainVISA is developed by the french government founded research organizations in a grouped federative research institute: IFR 49. BrianVISA is a free and open-source software written in Python. The BrainVISA project is focused on neuroimaging only in the context of research. BrainVISA offers a database manager and gives automatically access to the visualization tool Anatomist.

Step 1: Download BrainVISA

Download BrainVISA from: `http://www.brainvisa.info/download.html` and run "BrainVISA.bat". Version 4.3.0 is used (the newest at the date of writing).

To access all functionalities in BrainVISA the user level have to be "expert":

BrainVISA -> Preferences -> BrainVISA

- `userLevel`: Choose `expert` in the dropdown menu
- Click `ok` to close the preference panel

Step 2: Create database

The next step is to create a database in BrainVISA to hold both input data and results (Figure A.1.).

BrainVISA -> Preferences -> Databases ->Add

1. Click on the select input directory icon
2. Navigate to the location where the database should be located
3. Create a new folder that holds the name of the database
4. Click `Choose`
5. Click `ok` to add the database
6. Click `ok` to close the preference panel

Step 3: Import images into BrainVISA

The NiFTI images needs to imported into the created database.

Morphologist -> Import -> Import T1 MRI

1. Click `Iterate`
2. Input: Click on the select input directory icon
    - Navigate to the location of the NiFTI images
    - Click `Open`
    - Click `Ok`
3. Output: Click on the output database icon (red)

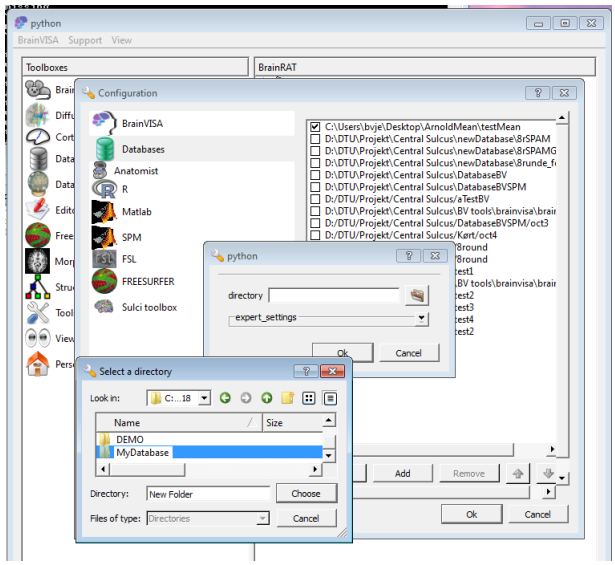

Figure A.1: To access input data and to store the results a database needs to be created.

- Database: Choose the database created in step 2
- Data type: Raw T1 image
- File format: NIFTI-1
- Protocol: Name the protocol
- Subject: Subject names have to be entered manually (e.g. *Test*1 *Test*2 ...)
- Mark all files in the upper right window "Resultats du filtre"
- Click `Ok`

4. Click `Ok`

5. An overview is given of the import. Click `Run`

A status will be given for each image. A correction mark in front of a subject insure that the image has been imported successfully (Figure A.2).

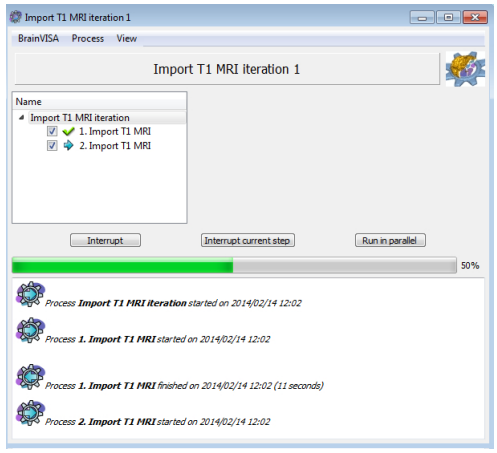

Figure A.2: Import of NiFTI images into BrainVISA. An overview is given of the process.

Step 4: Label sulci

The sulci in the brain is labeled in a pipeline in BrianVISA. This pipeline include 12 steps that include all steps from bias correction of the MR image to the location of the sulci in brain to a final labeling of all sulci. The sulci are represented by the medial surfaces of 2 opposing gyral banks [178].

`Morphologist-> Morphologist 2012`

1. Scroll down to the check up box `Sulci Recognition (both hemispheres)` and check it of
2. A window will appear that allows one to download the SPAM model. This step is only done once:
   - Click `Yes`.
   - Destination_database_directory: Click on the select input directory icon
   - Navigate to a location where the SPAM model should be saved
   - Click `Run`
   - Close the SPAM model installation window
3. In the window `Sulci Recognition (Both hemispheres)`

- Side: Both
- Model: SPAM
- Spam_model: Global+local

4. Click `Iterate`
5. MRI: Click on the input database icon (green)
   - Database: Choose the database created in step 2
   - Data type: Raw T1 MRI
   - File format: NIFTI-1
   - Protocol: Choose the protocol name that was created in step 3.
   - Mark all files in the upper right window "Resultats du filtre"
   - Click `Ok`
6. MRI_corrected: Click on the output database icon (red)
   - Database: Choose the database created in step 2
   - Data type: T1 MRI Bias Corrected
   - File format: NIFTI-1
   - Protocol: Choose the name the protocol was given
   - Subject: Subject names have to be entered manually (e.g. $Test1$ $Test2$ ...)
   - Mark all files in the upper right window "Resultats du filtre"
   - Click `Ok`
7. Normalised: Click `...`
   - Choose `MNI from SPM`
   - Click `Add` the same number of times as there is images to be imported
   - Click `Ok`
8. Click `Ok`
9. An overview is given of the morphologist pipeline. Click `Run`

A status will be given for each subject (Figure A.3). A correction mark in front of a subject ensures that the pipeline have been processed successfully.

The output sulci will be stored in the BrainVISA sulci graphs format (.arg) and holds both a mesh and a voxel list of the CS.

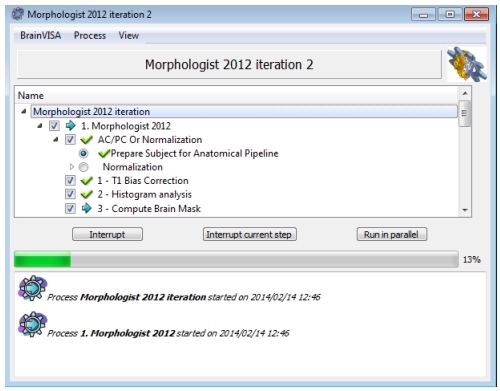

Figure A.3: BrainVISA encompass a pipeline that contain all the steps in labeling the sulci in the brain.

Step 5: Extracting central sulcus

The next step is to extract just the CS.

`Morphologist-> Sulci-> Recognition-> Create Sulcus Volume`

1. Click `Iterate`
2. Graph: Click on the input database icon (green)
   - Database: Choose the database created in step 2
   - Datatype: Labeled cortical folds
   - File format: Graph and data
   - Protocol: Choose the protocol that was created in step 3
   - Side: left
   - Mark all files in the upper right window "Resultats du filtre"
   - Click `Ok`
3. MRI: Click on the input database icon (green)
   - Database: Choose the database created in step 2
   - Data type: T1 MRI Bias Corrected
   - File format: NIFTI-1 image
   - Protocol: Choose the protocol name that was created in step 3

- Mark all files in the upper right window "Resultats du filtre"
- Click `Ok`

4. Sulci: Click on the output database icon (red)
   - Database: Choose the database created in step 2
   - Data type: Sulci Volume
   - File format: NIFTI-1 image
   - Protocol: Choose the protocol that was created in step 3
   - Graph version: 3.1
   - Side: Left (or Right)
   - Manually_labelled: No
   - Automatically_labelled: Yes
   - Best: No
   - Labelled: Yes
   - Mark all files in the upper right window("Resultats du filtre")
   - Click `Ok`
5. Label_values: S.C._left or S.C._right
6. Click `Ok`
7. An overview is given of the import. Click `Run`

A status will be given for each image (Figure A.4). A correction mark in front of a subject means that the CS have been found successfully. The extracted CS are NifTI images.

Step 6: Visually inspection

To perform a visually inspect of the extracted sulci an option is to convert the NifTI files into a mesh.

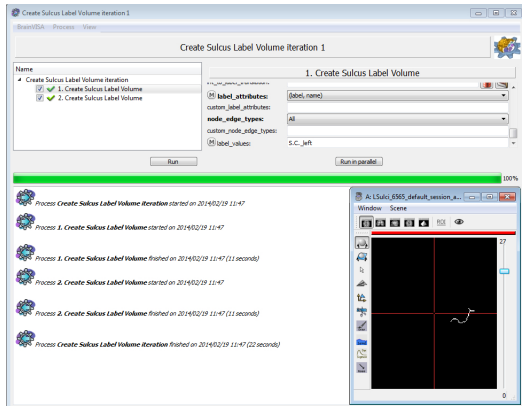

Figure A.4: Extraction of the CS in BrainVISA. One of the extracted CS is here visualized along with an overview of the process.

Convert CS into mesh

BrainVisa holds a number of commands called AIMS (Analyse d'IMage et de Signaux -Image and signal analysis). These commands can be run outside BrainVISA from a batch.

All sulci are converted into a mesh (.ply) for visual inspection by the `AimMeshBrain` command:

```
AimsMeshBrain -i L6565.nii -o L6565.ply
```

The AimsMeshBrain command also include morphological operations that remove noise.

Visualizing the mesh

In connection to BrainVISA a visualization software is developed called Anatomist. Anatomist is downloaded along with the BrainVISA package. Several images can be dragged to the same image enabling a detailed inspection of the extracted sulci (Figure A.5).

1. Run "anatomist.bat".

2. File-> Open
3. Choose a whole brain image (.nii)
4. File-> Open
5. Choose the sulci mesh (.ply)
6. Drag the two image to a chosen view (3D, Axial, Sagittal, Coronal)
7. Hold down the middle button on the mouse to rotate the image in 3D. The extraction of CS can now be inspected in all orientations.

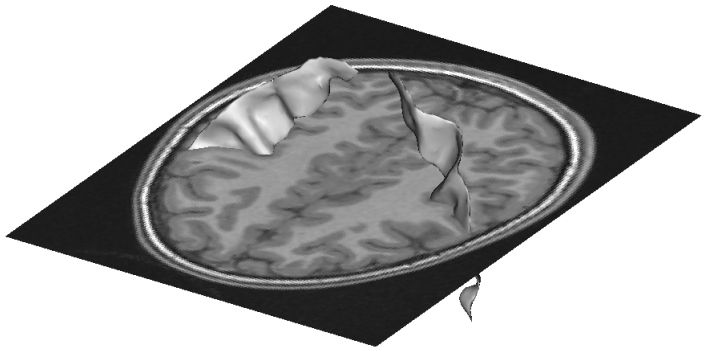

Figure A.5: Visual inspection of the sulci in Anatomist.

Step 7: Correcting sulci

The extracted sulci often show parts of connected side sulci or missing parts of the sulci.

To much sulci extracted

Superfluous sulci can be removed in bigger parts in BrainVISA and by manually editing.

Removing bigger parts in BrainVISA

If other sulci are extracted along with CS, the extracted sulci can be split up into minor objects. The objects that make up the sulci can be selected and merged.

To split the extracted sulci into one mesh for every object `AimsMesh` is used:

```
AimsMesh -i L6565.nii -o L6565.ply
```

Afterwards the meshes that make up central sulcus can be joined by using `AimsZCat`:

```
AimsZCat -i L6565_1_0.ply L6565_1_3.ply -o jointed6565.ply
```

Manually editing

Manually editing can be used to remove additional sulci. This can be accomplished in a free program called MeshLab (Figure A.6).

Download MeshLab from `http://meshlab.sourceforge.net/Download`

1. Open a mesh `File-> Import mesh`
2. Click `Select vertexes` in the menu
3. Mark the vertexes that are not a part of the sulci
4. Click `Delete the current set of selected vertices`
5. Close holes (if needed): `Filters -> Remeshing, Simplifications and Reconstructing -> Close holes`
6. Change `Max size to be closed` (the default will do fine in most cases)
7. Click apply
8. To save the mesh: File-> Export Mesh

.

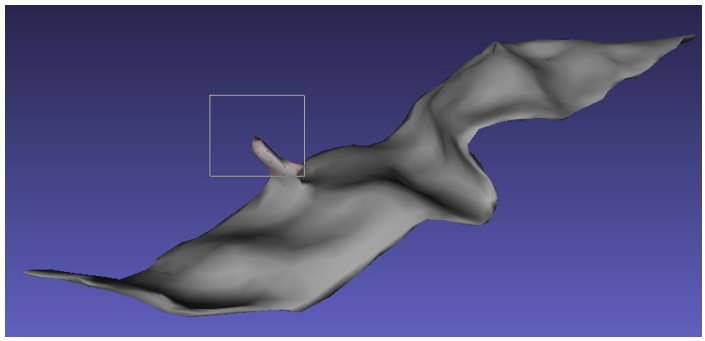

Figure A.6: Manually editing of a mesh in MeshLab. Vertices can be selected and afterwards deleted.

Restoring missing sulci

If parts of a CS is missing other candidate sulci from the same side of the brain can adding or another model can be used in BrainVISA.

Adding other candidate sulci

If parts of CS is missing other meshes from the same side of the brain can be fused with an extracted sulcus. To do this the same steps must be taken as in chapter A.

Extraction of sulci using other models

If the entire sulci is not extracted an alternative approach is to use another model in BrainVISA. The SPAM model could for example be run with the another method (global or Talairach) or the model could be changed to ANN. In this way other models may fit the sulci better and an initial extracted sulci can be extracted.

Bibliography

[1] Nasreddin D. Abolmaali, Volker Hietschold, Thomas J. Vogl, Karl-Bernd Huttenbrink, and Thomas Hummel. MR Evaluation in Patients with Isolated Anosmia Since Birth or Early Childhood. *AJNR Am. J. Neuroradiol.*, 23(1):157–164, 2002.

[2] Daniel J Acheson and Peter Hagoort. Stimulating the brain's language network: syntactic ambiguity resolution after TMS to the inferior frontal gyrus and middle temporal gyrus. *Journal of cognitive neuroscience*, 25(10):1664–77, oct 2013.

[3] Afif Afif, Jacqueline Trouillas, and Patrick Mertens. Development of the sensorimotor cortex in the human fetus: a morphological description. *Surgical and radiologic anatomy*, 37(2):153–160, 2014.

[4] H. Alkadhi and Spyros S. Kollias. Pli de passage fronto-parietal moyen of Broca separates the motor homunculus. *American Journal of Neuroradiology*, 25(May):809–812, 2004.

[5] K. Amunts, L. Jäncke, H. Mohlberg, H. Steinmetz, and K. Zilles. Interhemispheric asymmetry of the human motor cortex related to handedness and gender. *Neuropsychologia*, 38(3):304–12, jan 2000.

[6] K. Amunts, G. Schlaug, A. Schleicher, H. Steinmetz, A. Dabringhaus, P. E. Roland, and K. Zilles. Asymmetry in the human motor cortex and handedness. *NeuroImage*, 4(3):216–222, dec 1996.

[7] A.K. Anderson, K. Christoff, I. Stappen, D. Panitz, D. G. Ghahremani, G. Glover, J.D.E. Gabrieli, and N. Sobel. Dissociated neural representa-

tions of intensity and valence in human olfaction. *Nature Neuroscience*, 6(2):196–202, 2003.

[8] Yoko Arai and Alessandra Pierani. Development and evolution of cortical fields. *Neuroscience research*, 86:66–76, sep 2014.

[9] E. Armstrong, M. Curtis, D. P. Buxhoeveden, C. Fregoe, K. Zilles, M. F. Casanova, and W. F. McCarthy. Cortical gyrification in the rhesus monkey: a test of the mechanical folding hypothesis. *Cerebral cortex*, 1(5):426–32, jan 1991.

[10] E. Armstrong, A. Schleicher, H. Omran, M. Curtis, and K. Zilles. The ontogeny of human gyrification. *Cerebral cortex (New York, N.Y. : 1991)*, 5(1):56–63, jan 1995.

[11] J. Ashburner, P. Neelin, D. L. Collins, A. Evans, and K. Friston. Incorporating prior knowledge into image registration. *NeuroImage*, 6(4):344–52, nov 1997.

[12] John Ashburner. A fast diffeomorphic image registration algorithm. *NeuroImage*, 38(1):95–113, 2007.

[13] G. Auzias, M. Viellard, S. Takerkart, N. Villeneuve, F. Poinso, D. Da Fonséca, N. Girard, and C. Deruelle. Atypical sulcal anatomy in young children with autism spectrum disorder. *NeuroImage: Clinical*, 4:593–603, 2014.

[14] Guillaume Auzias, Joan Glaunès, Olivier Colliot, Matthieu Perrot, Jean-François Mangin, Alain Trouvé, and Sylvain Baillet. Medical Image Computing and Computer-Assisted Intervention. Technical Report 1, ., jan 2009.

[15] Brian Avants and James C Gee. Geodesic estimation for large deformation anatomical shape averaging and interpolation. *NeuroImage*, 23 Suppl 1:S139–50, jan 2004.

[16] W F Baaré, H E Hulshoff Pol, D I Boomsma, D Posthuma, E J de Geus, H G Schnack, N E van Haren, C J van Oel, and R S Kahn. Quantitative genetic modeling of variation in human brain morphology. *Cerebral cortex (New York, N.Y. : 1991)*, 11(9):816–24, 2001.

[17] Helen Barbas. Organization of cortical afferent input to orbitofrontal areas in the rhesus monkey. *Neuroscience*, 56(4):841–864, 1993.

[18] S. H. Barondes, B. M. Alberts, N. C. Andreasen, C. Bargmann, F. Benes, P. Goldman-Rakic, I. Gottesman, S. F. Heinemann, E. G. Jones, M. Kirschner, D. Lewis, M. Raff, A. Roses, J. Rubenstein, S. Snyder, S. J. Watson, D. R. Weinberger, and R. H. Yolken. Workshop on schizophrenia.

Proceedings of the National Academy of Sciences of the United States of America, 94(5):1612–4, mar 1997.

[19] A. J. Bartley, D. W. Jones, and D. R. Weinberger. Genetic variability of human brain size and cortical gyral patterns. *Brain : a journal of neurology*, 120:257–69, feb 1997.

[20] George Bartzokis, Jeffrey L. Cummings, David Sultzer, Victor W. Henderson, Keith H. Nuechterlein, and Jim Mintz. White matter structural integrity in healthy aging adults and patients with Alzheimer disease: a magnetic resonance imaging study. *Archives of neurology*, 60(3):393–8, mar 2003.

[21] Kirsten J Behnke, Maryam E Rettmann, Dzung L Pham, Dinggang Shen, Susan M Resnick, Christos Davatzikos, and Jerry L Prince. Automatic classification of sulcal regions of the human brain cortex using pattern recognition sulcal region gyrus. In *SPIE Med. Imaging*, volume 5032, pages 1499–1510, 2003.

[22] G. Van Belle, Ld Fisher, Pj Heagerty, and T. Lumley. Longitudinal Data Analysis. *Biostatistics: A Methodology for the Health Sciences*, pages 1–63, 2004.

[23] Sarah-Jayne Blakemore. Imaging brain development: the adolescent brain. *NeuroImage*, 61(2):397–406, jun 2012.

[24] D. D. Blatter, E. D. Bigler, S. D. Gale, S. C. Johnson, C. V. Anderson, B. M. Burnett, N. Parker, S. Kurth, and S. D. Horn. Quantitative volumetric analysis of brain MR: normative database spanning 5 decades of life. *AJNR. American journal of neuroradiology*, 16(2):241–51, feb 1995.

[25] Gabriëlla A M Blokland, Greig I de Zubicaray, Katie L McMahon, and Margaret J Wright. Genetic and environmental influences on neuroimaging phenotypes: a meta-analytical perspective on twin imaging studies. *Twin research and human genetics : the official journal of the International Society for Twin Studies*, 15(3):351–71, jun 2012.

[26] William T Blows. Child brain development. *Nursing times*, 99(17):28–31, jan 2003.

[27] Warren W Boling and André Olivier. Localization of hand sensory function to the pli de passage moyen of Broca. *Journal of neurosurgery*, 101(2):278–83, aug 2004.

[28] F. L. Bookstein. Principal warps: thin-plate splines and the decomposition of deformations. *IEEE Transactions on Pattern Analysis and Machine Intelligence*, 11(6):567–585, jun 1989.

[29] Nicholas E Bowman, Konrad P Kording, and Jay A Gottfried. Temporal Integration of Olfactory Perceptual Evidence in Human Orbitofrontal Cortex. *Neuron*, 75(5):916–927, 2012.

[30] P. Broca. M \'{e} moires d'anthropologie. Technical report, Paris: Reinwald., 1888.

[31] Steven Brown, Roger J Ingham, Janis C Ingham, Angela R Laird, and Peter T Fox. Stuttered and fluent speech production: an ALE meta-analysis of functional neuroimaging studies. *Human brain mapping*, 25(1):105–17, may 2005.

[32] R. D. Bucholz. The central sulcus and surgical planning. *AJNR. American journal of neuroradiology*, 14(4):926–7, jan 1993.

[33] Silvia Budday, Paul Steinmann, and Ellen Kuhl. Physical biology of human brain development. *Frontiers in Cellular Neuroscience*, 9(July):1–17, 2015.

[34] Kate Bunton. Speech versus nonspeech: different tasks, different neural organization. *Seminars in speech and language*, 29(4):267–75, nov 2008.

[35] Hartmut P. Burmeister, Thomas Bitter, Patrick M. Heiler, Andrey Irintchev, Rosemarie Fröber, Matthias Dietzel, Pascal a. Baltzer, Lothar R. Schad, Jürgen R. Reichenbach, Hilmar Gudziol, Orlando Guntinas-Lichius, and Werner a. Kaiser. Imaging of lamination patterns of the adult human olfactory bulb and tract: In vitro comparison of standard- and high-resolution 3T MRI, and MR microscopy at 9.4T. *NeuroImage*, 60(3):1662–1670, 2012.

[36] Hartmut Peter Burmeister, Pascal Andreas Thomas Baltzer, Constanze Möslein, Thomas Bitter, Hilmar Gudziol, Matthias Dietzel, Orlando Guntinas-Lichius, and Werner Alois Kaiser. Reproducibility and Repeatability of Volumetric Measurements for Olfactory Bulb Volumetry: Which Method Is Appropriate? An Update Using 3 Tesla MRI. *Academic Radiology*, 18(7):842–849, 2011.

[37] D Buschhüter, M Smitka, S Puschmann, J C Gerber, M Witt, N D Abolmaali, and T Hummel. Correlation between olfactory bulb volume and olfactory function. *NeuroImage*, 42(2):498–502, 2008.

[38] J. A. Butman and M. K. Floeter. Decreased thickness of primary motor cortex in primary lateral sclerosis. *AJNR. American journal of neuroradiology*, 28(1):87–91, jan 2007.

[39] Mariano Cabezas, Arnau Oliver, Xavier Lladó, Jordi Freixenet, and Meritxell Bach Cuadra. A review of atlas-based segmentation for magnetic

resonance brain images. *Computer methods and programs in biomedicine*, 104(3):e158–77, dec 2011.

[40] Pascal Cachier, Xavier Pennec, Denis Rivi, Nicholas Ayache, Dimitri Papadopoulos-orfanos, and R Jean. Multisubject Non-rigid Registration of Brain MRI Using Intensity and Geometric Features. *Miccai*, 16:734–742, 2001.

[41] Alfred Campbell. Histological studies on the localisation of cerebral function. *Cambridge University Press. Cambridge, UK*, 1905.

[42] S. T. Carmichael, M. C. Clugnet, and J. L. Price. Central olfactory connections in the macaque monkey. *Journal of Comparative Neurology*, 346(3):403–434, 1994.

[43] Lisa Cashmore, Natalie Uomini, and Amandine Chapelain. The evolution of handedness in humans and great apes:a review and current issues. *J Anthropol Sci*, 86:7–35, jan 2008.

[44] Pauline Chatagny, Simon Badoud, Mélanie Kaeser, Anne-Dominique Gindrat, Julie Savidan, Michela Fregosi, Véronique Moret, Christine Roulin, Eric Schmidlin, and Eric M Rouiller. Distinction between hand dominance and hand preference in primates: a behavioral investigation of manual dexterity in nonhuman primates (macaques) and human subjects. *Brain and behavior*, 3(5):575–95, sep 2013.

[45] J. G. Chi, E. C. Dooling, and F. H. Gilles. Gyral development of the human brain. *Annals of neurology*, 1(1):86–93, 1977.

[46] H. Chui, J. Rambo, and J. Duncan. Registration of cortical anatomical structures via robust 3D point matching. *... Processing in Medical ...*, 1999.

[47] Haili Chui and Anand Rangarajan. A new point matching algorithm for non-rigid registration. *Computer Vision and Image Understanding*, 89(2-3):114–141, 2003.

[48] D. Louis Collins, Georges Le Goualher, and Alan C. Evans. Non-linear Cerebral Registration with Sulcal Constraints. *In Medical Image Computing and Computer Assisted intervention*, pages 974–984, 1998.

[49] D. Louis Collins, C. J. Holmes, T. M. Peters, and A. C. Evans. Automatic 3-D model-based neuroanatomical segmentation. *Human Brain Mapping*, 3(3):190–208, 1995.

[50] T. F. Cootes, G. J. Edwards, and C. J. Taylor. Active Appearance Models. *Proc. ECCV*, pages 1–2, 1998.

[51] T.F. Cootes, C.J. Taylor, D.H. Cooper, and J. Graham. Active Shape Models-Their Training and Application, 1995.

[52] O Coulon, C Clouchoux, G Operto, K Dauchot, A Sirigu, and JL Anton. Cortical localization via surface parameterization: a sulcus-based approach. *NeuroImage*, 31:S46, jan 2006.

[53] Olivier Coulon, Fabrizio Pizzagalli, Grégory Operto, Guillaume Auzias, Chantal Delon-Martin, and Michel Dojat. Two new stable anatomical landmarks on the Central Sulcus: definition, automatic detection, and their relationship with primary motor functions of the hand. *Annual International Conference of the IEEE Engineering in Medicine and Biology Society.*, 2011:7795–8, jan 2011.

[54] Olivier Coulon, Fabrizio Pizzagalli, Grégory Operto, Guillaume Auzias, Chantal Delon-Martin, and Michel Dojat. Two new stable anatomical landmarks on the Central Sulcus: Definition, automatic detection, and their relationship with primary motor functions of the hand. *Proceedings of the Annual International Conference of the IEEE Engineering in Medicine and Biology Society, EMBS*, pages 7795–7798, jan 2011.

[55] W. M. Cowan, J. W. Fawcett, D. D. O'Leary, and B. B. Stanfield. Regressive events in neurogenesis. *Science (New York, N.Y.)*, 225(4668):1258–65, sep 1984.

[56] Fergus I M Craik and Ellen Bialystok. Cognition through the lifespan: mechanisms of change. *Trends in cognitive sciences*, 10(3):131–8, mar 2006.

[57] Bruce Crosson, Anastasia Ford, Keith M McGregor, Marcus Meinzer, Sergey Cheshkov, Xiufeng Li, Delaina Walker-Batson, and Richard W Briggs. Functional imaging and related techniques: an introduction for rehabilitation researchers. *Journal of rehabilitation research and development*, 47(2):vii–xxxiv, jan 2010.

[58] John G Csernansky, Sarah K Gillespie, Donna L Dierker, Alan Anticevic, Lei Wang, Deanna M Barch, and David C Van Essen. Symmetric abnormalities in sulcal patterning in schizophrenia. *NeuroImage*, 43(3):440–6, nov 2008.

[59] P. K. Curiati, J. H. Tamashiro, P. Squarzoni, F. L S Duran, L. C. Santos, M. Wajngarten, C. C. Leite, H. Vallada, P. R. Menezes, M. Scazufca, G. F. Busatto, and Tânia C. T. Ferraz Alves. Brain structural variability due to aging and gender in cognitively healthy elders: Results from the São Paulo ageing and health study. *American Journal of Neuroradiology*, 30(10):1850–1856, 2009.

[60] Matthew D. Cykowski, Olivier Coulon, Peter V. Kochunov, Katrin Amunts, Jack L. Lancaster, Angela R. Laird, David C. Glahn, and Peter T. Fox. The central sulcus: an observer-independent characterization of sulcal landmarks and depth asymmetry. *Cerebral cortex*, 18(9):1999–2009, sep 2008.

[61] T. Darvann. Landmarker: a vtk-based tool for landmarking of polygonal surfaces. *SilicoDentistry -The Evolution of Computational Oral Health Science*, pages 160–162, 2008.

[62] C Davatzikos. Mapping image data to stereotaxic spaces: applications to brain mapping. *Human brain mapping*, 6(5-6):334–8, jan 1998.

[63] Christos Davatzikos and R. Nick Bryan. Morphometric Analysis of Cortical Sulci Using Parametric Ribbons : A Study of the Central Sulcus. *Journal of Computer Assisted Tomography*, 26(2):298–307, 2002.

[64] François De Guio, Jean-François Mangin, Denis Rivière, Matthieu Perrot, Christopher D. Molteno, Sandra W. Jacobson, Ernesta M. Meintjes, and Joseph L. Jacobson. A study of cortical morphology in children with fetal alcohol spectrum disorders. *Human brain mapping*, 35(5):2285–96, may 2014.

[65] Anatole S. Dekaban and Doris Sadowsky. Changes in brain weights during the span of human life: Relation of brain weights to body heights and body weights. *Annals of Neurology*, 4(4):345–356, oct 1978.

[66] Chantal Delon-Martin, Jane Plailly, Pierre Fonlupt, Alexandra Veyrac, and Jean Pierre Royet. Perfumers' expertise induces structural reorganization in olfactory brain regions. *NeuroImage*, 68:55–62, 2013.

[67] Rahul S Desikan, Florent Ségonne, Bruce Fischl, Brian T Quinn, Bradford C Dickerson, Deborah Blacker, Randy L Buckner, Anders M Dale, R Paul Maguire, Bradley T Hyman, Marilyn S Albert, and Ronald J Killiany. An automated labeling system for subdividing the human cerebral cortex on MRI scans into gyral based regions of interest. *NeuroImage*, 31(3):968–80, 2006.

[68] Richard L Doty. Olfactory dysfunction in Parkinson disease. *Nature reviews. Neurology*, 8(6):329–39, jun 2012.

[69] J Duchon. Splines minimizing rotation-invariant semi-norms in Sobolev spaces. *Constructive theory of functions of several variables*, 1977.

[70] H.M. Duvernoy. *The human brain: surface, three-dimensional sectional anatomy with MRI, and vascularization*. 1999.

[71] Bradley Efron. Large-Scale Simultaneous The Choice Hypothesis Testing : of a Null Hypothesis. *Journal of the American Statistical Association*, 99(465):96–104, 2014.

[72] H Henrik Ehrsson, Stefan Geyer, and Eiichi Naito. Imagery of voluntary movement of fingers, toes, and tongue activates corresponding body-part-specific motor representations. *Journal of neurophysiology*, 90(5):3304–16, nov 2003.

[73] Susan Elmore. Apoptosis: a review of programmed cell death. *Toxicologic pathology*, 35(4):495–516, jun 2007.

[74] A.C. Evans, W. Dai, D.L. Collins, P. Neelin, and S. Marrett. Warping of a computerzied 3D atlas to match brain image volumes for quantitative neuroanatomical and functional analysis. *SPIE Med. Imaging*, 1445:236 –247, 1991.

[75] Alan C. Evans. The NIH MRI study of normal brain development. *NeuroImage*, 30(1):184–202, mar 2006.

[76] G. Fesl, B. Moriggl, U. D. Schmid, T. P. Naidich, K. Herholz, and T. A. Yousry. Inferior central sulcus: variations of anatomy and function on the example of the motor tongue area. *NeuroImage*, 20(1):601–610, sep 2003.

[77] Bruce Fischl, André van der Kouwe, Christophe Destrieux, Eric Halgren, Florent Ségonne, David H. Salat, Evelina Busa, Larry J. Seidman, Jill Goldstein, David Kennedy, Verne Caviness, Nikos Makris, Bruce Rosen, and Anders M. Dale. Automatically parcellating the human cerebral cortex. *Cerebral cortex (New York, N.Y. : 1991)*, 14(1):11–22, jan 2004.

[78] J Michael Fitzpatrick, Derek L G Hill, and Calvin R Maurer. Image Registration. *Handbook of Medical Imaging, Volume2: Medical Image Processing and Analysis*, pages 447–514, 2000.

[79] O. Foester. The Motor Cortex in Man in the Light of Hughlings Jackson's Doctrines. (Brain, vol. lix, p. 135, June, 1936.) Foerster, O. *The British Journal of Psychiatry*, 82(340):677–678, sep 1936.

[80] A. L. Foundas, K. Hong, C. M. Leonard, and K. M. Heilman. Hand preference and magnetic resonance imaging asymmetries of the central sulcus. *Neuropsychiatry, neuropsychology, and behavioral neurology*, 11(2):65–71, apr 1998.

[81] P. T. Fox, J. S. Perlmutter, and M. E. Raichle. A stereotactic method of anatomical localization for positron emission tomography. *Journal of computer assisted tomography*, 9(1):141–53, jan 1985.

[82] K L Francis and W W Spirduso. Age differences in the expression of manual asymmetry. *Experimental aging research*, 26(2):169–80, jan.

[83] Johannes Frasnelli, Therese Fark, Jacqueline Lehmann, Johannes Gerber, and Thomas Hummel. Brain structure is changed in congenital anosmia. *NeuroImage*, 83:1074–1080, 2013.

[84] Johannes Frasnelli, Johan N. Lundström, Julie A. Boyle, Jelena Djordjevic, Robert J. Zatorre, and Marilyn Jones-Gotman. Neuroanatomical correlates of olfactory performance. *Experimental Brain Research*, 201(1):1–11, 2010.

[85] David W. Frayer, Marina Lozano, José M. Bermúdez de Castro, Eudald Carbonell, Juan Luis Arsuaga, Jakov Radovčić, Ivana Fiore, and Luca Bondioli. More than 500,000 years of right-handedness in Europe. Laterality: Asymmetries of Body. *Brain and Cognition*, 17(1):51–69, jan 2012.

[86] Juanma De La Fuente, Julio Santiago, Antonio Román, Cristina Dumitrache, and Daniel Casasanto. When you think about it, your past is in front of you: How culture shapes spatial conceptions of time. *Psychological Science*, 25(9):1682–1690, 2014.

[87] Hironobu Fujiwara, Kazuyuki Hirao, Chihiro Namiki, Makiko Yamada, Mitsuaki Shimizu, Hidenao Fukuyama, Takuji Hayashi, and Toshiya Murai. Anterior cingulate pathology and social cognition in schizophrenia: a study of gray matter, white matter and sulcal morphometry. *NeuroImage*, 36(4):1236–45, jul 2007.

[88] A. M. Galaburda, J. E. Schmitt, S. W. Atlas, S. Eliez, U. Bellugi, and A. L. Reiss. Dorsal forebrain anomaly in Williams syndrome. *Archives of neurology*, 58(11):1865–9, nov 2001.

[89] Adriana Galván, Linda Van Leijenhorst, and Kristine M McGlennen. Considerations for imaging the adolescent brain. *Developmental cognitive neuroscience*, 2(3):293–302, jul 2012.

[90] Prapti Gautam, Kaarin J. Anstey, Wei Wen, Perminder S. Sachdev, and Nicolas Cherbuin. Cortical gyrification and its relationships with cortical volume, cortical thickness, and cognitive performance in healthy mid-life adults. *Behavioural brain research*, 287:331–9, jul 2015.

[91] Jay N Giedd and Judith L Rapoport. Structural MRI of pediatric brain development: what have we learned and where are we going? *Neuron*, 67(5):728–34, sep 2010.

[92] Nitin Gogtay, Jay N. Giedd, Leslie Lusk, Kiralee M. Hayashi, Deanna Greenstein, A. Catherine Vaituzis, Tom F. Nugent, David H. Herman,

Liv S. Clasen, Arthur W. Toga, Judith L. Rapoport, and Paul M. Thompson. Dynamic mapping of human cortical development during childhood through early adulthood. *Proceedings of the National Academy of Sciences of the United States of America*, 101(21):8174–9, may 2004.

[93] Yucel Gonul, Ahmet Songur, Ibrahim Uzun, Ramazan Uygur, Ozan Alper Alkoc, Veli Caglar, and Hudaverdi Kucuker. Morphometry, asymmetry and variations of cerebral sulci on superolateral surface of cerebrum in autopsy cases. *Surgical and radiologic anatomy : SRA*, nov 2013.

[94] Jay a. Gottfried and Raymond J. Dolan. The nose smells what the eye sees: Crossmodal visual facilitation of human olfactory perception. *Neuron*, 39(2):375–386, 2003.

[95] G. Le Goualher, A. M. Argenti, M. Duyme, W. F. Baaré, H. E. Hulshoff Pol, D. I. Boomsma, A. Zouaoui, C. Barillot, and A. C. Evans. Statistical sulcal shape comparisons: application to the detection of genetic encoding of the central sulcus shape. *NeuroImage*, 11(5 Pt 1):564–74, may 2000.

[96] Georges Le Goualher and DL Collins. Automatic identificaiton of cortical sulci using a 3D probabilistic atlas. In *Proc. 1st MICCAI*, volume 1496, pages 509–518, 1998.

[97] Anna Grabowska, Malgorzata Gut, Marek Binder, Lars Forsberg, Krystyna Rymarczyk, and Andrzej Urbanik. Switching handedness: fMRI study of hand motor control in right-handers, left-handers and converted left-handers. *Acta neurobiologiae experimentalis*, 72(4):439–51, jan 2012.

[98] Krystyna Grabski, Laurent Lamalle, Coriandre Vilain, Jean-Luc Schwartz, Nathalie Vallée, Irène Tropres, Monica Baciu, Jean-François Le Bas, and Marc Sato. Functional MRI assessment of orofacial articulators: Neural correlates of lip, jaw, larynx, and tongue movements. *Human Brain Mapping*, 33(10):2306–2321, 2012.

[99] Oliver Granert, Martin Peller, Christian Gaser, Sergiu Groppa, Mark Hallett, Arne Knutzen, Günther Deuschl, Kirsten E. Zeuner, and Hartwig R. Siebner. Manual activity shapes structure and function in contralateral human motor hand area. *NeuroImage*, 54(1):32–41, jan 2011.

[100] R C Gur, P D Mozley, S M Resnick, G L Gottlieb, M Kohn, R Zimmerman, G Herman, S Atlas, R Grossman, and D Berretta. Gender differences in age effect on brain atrophy measured by magnetic resonance imaging. *Proceedings of the National Academy of Sciences of the United States of America*, 88(7):2845–9, apr 1991.

[101] Malgorzata Gut, Andrzej Urbanik, Lars Forsberg, Marek Binder, Krystyna Rymarczyk, Barbara Sobiecka, Justyna Kozub, and Anna

Grabowska. Brain correlates of right-handedness. *Acta neurobiologiae experimentalis*, 67(1):43–51, jan 2007.

[102] Tadashi Hamasaki, Jun-ichi Imamura, Hiroshi Kawai, and Jun-ichi Kuratsu. A three-dimensional MRI study of variations in central sulcus location in 40 normal subjects. *Journal of clinical neuroscience : official journal of the Neurosurgical Society of Australasia*, 19(1):115–20, jan 2012.

[103] R. Hamer and P. M. Simpson. Mixed-Up Mixed Models: Things That Look Like They Should Work But Don't, and Things That Look Like They Shouldn't Work But Do. *Proceedings of the Twenty-Fifth Annual SAS® Users Group International Conference*, pages 20–25, 2000.

[104] Geoffrey Hammond. Correlates of human handedness in primary motor cortex: a review and hypothesis. *Neuroscience and biobehavioral reviews*, 26(3):285–92, may 2002.

[105] L. G. Hansen. Introduction to magnetic resonance imaging techniques, 2015.

[106] Alkomiet Hasan, Andrew M. McIntosh, Uta Aglaia Droese, Thomas Schneider-Axmann, Stephen M. Lawrie, Thomas William Moorhead, Ralf Tepest, Wolfgang Maier, Peter Falkai, and Thomas Wobrock. Prefrontal cortex gyrification index in twins: An MRI study. *European Archives of Psychiatry and Clinical Neuroscience*, 261(7):459–465, 2011.

[107] Christopher Hawkes. Olfaction in neurodegenerative disorder. *Movement disorders : official journal of the Movement Disorder Society*, 18(4):364–72, apr 2003.

[108] Norio Hayashi, Keita Sakuta, Kaori Minehiro, Masako Takanaga, Shigeru Sanada, Masayuki Suzuki, Tosiaki Miyati, Tomoyuki Yamamoto, and Osamu Matsui. Development of identification of the central sulcus in brain magnetic resonance imaging. *Radiological physics and technology*, 4(1):53–60, jan 2011.

[109] Anna M. Hedman, Neeltje E. M. van Haren, Hugo G. Schnack, René S. Kahn, and Hilleke E. Hulshoff Pol. Human brain changes across the life span: a review of 56 longitudinal magnetic resonance imaging studies. *Human brain mapping*, 33(8):1987–2002, aug 2012.

[110] V. Henkel, R. Mergl, G. Juckel, D. Rujescu, P. Mavrogiorgou, I. Giegling, H. Möller, and U. Hegerl. Assessment of handedness using a digitizing tablet: a new method. *Neuropsychologia*, 39(11):1158–66, jan 2001.

[111] Pierre-Yves Hervé, Bernard Mazoyer, Fabrice Crivello, Guy Perchey, and Nathalie Tzourio-Mazoyer. Finger tapping, handedness and grey matter

amount in the Rolando's genu area. *NeuroImage*, 25(4):1133–45, may 2005.

[112] Claus C. Hilgetag and Helen Barbas. Developmental mechanics of the primate cerebral cortex. *Anatomy and Embryology*, 210(5-6):411–417, 2005.

[113] Claus C. Hilgetag and Helen Barbas. Role of Mechanical Factors in the Morphology of the Primate Cerebral Cortex. *PLoS Computational Biology*, 2(3):e22, 2006.

[114] D L Hill, P G Batchelor, M Holden, and D J Hawkes. Medical image registration. *Physics in medicine and biology*, 46(3):R1–45, mar 2001.

[115] T Duelund Hjortshoj, K Grønskov, K Brøndum-Nielsen, and T Rosenberg. A novel founder BBS1 mutation explains a unique high prevalence of Bardet-Biedl syndrome in the Faroe Islands. *The British journal of ophthalmology*, 93(3):409–13, mar 2009.

[116] Michel A. Hofman. On the evolution and geometry of the brain in mammals. *Progress in Neurobiology*, 32(2):137–158, jan 1989.

[117] Larson J. Hogstrom, Lars T. Westlye, Kristine B. Walhovd, and Anders M. Fjell. The structure of the cerebral cortex across adult life: Age-related patterns of surface area, thickness, and gyrification. *Cerebral Cortex*, 23(11):2521–2530, 2013.

[118] W. D. Hopkins, O. Coulon, and J. F. Mangin. Observer-independent characterization of sulcal landmarks and depth asymmetry in the central sulcus of the chimpanzee brain. *Journal of Neuroscience*, 171(2):544–551, sep 2010.

[119] James D. Howard, Jay A. Gottfried, Philippe N. Tobler, and Thorsten Kahnt. Identity-specific coding of future rewards in the human orbitofrontal cortex. *Proceedings of the National Academy of Sciences*, 112(16):201503550, 2015.

[120] Caroline Huart, T. Meusel, J. Gerber, T. Duprez, P. Rombaux, and T. Hummel. The depth of the olfactory sulcus is an indicator of congenital anosmia. *American Journal of Neuroradiology*, 32(10):1911–1914, 2011.

[121] Caroline Huart, T. Meusel, J. Gerber, T. Duprez, P. Rombaux, and T. Hummel. The depth of the olfactory sulcus is an indicator of congenital anosmia. *American Journal of Neuroradiology*, 32(10):1911–1914, 2011.

[122] T. Hummel, G. Kobal, H. Gudziol, and a. Mackay-Sim. Normative data for the "Sniffin' Sticks" including tests of odor identification, odor discrimination, and olfactory thresholds: An upgrade based on a group of more than 3,000 subjects. *European Archives of Oto-Rhino-Laryngology*, 264(3):237–243, 2007.

[123] Thomas Hummel, Michael Damm, Julia Vent, Matthias Schmidt, Peter Theissen, Maria Larsson, and Jens Peter Klussmann. Depth of olfactory sulcus and olfactory function. *Brain Research*, 975:85–89, 2003.

[124] Thomas Hummel, Antje Urbig, Caroline Huart, Thierry Duprez, and Philippe Rombaux. Volume of olfactory bulb and depth of olfactory sulcus in 378 consecutive patients with olfactory loss. *Journal of Neurology*, pages 1046–1051, 2015.

[125] P. R. Huttenlocher. Synaptic density in human frontal cortex - developmental changes and effects of aging. *Brain research*, 163(2):195–205, mar 1979.

[126] P. R. Huttenlocher and C. de Courten. The development of synapses in striate cortex of man. *Human neurobiology*, 6(1):1–9, jan 1987.

[127] Krista L. Hyde, Jason Lerch, Andrea Norton, Marie Forgeard, Ellen Winner, Alan C. Evans, and Gottfried Schlaug. The Effects of Musical Training on Structural Brain Development. *Annals of the New York Academy of Sciences*, 1169(1):182–186, 2009.

[128] Kiho Im, Hang Joon Jo, Jean-François Mangin, Alan C. Evans, Sun I. Kim, and Jong-Min Lee. Spatial distribution of deep sulcal landmarks and hemispherical asymmetry on the cortical surface. *Cerebral cortex (New York, N.Y. : 1991)*, 20(3):602–11, mar 2010.

[129] Kiho Im, Jong-Min Lee, Sang Won Seo, Sun Hyung Kim, Sun I. Kim, and Duk L. Na. Sulcal morphology changes and their relationship with cortical thickness and gyral white matter volume in mild cognitive impairment and Alzheimer's disease. *NeuroImage*, 43(1):103–13, oct 2008.

[130] M Imagawa and T Yamadori. Phylogenetic development of brain and brain sulci in primates. *The Kobe journal of medical sciences*, 42(1):61–72, feb 1996.

[131] Noritaka Imai, Kazuhiko Sawada, Katsuhiro Fukunishi, Hiromi Sakata-Haga, and Yoshihiro Fukui. Sexual dimorphism of sulcal length asymmetry in the cerebrum of adult cynomolgus monkeys (Macaca fascicularis). *Congenital anomalies*, 51(4):161–6, dec 2011.

[132] C R Jack, R M Thompson, R K Butts, F W Sharbrough, P J Kelly, D P Hanson, S J Riederer, R L Ehman, N J Hangiandreou, and G D Cascino. Sensory motor cortex: correlation of presurgical mapping with functional MR imaging and invasive cortical mapping. *Radiology*, 190(1):85–92, jan 1994.

[133] Andrea P. Jackowski and Robert T. Schultz. Foreshortened dorsal extension of the central sulcus in Williams syndrome. *Cortex*, 41:282—-290, 1994.

[134] Anand A. Joshi, David W. Shattuck, Paul M. Thompson, and Richard M. Leahy. A framework for registration, statistical characterization and classification of cortically constrained functional imaging data. *Inf Process Med Imaging*, 19:186–196, jan 2005.

[135] Eric Jouvent, Jean-François Mangin, Edouard Duchesnay, Raphael Porcher, Marco Düring, Yvonne Mewald, Jean-Pierre Guichard, Dominique Hervé, Sonia Reyes, Nikola Zieren, Martin Dichgans, and Hugues Chabriat. Longitudinal changes of cortical morphology in CADASIL. *Neurobiology of aging*, 33(5):1002.e29–36, may 2012.

[136] Jorge Jovicich, Silvester Czanner, Douglas Greve, Elizabeth Haley, Andre van der Kouwe, Randy Gollub, David Kennedy, Franz Schmitt, Gregory Brown, James Macfall, Bruce Fischl, and Anders Dale. Reliability in multi-site structural MRI studies: effects of gradient non-linearity correction on phantom and human data. *NeuroImage*, 30(2):436–43, apr 2006.

[137] Henry F. Kaiser. The varimax criterion for analytic rotation in factor analysis. *Psychometrika*, 23(3):187–200, sep 1958.

[138] M. Karstensen, H.G. Vestergaard, A. Baar\'{e} , W. F, Skimminge, B. Djurhuus, B. Ellefsen, N. Brüggemann, C. Klausen, A. Leffers, N Tommerup, and H.R Siebner. Grey matter volume in prefrontal and limbic cortical regions is linked to smell ability in isolated congenital olfactory impairment. *in Submission*, 2015.

[139] Regina Katzenschlager and Andrew J Lees. Olfaction and Parkinson's syndromes: its role in differential diagnosis. *Current opinion in neurology*, 17(4):417–23, aug 2004.

[140] D. G. Kendall. Shape Manifolds, Procrustean Metrics, and Complex Projective Spaces. *Bulletin of the London Mathematical Society*, 16(2):81–121, 1984.

[141] J. F. Kerr, A. H. Wyllie, and A. R. Currie. Apoptosis: a basic biological phenomenon with wide-ranging implications in tissue kinetics. *British journal of cancer*, 26(4):239–57, aug 1972.

[142] R Kikinis, M E Shenton, G Gerig, H Hokama, J Haimson, B F O'Donnell, C G Wible, R W McCarley, and F A Jolesz. Temporal lobe sulco-gyral pattern anomalies in schizophrenia: an in vivo MR three-dimensional surface rendering study. *Neuroscience letters*, 182(1):7–12, nov 1994.

[143] Bjarne Kj\aer Ersb{\o}l and Knut Conradsen. *Multivariate Statistics -An Introduction*. DTU Informatics, Kgs. Lyngby, 2012.

[144] Arno Klein, Jesper Andersson, Babak A. Ardekani, John Ashburner, Brian Avants, Ming-Chang Chiang, Gary E. Christensen, D. Louis Collins, James Gee, Pierre Hellier, Joo Hyun Song, Mark Jenkinson, Claude Lepage, Daniel Rueckert, Paul Thompson, Tom Vercauteren, Roger P. Woods, J. John Mann, and Ramin V. Parsey. Evaluation of 14 nonlinear deformation algorithms applied to human brain MRI registration. *NeuroImage*, 46(3):786–802, 2009.

[145] Daniel Klein, Anna Rotarska-Jagiela, Erhan Genc, Sharmili Sritharan, Harald Mohr, Frederic Roux, Cheol E. Han, Marcus Kaiser, Wolf Singer, and Peter J. Uhlhaas. Adolescent Brain Maturation and Cortical Folding: Evidence for Reductions in Gyrification. *PLoS ONE*, 9(1):e84914, 2014.

[146] Stefan Klöppel, Jean-Francois Mangin, Anna Vongerichten, Richard S. J. Frackowiak, and Hartwig R. Siebner. Nurture versus nature: long-term impact of forced right-handedness on structure of pericentral cortex and basal ganglia. *Journal of Neuroscience*, 30(9):3271–3275, mar 2010.

[147] Stefan Klöppel, Anna Vongerichten, Thilo van Eimeren, Richard S. J. Frackowiak, and Hartwig R. Siebner. Can left-handedness be switched? Insights from an early switch of handwriting. *The Journal of neuroscience : the official journal of the Society for Neuroscience*, 27(29):7847–53, jul 2007.

[148] G. Kobal, L. Klimek, M. Wolfensberger, H. Gudziol, A. Temmel, C. M. Owen, H. Seeber, E. Pauli, and T. Hummel. Multicenter investigation of 1,036 subjects using a standardized method for the assessment of olfactory function combining tests of odor identification, odor discrimination, and olfactory thresholds. *European archives of oto-rhino-laryngology : official journal of the European Federation of Oto-Rhino-Laryngological Societies (EUFOS) : affiliated with the German Society for Oto-Rhino-Laryngology - Head and Neck Surgery*, 257(4):205–11, jan 2000.

[149] P. Kochunov, D. C. Glahn, P. T. Fox, J. L. Lancaster, K. Saleem, W. Shelledy, K. Zilles, P. M. Thompson, O. Coulon, J. F. Mangin, J. Blangero, and J. Rogers. Genetics of primary cerebral gyrification: Heritability of length, depth and area of primary sulci in an extended pedigree of Papio baboons. *NeuroImage*, 53(3):1126–34, nov 2010.

[150] Peter Kochunov, Jean François Mangin, Thomas Coyle, Jack Lancaster, Paul Thompson, Dennis Rivière, Yann Cointepas, Jean Régis, Anita Schlosser, Don R. Royall, Karl Zilles, John Mazziotta, Arthur Toga, and Peter T. Fox. Age-related morphology trends of cortical sulci. *Human Brain Mapping*, 26(3):210–220, 2005.

[151] A. Kumar, C. Juhasz, E. Asano, S. K. Sundaram, M. I. Makki, D. C. Chugani, and Harry T. Chugani. Diffusion tensor imaging study of the cortical origin and course of the corticospinal tract in healthy children. *American Journal of Neuroradiology*, 30(10):1963–1970, 2009.

[152] K. Ladeji-Osias. Medical image registration [Book Review]. *IEEE Engineering in Medicine and Biology Magazine*, 21(6):619–660, 2002.

[153] R Larsen, K B Hilger, and M C Wrobel. Statistical 2{D} and 3{D} shape analysis using Non-{E}uclidean Metrics. *Proceedings of Medical Image Computing and Computer-Assisted Intervention*, 2489:428–435, 2002.

[154] G. Le Goualher, E. Procyk, D. L. Collins, R. Venugopal, C. Barillot, and A. C. Evans. Automated extraction and variability analysis of sulcal neuroanatomy. *IEEE transactions on medical imaging*, 18(3):206–17, mar 1999.

[155] George Le Goualher, Christian Barillot, and Yves Bizais. Modeling Cortical Sulci with Active Ribbons. *International Journal of Pattern Recognition and Artificial Intelligence*, 11(08):1295–1315, dec 1997.

[156] R. N. Lemon. Neural control of dexterity: what has been achieved? *Experimental brain research*, 128(1-2):6–12, sep 1999.

[157] Lucien M Levy, Andrew J Degnan, Ila Sethi, and Robert I Henkin. Anatomic olfactory structural abnormalities in congenital smell loss: magnetic resonance imaging evaluation of olfactory bulb, groove, sulcal, and hippocampal morphology. *Journal of computer assisted tomography*, 37(5):650–7, jan 2013.

[158] Gang Li, Lei Guo, Jingxin Nie, and Tianming Liu. Automatic cortical sulcal parcellation based on surface principal direction flow field tracking. *NeuroImage*, 46(4):923–37, jul 2009.

[159] Gang Li, Jingxin Nie, Li Wang, Feng Shi, Amanda E. Lyall, Weili Lin, John H. Gilmore, and Dinggang Shen. Mapping longitudinal hemispheric structural asymmetries of the human cerebral cortex from birth to 2 years of age. *Cerebral Cortex*, 24(5):1289–1300, 2014.

[160] Shuyu Li, Ying Han, Deyi Wang, Hong Yang, Yubo Fan, Yating Lv, Hehan Tang, Qiyong Gong, Yufeng Zang, and Yong He. Mapping surface variability of the central sulcus in musicians. *Cerebral cortex*, 20(1):25–33, jan 2010.

[161] Shuyu Li, Shaoyi Wang, Xinwei Li, Qiongling Li, and Xiaobo Li. Abnormal surface morphology of the central sulcus in children with attention-deficit/hyperactivity disorder. *Frontiers in neuroanatomy*, 9:114, jan 2015.

[162] Shuyu Li, Mingrui Xia, Fang Pu, Deyu Li, Yubo Fan, Haijun Niu, Baoqing Pei, and Yong He. Age-related changes in the surface morphology of the central sulcus. *NeuroImage*, 58(2):381–390, sep 2011.

[163] Wen Li, James D Howard, Todd B Parrish, and Jay a Gottfried. Aversive learning enhances perceptual and cortical discrimination of indiscriminable odor cues. *Science (New York, N.Y.)*, 319(5871):1842–1845, 2008.

[164] Fang Liu, Logi Vidarsson, Jeff D Winter, Hien Tran, and Andrea Kassner. Sex differences in the human corpus callosum microstructure: A combined T2 myelin-water and diffusion tensor magnetic resonance imaging study. *Brain Research*, 1343:37–45, 2010.

[165] Tao Liu, Perminder S Sachdev, Darren M Lipnicki, Jiyang Jiang, Yue Cui, Nicole A Kochan, Simone Reppermund, Julian N Trollor, Henry Brodaty, and Wei Wen. Longitudinal changes in sulcal morphology associated with late-life aging and MCI. *NeuroImage*, 74:337–42, jul 2013.

[166] G. Lohmann, D. Y. von Cramon, and H. Steinmetz. Sulcal variability of twins. *Cerebral cortex*, 9(7):754–63, jan 1999.

[167] Gabriele Lohmann and D. Yves Von Cramon. Automatic labelling of the human cortical surface using sulcal basins. *Medical Image Analysis*, 4(3):179–188, 2000.

[168] M. Lotze, M. Erb, H. Flor, E. Huelsmann, B. Godde, and W. Grodd. fMRI evaluation of somatotopic representation in human primary motor cortex. *NeuroImage*, 11(5):473–481, 2000.

[169] E. Luders, K. L. Narr, R. M. Bilder, P. R. Szeszko, M. N. Gurbani, L. Hamilton, A. W. Toga, and C. Gaser. Mapping the Relationship between Cortical Convolution and Intelligence: Effects of Gender. *Cerebral Cortex*, 18(9):2019–2026, dec 2007.

[170] L. Lui, Y. Wang, T. Chan, and P. Thompson. Landmark constrained genus zero surface conformal mapping and its application to brain mapping research. *Applied Numerical Mathematics*, 57(5-7):847–858, 2007.

[171] C S Lygonis. Familiar absence of olfaction. *Hereditas*, 61(3):413–6, jan 1969.

[172] Oliver Lyttelton, Maxime Boucher, Steven Robbins, and Alan Evans. An unbiased iterative group registration template for cortical surface analysis. *NeuroImage*, 34(4):1535–44, feb 2007.

[173] Kathrine Skak Madsen, William F. C. Baaré, Martin Vestergaard, Arnold Skimminge, Lisser Rye Ejersbo, Thomas Z. Ramsøy, Christian Gerlach, Per Akeson, Olaf B Paulson, and Terry L. Jernigan. Response inhibition is associated with white matter microstructure in children. *Neuropsychologia*, 48(4):854–62, mar 2010.

[174] V. A. Magnotta. Quantitative In Vivo Measurement of Gyrification in the Human Brain: Changes Associated with Aging. *Cerebral Cortex*, 9(2):151–160, mar 1999.

[175] E A Maguire, D G Gadian, I S Johnsrude, C D Good, J Ashburner, R S Frackowiak, and C D Frith. Navigation-related structural change in the hippocampi of taxi drivers. *Proceedings of the National Academy of Sciences of the United States of America*, 97(8):4398–403, apr 2000.

[176] J B Maintz and M a Viergever. A survey of medical image registration. *Medical image analysis*, 2(1):1–36, 1998.

[177] J. Mangin, O. Coulon, and V. Frouin. Robust Brain Segmentation Using Histogram Scale-Space Analysis. In *MICCAI*, volume 1496, pages 1230–1241, 1998.

[178] J. Mangin, D. Rivière, A. Cachia, E. Duchesnay, Y. Cointepas, D. L. Collins, A. C. Evans, and J. Régis. Object-Based Morphometry of the Cerebral Cortex. *IEEE Transactions on Medical Imaging*, 23(8):968–982, 2004.

[179] Jean-Fran\c{c}ois Mangin, Vincent Frouin, Isabelle Bloch, Jean R \'{e}gis, and Jaime Lopez-Krahe. From 3D magnetic resonance images to structural representations of the cortex topography using topology preserving deformations. *Journal of Mathematical Imaging and Vision*, 5(4):297–318, dec 1995.

[180] JF Mangin. Entropy minimization for automatic correction of intensity nonuniformity. *Proceedings IEEE Workshop on Mathematical Methods in Biomedical Image Analysis. MMBIA-2000 (Cat. No.PR00737)*, 00(c):162–169, 2000.

[181] C. Marquardt, W. Gentz, and N. Mai. Visual control of automated handwriting movements. *Experimental Brain Research*, 128(1):224–228, 1999.

[182] Ruth E Martin, Bradley J MacIntosh, Rebecca C Smith, Amy M Barr, Todd K Stevens, Joseph S Gati, and Ravi S Menon. Cerebral areas processing swallowing and tongue movement are overlapping but distinct: a functional magnetic resonance imaging study. *Journal of neurophysiology*, 92(4):2428–43, oct 2004.

[183] Massaachusetts General Hospita. Internet Brain Segmentaion Respository, 2015.

[184] J. Mazziotta, A. Toga, A. Evans, P. Fox, J. Lancaster, K. Zilles, R. Woods, T. Paus, G. Simpson, B. Pike, C. Holmes, L. Collins, P. Thompson, D. MacDonald, M. Iacoboni, T. Schormann, K. Amunts, N. Palomero-Gallagher, S. Geyer, L. Parsons, K. Narr, N. Kabani, G. L. Goualher, D. Boomsma, T. Cannon, R. Kawashima, and B. Mazoyer. A probabilistic atlas and reference system for the human brain: International Consortium for Brain Mapping (ICBM). *Philosophical Transactions of the Royal Society B: Biological Sciences*, 356(1412):1293–1322, aug 2001.

[185] J C Mazziotta, A W Toga, A Evans, P Fox, and J Lancaster. A probabilistic atlas of the human brain: theory and rationale for its development. The International Consortium for Brain Mapping (ICBM). *NeuroImage*, 2(2):89–101, jun 1995.

[186] D Reese McKay, Peter Kochunov, Matthew D Cykowski, Jack W Kent, Angela R Laird, Jack L Lancaster, John Blangero, David C Glahn, and Peter T Fox. Sulcal depth-position profile is a genetically mediated neuroscientific trait: description and characterization in the central sulcus. *Journal of Neuroscience*, 33(39):15618–15625, sep 2013.

[187] J. R. Meyer, S. Roychowdhury, E. J. Russell, C. Callahan, D. Gitelman, and M. M. Mesulam. Location of the central sulcus via cortical thickness of the precentral and postcentral gyri on MR. *AJNR. American journal of neuroradiology*, 17(9):1699–706, oct 1996.

[188] O Missir, C Dutheil-Desclercs, J F Meder, A Musolino, and D Fredy. Central sulcus patterns at MRI. *Journal of neuroradiology. Journal de neuroradiologie*, 16(2):133–44, jan 1989.

[189] Anna L Mitchell, Andrew Dwyer, Nelly Pitteloud, and Richard Quinton. Genetic basis and variable phenotypic expression of Kallmann syndrome: towards a unifying theory. *Trends in endocrinology and metabolism: TEM*, 22(7):249–58, jul 2011.

[190] Wayne L. Monsky, Armando S. Garza, Isaac Kim, Shaun Loh, Tzu Chun Lin, Chin Shang Li, Jerron Fisher, Parmbir Sandhu, Vishal Sidhar, Abhijit J. Chaudhari, Frank Lin, Larry Stuart Deutsch, and Ramsey D. Badawi. Treatment planning and volumetric response assessment for yttrium-90 Radioembolization: Semiautomated determination of liver volume and volume of tumor necrosis in patients with hepatic malignancy. *CardioVascular and Interventional Radiology*, 34(2):306–318, 2011.

[191] Torben Moos and Morten Moller. *Basal neuroanatomi*. FADL, 2006.

[192] R J Morecraft, C Geula, and M M Mesulam. Cytoarchitecture and neural afferents of orbitofrontal cortex in the brain of the monkey. *The Journal of comparative neurology*, 323(3):341–358, 1992.

[193] a. Kadir Mutlu, Maude Schneider, Martin Debbané, Deborah Badoud, Stephan Eliez, and Marie Schaer. Sex differences in thickness, and folding developments throughout the cortex. *NeuroImage*, 82:200–207, 2013.

[194] T. P. Naidich, J. L. Grant, N. Altman, R. A. Zimmerman, S. B. Birchansky, B. Braffman, and J. L. Daniel. The developing cerebral surface. Preliminary report on the patterns of sulcal and gyral maturation–anatomy, ultrasound, and magnetic resonance imaging. *Neuroimaging clinics of North America*, 4(2):201–40, may 1994.

[195] Ziad S Nasreddine, Natalie A Phillips, Valérie Bédirian, Simon Charbonneau, Victor Whitehead, Isabelle Collin, Jeffrey L Cummings, and Howard Chertkow. The Montreal Cognitive Assessment, MoCA: a brief screening tool for mild cognitive impairment. *Journal of the American Geriatrics Society*, 53(4):695–9, apr 2005.

[196] Koshiro Nishikuni and Guilherme Carvalhal Ribas. Study of fetal and postnatal morphological development of the brain sulci. *Journal of neurosurgery. Pediatrics*, 11(January):1–11, 2013.

[197] Taku Ochiai, Stephan Grimault, Didier Scavarda, Giorgi Roch, Tomokatsu Hori, Denis Rivière, Jean François Mangin, and Jean Régis. Sulcal pattern and morphology of the superior temporal sulcus. *NeuroImage*, 22(2):706–719, jun 2004.

[198] R. C. Oldfield. The assessment and analysis of handedness: the Edinburgh inventory. *Neuropsychologia*, 9(1):97–113, mar 1971.

[199] Michio Ono, Stefan Kubik, and Chad D. Abernathey. *Atlas of the Cerebral Sulci*. Thieme, 1990.

[200] Grégory Operto, G. Auzias, Arnaud Le Troter, Matthieu Perrot, D. Riviere, J. Dubois, P. Huppi, Olivier Coulon, and Jean-François Mangin. Structural group analysis of cortical curvature and depth patterns in the developing brain. In *IEEE International Symposium on Biomedical Imaging (ISBI)*, number October, pages 422–425. ResearchGate, 2012.

[201] Elsebet Ostergaard, Flemming J Hansen, Nicolina Sorensen, Morten Duno, John Vissing, Pernille L Larsen, Oddmar Faeroe, Sigurdur Thorgrimsson, Flemming Wibrand, Ernst Christensen, and Marianne Schwartz. Mitochondrial encephalomyopathy with elevated methylmalonic acid is caused by SUCLA2 mutations. *Brain : a journal of neurology*, 130(Pt 3):853–61, mar 2007.

[202] M. S. Panizzon, C. Fennema-Notestine, L. T. Eyler, T. L. Jernigan, E. Prom-Wormley, M. Neale, K. Jacobson, M. J. Lyons, M. D. Grant, C. E. Franz, H. Xian, M. Tsuang, B. Fischl, L. Seidman, A. Dale, and W. S. Kremen. Distinct Genetic Influences on Cortical Surface Area and Cortical Thickness. *Cerebral Cortex*, 19(11):2728–2735, 2009.

[203] Wilder Penfield and Edwin Boldrey. Somatic motor and sensory representation in the cerebral cortex of man as studied by electrical stimulation. *Brain*, 60(4):389–443, dec 1937.

[204] Wilder Penfield and Theodore Rasmussen. *The cerebral cortex of man; a clinical study of localization of function.*

[205] Jiska S. Peper, Rachel M. Brouwer, Dorret I. Boomsma, René S. Kahn, and Hilleke E. Hulshoff Pol. Genetic influences on human brain structure: a review of brain imaging studies in twins. *Human brain mapping*, 28(6):464–73, jun 2007.

[206] Matthieu Perrot, Denis Rivière, and Jean-François Mangin. Cortical sulci recognition and spatial normalization. *Medical image analysis*, 15(4):529–550, aug 2011.

[207] Ruth E. Propper, Lauren J. O'Donnell, Stephen Whalen, Yanmei Tie, Isaiah H. Norton, Ralph O. Suarez, Lilla Zollei, Alireza Radmanesh, and Alexandra J. Golby. A combined fMRI and DTI examination of functional language lateralization and arcuate fasciculus structure: Effects of degree versus direction of hand preference. *Brain and cognition*, 73(2):85–92, jul 2010.

[208] P Rakic. A small step for the cell, a giant leap for mankind: a hypothesis of neocortical expansion during evolution. *Trends in neurosciences*, 18(9):383–8, sep 1995.

[209] S M Rao, J R Binder, T A Hammeke, P A Bandettini, J A Bobholz, J A Frost, B M Myklebust, R D Jacobson, and J S Hyde. Somatotopic mapping of the human primary motor cortex with functional magnetic resonance imaging. *Neurology*, 45(5):919–24, may 1995.

[210] N. Raz, F. M. Gunning, D. Head, J. H. Dupuis, J. McQuain, S. D. Briggs, W. J. Loken, A. E. Thornton, and J. D. Acker. Selective aging of the human cerebral cortex observed in vivo: differential vulnerability of the prefrontal gray matter. *Cerebral cortex*, 7(3):268–82, jan 1997.

[211] Armin Raznahan, Jason P. Lerch, Nancy Lee, Dede Greenstein, Gregory L. Wallace, Michael Stockman, Liv Clasen, Phillip W. Shaw, and Jay N. Giedd. Patterns of Coordinated Anatomical Change in Human Cortical Development: A Longitudinal Neuroimaging Study of Maturational Coupling. *Neuron*, 72(5):873–884, 2011.

[212] Jean Régis, Jean-François Mangin, Taku Ochiai, Vincent Frouin, Denis Riviére, Arnaud Cachia, Manabu Tamura, and Yves Samson. "Sulcal root" generic model: a hypothesis to overcome the variability of the human cortex folding patterns. *Neurologia medico-chirurgica*, 45(1):1–17, jan 2005.

[213] Peggy Reiner, Eric Jouvent, Edouard Duchesnay, Rémi Cuingnet, Jean-François Mangin, and Hugues Chabriat. Sulcal span in Azheimer's disease, amnestic mild cognitive impairment, and healthy controls. *Journal of Alzheimer's disease : JAD*, 29(3):605–13, jan 2012.

[214] A. G. Renehan, C. Booth, and C. S. Potten. What is apoptosis, and why is it important? *BMJ (Clinical research ed.)*, 322(7301):1536–8, jun 2001.

[215] S. M. Resnick, A. F. Goldszal, C. Davatzikos, S. Golski, M. A. Kraut, E. J. Metter, R. N. Bryan, and A. B. Zonderman. One-year age changes in MRI brain volumes in older adults. *Cerebral cortex (New York, N.Y. : 1991)*, 10(5):464–72, may 2000.

[216] Susan M Resnick, Dzung L Pham, Michael A Kraut, Alan B Zonderman, and Christos Davatzikos. Longitudinal magnetic resonance imaging studies of older adults: a shrinking brain. *The Journal of neuroscience : the official journal of the Society for Neuroscience*, 23(8):3295–301, apr 2003.

[217] Maryam E Rettmann, Xiao Han, Chenyang Xu, and Jerry L Prince. Automated sulcal segmentation using watersheds on the cortical surface. *NeuroImage*, 15(2):329–44, feb 2002.

[218] Maryam E. Rettmann, Michael A. Kraut, Jerry L. Prince, and Susan M. Resnick. Cross-sectional and longitudinal analyses of anatomical sulcal changes associated with aging. *Cerebral cortex (New York, N.Y. : 1991)*, 16(11):1584–94, nov 2006.

[219] Maryam E Rettmann, Duygu Tosun, Xiaodong Tao, Susan M Resnick, and Jerry L Prince. Program for Assisted Labeling of Sulcal Regions (PALS): description and reliability. *NeuroImage*, 24(2):398–416, jan 2005.

[220] David P Richman, R Malcolm Stewart, John W Hutchinson, and Verne S Caviness. Mechanical Model of Brain Convolutinal Development, 1975.

[221] Denis Rivière, Jean-François Mangin, Dimitri Papadopoulos-Orfanos, Jean-Marc Martinez, Vincent Frouin, and Jean Régis. Automatic recognition of cortical sulci of the human brain using a congregation of neural networks. *Medical image analysis*, 6(2):77–92, jun 2002.

[222] M. R. Roesch, T. A. Stalnaker, and G. Schoenbaum. Associative Encoding in Anterior Piriform Cortex versus Orbitofrontal Cortex during Odor

Discrimination and Reversal Learning. *Cerebral Cortex*, 17(3):643–652, 2006.

[223] Jeffrey Rogers, Peter Kochunov, Karl Zilles, Wendy Shelledy, Jack Lancaster, Paul Thompson, Ravindranath Duggirala, John Blangero, Peter T Fox, and David C Glahn. On the genetic architecture of cortical folding and brain volume in primates. *NeuroImage*, 53(3):1103–8, 2010.

[224] P E Roland and K Zilles. Brain atlases–a new research tool. *Trends in neurosciences*, 17(11):458–67, nov 1994.

[225] E T Rolls and L L Baylis. Gustatory, olfactory, and visual convergence within the primate orbitofrontal cortex. *The Journal of neuroscience : the official journal of the Society for Neuroscience*, 14(9):5437–5452, 1994.

[226] E T Rolls, H D Critchley, and A Treves. Representation of olfactory information in the primate orbitofrontal cortex. *Journal of Neurophysiology*, 75(5):1982–1996, 1996.

[227] Ph. Rombaux, H. Potier, E. Markessis, T. Duprez, and T. Hummel. Olfactory bulb volume and depth of olfactory sulcus in patients with idiopathic olfactory loss. *European Archives of Oto-Rhino-Laryngology*, 267(10):1551–1556, 2010.

[228] Lisa Ronan, Natalie Voets, Catarina Rua, Aaron Alexander-Bloch, Morgan Hough, Clare Mackay, Tim J. Crow, Anthony James, Jay N. Giedd, and Paul C. Fletcher. Differential tangential expansion as a mechanism for cortical gyrification. *Cerebral Cortex*, 24(8):2219–2228, 2014.

[229] E. M. Rouiller, X. H. Yu, V. Moret, a. Tempini, M. Wiesendanger, and F. Liang. Dexterity in adult monkeys following early lesion of the motor cortical hand area: The role of cortex adjacent to the lesion. *European Journal of Neuroscience*, 10(2):729–740, 1998.

[230] David H. Salat, Randy L. Buckner, Abraham Z. Snyder, Douglas N. Greve, Rahul S. R. Desikan, Evelina Busa, John C. Morris, Anders M. Dale, and Bruce Fischl. Thinning of the cerebral cortex in aging. *Cerebral cortex (New York, N.Y. : 1991)*, 14(7):721–30, jul 2004.

[231] S. Sandor and R. Leahy. Surface-based labeling of cortical anatomy using a deformable atlas. *IEEE transactions on medical imaging*, 16(1):41–54, feb 1997.

[232] Silvio Sarubbo, Alessandro De Benedictis, Igor L. Maldonado, Gianpaolo Basso, and Hugues Duffau. Frontal terminations for the inferior fronto-occipital fascicle: Anatomical dissection, DTI study and functional considerations on a multi-component bundle. *Brain Structure and Function*, 218(1):21–37, 2013.

[233] F. Sastre-Janer. Three-dimensional reconstruction of the human central sulcus reveals a morphological correlate of the hand area. *Cerebral Cortex*, 8(7):641–647, 1998.

[234] K Sawada, K Hikishima, a Y Murayama, H J Okano, E Sasaki, and H Okano. Fetal Sulcation And Gyrification In Common Marmosets (Callithrix Jacchus) Obtained By Ex Vivo Magnetic Resonance Imaging. *Neuroscience*, (November), nov 2013.

[235] A Sawczuk and K M Mosier. Neural control of tongue movement with respect to respiration and swallowing. *Critical reviews in oral biology and medicine : an official publication of the American Association of Oral Biologists*, 12(1):18–37, jan 2001.

[236] Rachael I. Scahill, Chris Frost, Rhian Jenkins, Jennifer L. Whitwell, Martin N. Rossor, and Nick C. Fox. A longitudinal study of brain volume changes in normal aging using serial registered magnetic resonance imaging. *Archives of neurology*, 60(7):989–94, jul 2003.

[237] Marie Schaer, Meritxell Bach Cuadra, Lucas Tamarit, François Lazeyras, Stephan Eliez, and Jean Philippe Thiran. A Surface-based approach to quantify local cortical gyrification. *IEEE Transactions on Medical Imaging*, 27(2):161–170, 2008.

[238] G Schoenbaum and H Eichenbaum. Information coding in the rodent prefrontal cortex. I. Single-neuron activity in orbitofrontal cortex compared with that in pyriform cortex. *Journal of neurophysiology*, 74(2):733–750, 1995.

[239] Jan Scholz, Miriam C Klein, Timothy E J Behrens, and Heidi Johansen-Berg. Training induces changes in white-matter architecture. *Nature neuroscience*, 12(11):1370–1, nov 2009.

[240] Renate Schweizer, Gunther Helms, and Jens Frahm. Revisiting a historic human brain with magnetic resonance imaging the first description of a divided central sulcus. *Frontiers in Neuroanatomy*, 8(May):1–7, 2014.

[241] N. Senthilkumaran and R. Rajesh. Edge detection techniques for image segmentation–a survey of soft computing approaches. *International Journal of Recent Trends in Engineering and Technology*, 1(2):250–254, 2009.

[242] Janina Seubert, Jessica Freiherr, Johannes Frasnelli, Thomas Hummel, and Johan N. Lundström. Orbitofrontal cortex and olfactory bulb volume predict distinct aspects of olfactory performance in healthy subjects. *Cerebral Cortex*, 23(October):2448–2456, 2013.

[243] Philip Shaw, Francois Lalonde, Claude Lepage, Cara Rabin, Kristen Eckstrand, Wendy Sharp, Deanna Greenstein, Alan Evans, J. N. Giedd, and Judith Rapoport. Development of cortical asymmetry in typically developing children and its disruption in attention-deficit/hyperactivity disorder. *Archives of general psychiatry*, 66(8):888–96, aug 2009.

[244] Philip Shaw, Meaghan Malek, Bethany Watson, Wendy Sharp, Alan Evans, and Deanna Greenstein. Development of Cortical Surface Area and Gyrification in Attention-Deficit/Hyperactivity Disorder. *Biological Psychiatry*, 72(3):191–197, aug 2012.

[245] Y. Shi, P. M. Thompson, I. Dinov, and A. W. Toga. Hamilton-Jacobi skeleton on cortical surfaces. *IEEE transactions on medical imaging*, 27(5):664–73, may 2008.

[246] Yonggang Shi, Zhuowen Tu, Allan L Reiss, Rebecca A. Dutton, Agatha D. Lee, Albert M. Galaburda, Ivo Dinov, Paul M. Thompson, and Arthur W. Toga. Joint sulcal detection on cortical surfaces with graphical models and boosted priors. *IEEE transactions on medical imaging*, 28(3):361–73, mar 2009.

[247] Hartwig R Siebner, Claus Limmer, Alexander Peinemann, Alexander Drzezga, Bastiaan R Bloem, Markus Schwaiger, and Bastian Conrad. Long-Term Consequences of Switching Handedness: A Positron Emission Tomography Study on Handwriting in " Converted " Left-Handers. *Journal of Neuroscience*, 22(7):2816–2825, 2002.

[248] E. R. Sowell. Longitudinal Mapping of Cortical Thickness and Brain Growth in Normal Children. *Journal of Neuroscience*, 24(38):8223–8231, 2004.

[249] Elizabeth R. Sowell and Bradley S. Peterson. Sex differences in cortical thickness mapped in 176 healthy individuals between 7 and 87 years of age. *October*, 28(30):4439–4448, 2008.

[250] Elizabeth R. Sowell, Doris A. Trauner, Anthony Gamst, and Terry L. Jernigan. Development of cortical and subcortical brain structures in childhood and adolescence: a structural MRI study. *Developmental medicine and child neurology*, 44(1):4–16, 2002.

[251] R Grant Steen, Courtney Mull, Robert McClure, Robert M Hamer, and Jeffrey A Lieberman. Brain volume in first-episode schizophrenia: systematic review and meta-analysis of magnetic resonance imaging studies. *The British journal of psychiatry : the journal of mental science*, 188(6):510–8, jun 2006.

[252] Mb B B Stegmann and Dd D D Gomez. A brief introduction to statistical shape analysis. *Informatics and Mathematical ...*, (March):1–15, 2002.

[253] H Steinmetz, G Fürst, and H J Freund. Cerebral cortical localization: application and validation of the proportional grid system in MR imaging. *Journal of computer assisted tomography*, 13(1):10–9, jan.

[254] Joan Stiles and Terry L. Jernigan. The Basics of Brain Development. *Neuropsychology Review*, 20(4):327–348, 2010.

[255] M Styner, G Gerig, J Lieberman, D Jones, and D Weinberger. Statistical shape analysis of neuroanatomical structures based on medial models. *Medical Image Analysis*, 7(3):207–220, sep 2003.

[256] Bo Sun, Haitao Ge, Yuchun Tang, Zhongyu Hou, Junhai Xu, Xiangtao Lin, and Shuwei Liu. Asymmetries of the central sulcus in young adults: Effects of gender, age and sulcal pattern. *International Journal of Developmental Neuroscience*, 44:65–74, 2015.

[257] Tao Sun and Robert F Hevner. Growth and folding of the mammalian cerebral cortex: from molecules to malformations. *Nature reviews. Neuroscience*, 15(4):217–32, apr 2014.

[258] Z. Y. Sun, P. Pinel, D. Rivière, A. Moreno, S. Dehaene, and J.-F. Mangin. Linking morphological and functional variability in hand movement and silent reading. *Brain Structure and Function*, 2015.

[259] Zhong Yi Sun, Stefan Klöppel, Denis Rivière, Matthieu Perrot, Richard Frackowiak, and Laboratoire De Neuroimagerie. Innate and experience-dependent brain markers of left-handedness.

[260] Zhong Yi Sun, Stefan Klöppel, Denis Rivière, Matthieu Perrot, Richard Frackowiak, Hartwig Siebner, and Jean-François Mangin. The effect of handedness on the shape of the central sulcus. *NeuroImage*, 60(1):332–339, mar 2012.

[261] Jean Talairach and G. Szikla. Atlas of stereotactic concepts to the surgery of epilepsy. Technical report, ., 1967.

[262] H. Tanga, E.X. Wua, Mab Q.Y., D Gallagherc, G.M. Pereraa, and T. Zhuangd. MRI brain image segmentation by multi-resolution edge detection and region selection. *Computerized Medical Imaging and Graphics*, 24(May):349–357, 2200.

[263] X Tao, X Han, M E Rettmann, and C Davatzikos. Statistical Study on Cortical Sulci of Human Brains. *Lect. Notes in Comp. Sci.: Proc. of Information Processing in Medical Imaging*, 2082:475–487, 2001.

[264] C J Taylor and A Caunce. Using local geometry to build 3D sulcal models. In *Information Processing in Medical Imaging*, volume 1613, pages 196–209. Springer, 1999.

[265] P M Thompson, T D Cannon, K L Narr, T van Erp, V P Poutanen, M Huttunen, J Lönnqvist, C G Standertskjöld-Nordenstam, J Kaprio, M Khaledy, R Dail, C I Zoumalan, and A W Toga. Genetic influences on brain structure. *Nature neuroscience*, 4(12):1253–8, dec 2001.

[266] P. M. Thompson, R. P. Woods, M. S. Mega, and A. W. Toga. Mathematical/computational challenges in creating deformable and probabilistic atlases of the human brain. *Human brain mapping*, 9(2):81–92, feb 2000.

[267] Paul M Thompson, Kiralee M Hayashi, Elizabeth R Sowell, Nitin Gogtay, Jay N Giedd, Judith L Rapoport, Greig I De Zubicaray, Andrew L Janke, Stephen E Rose, James Semple, David M Doddrell, Yalin Wang, Theo G M Van Erp, Tyrone D Cannon, and Arthur W Toga. Mapping cortical change in Alzheimer ' s disease , brain development , and schizophrenia. *Neuroscience*, 23:2–18, 2004.

[268] Paul M Thompson, David MacDonald, Michael S Mega, Colin J Holmes, Alan C Evans, and Arthur W Toga. Detection and Mapping of Abnormal Brain Structure with a Probabilistic Atlas of Cortical Surfaces. *Journal of Computer Assisted Tomography*, 21(4), 1997.

[269] Paul M. Thompson, Craig Schwartz, Robert T. Lin, Aelia A. Khan, and Arthur W. Toga. Three-Dimensional Statistical Analysis of Sulcal Variability in the Human Brain. *Brain*, 16(13):4261– 4274, 1996.

[270] Arthur W. Toga and Paul Thompson. *Multimodal Brain Atlases*, volume 465. Springer US, Boston, MA, 1998.

[271] Arthur W Toga and Paul M Thompson. New approaches in brain morphometry. *The American journal of geriatric psychiatry : official journal of the American Association for Geriatric Psychiatry*, 10(1):13–23, jan 2002.

[272] Duygu Tosun, Maryam E Rettmann, Xiao Han, Xiaodong Tao, Chenyang Xu, Susan M Resnick, Dzung L Pham, and Jerry L Prince. Cortical surface segmentation and mapping. *NeuroImage*, 23 Suppl 1:S108–18, jan 2004.

[273] U.S National libery of medicine. Visual Human Brain Project, 2015.

[274] M Vaillant and C Davatzikos. Finding parametric representations of the cortical sulci using an active contour model. *Medical image analysis*, 1(4):295–315, sep 1997.

[275] D. C. Van Essen, M. F. Glasser, D. L. Dierker, J. Harwell, and T. Coalson. Parcellations and Hemispheric Asymmetries of Human Cerebral Cortex Analyzed on Surface-Based Atlases. *Cerebral Cortex*, 22(10):2241–2262, 2012.

[276] D.C Van Essen and H.A. Drury. Structural and functional analyses of human human cerebral cortex using a surface-based atlas. *The Journal of Neuroscience*, 17(19):7079–7102, 1997.

[277] D.C. Van Essen, J. Harwell, D. Hanlon, and J. Dickson. Surface-Based Atlases and a Database of Cortical Structure and Function. In *In: Databasing the Brain: From Data to Knowledge (Neuroinformatics), S.H. Koslow and S. Subramaniam*, pages 369–387. John Wiley & Sons, 2005.

[278] Gregory L. Wallace, Briana Robustelli, Nathan Dankner, Lauren Kenworthy, Jay N. Giedd, and Alex Martin. Increased gyrification, but comparable surface area in adolescents with autism spectrum disorders. *Brain : a journal of neurology*, 136(Pt 6):1956–67, jun 2013.

[279] Wally Welker. *Why do the cerebral cortex fissure and fold*, volume 8B of *Cerebral Cortex*. Cerebral Cortex, 1990.

[280] L. E. White, T. J. Andrews, C. Hulette, A.. Richards, M. Groelle, J. Paydarfar, and D. Purves. Structure of the human sensorimotor system. I: Morphology and cytoarchitecture of the central sulcus. *Cerebral cortex*, 7(1):18–30, 1997.

[281] L. E. White, T. J. Andrews, C. Hulette, A. Richards, M. Groelle, J. Paydarfar, and D. Purves. Structure of the human sensorimotor system. II: Lateral symmetry. *Cerebral cortex (New York, N.Y. : 1991)*, 7(1):31–47, jan 1997.

[282] Tonya White, Nancy C. Andreasen, and Peggy Nopoulos. Brain volumes and surface morphology in monozygotic twins. *Cerebral cortex*, 12(5):486–493, 2002.

[283] Tonya White, Shu Su, Marcus Schmidt, Chiu-Yen Kao, and Guillermo Sapiro. NIH Public Access. *Brain Cogn*, 72(1), 2010.

[284] S F Witelson and D L Kigar. Sylvian fissure morphology and asymmetry in men and women: bilateral differences in relation to handedness in men. *The Journal of comparative neurology*, 323(3):326–40, sep 1992.

[285] Sandra F. Witelson and Debra L. Kigar. Asymmtery in brain function follows asymmetry in anatomical form: gross, microscopic, postmortem and imaging studies. *Elsevier, Amsterdam*, 1:111–142, 1988.

[286] Keng Nei Wu, Bruce K Tan, James D Howard, David B Conley, and Jay A Gottfried. Olfactory input is critical for sustaining odor quality codes in human orbitofrontal cortex. *Nature Neuroscience*, 15(9):1313–1319, 2012.

[287] Faguo Yang and Frithjof Kruggel. Automatic segmentation of human brain sulci. *Medical image analysis*, 12(4):442–51, aug 2008.

[288] David M. Yousem, Rena J. Geckle, Warren B. Bilker, D. A. McKeown, and Richard L. Doty. MR Evaluation of patients with congenital hyposmia or anosmia. *Ajr*, 166(2):439–443, 1996.

[289] T. A. Yousry, U. D. Schmid, H. Alkadhi, D. Schmidt, A. Peraud, A. Buettner, and P. Winkler. Localization of the motor hand area to a knob on the precentral gyrus. A new landmark. *Brain*, 120:141–157, jan 1997.

[290] Jana Zelinková, Daniel Joel Shaw, Radek Mareček, Michal Mikl, Tomáš Urbánek, Lenka Peterková, Petr Zámečník, and Milan Brázdil. Superior temporal sulcus and social cognition in dangerous drivers. *NeuroImage*, 83:1024–30, dec 2013.

[291] Haidong Zhang, Zhonghe Zhang, Xuntao Yin, Jinfeng Zhan, Zhenmei Zhao, Yuchun Tang, Chao Liu, Shuwei Liu, and Shizhen Zhong. Early development of the fetal central sulcus on 7.0T magnetic resonance imaging. *International journal of developmental neuroscience : the official journal of the International Society for Developmental Neuroscience*, nov 2015.

[292] Karl Zilles, Nicola Palomero-Gallagher, and Katrin Amunts. Development of cortical folding during evolution and ontogeny. *Trends in Neurosciences*, 36(5):275–284, 2013.

[293] Karl Zilles, Axel Schleicher, Christian Langemann, Katrin Amunts, Patricia Morosan, Nicola Palomero-gallagher, Thorsten Schormann, Hartmut Mohlberg, Uli Bu, Helmut Steinmetz, Gottfried Schlaug, and Per E. Roland. Quantitative Analysis of Sulci in the Human Cerebral Cortex : Development , Regional Heterogeneity , Gender Difference , Asymmetry , Intersubject Variability and Cortical Architecture. *Human Brain Mapping*, 221:218–221, 1997.